2007

Practical vibration evaluation and early warning of damage in post-tensioned tendons

Jaime Lopez-Sabando
University of South Florida

Practical Vibration Evaluation and Early Warning of Damage in Post-Tensioned Tendons

by

Jaime Lopez-Sabando

A thesis submitted in partial fulfillment
of the requirements for the degree of
Master of Science in Mechanical Engineering
College of Engineering
University of South Florida

Major Professor: Alberto A. Sagüés, Ph.D.
Daniel P. Hess, Ph.D.
Autar K. Kaw, Ph.D.

Date of Approval:
December 14, 2007

Keywords: Tendon anchorage, Non destructive methods, Corrosion monitoring, Probes, Electrochemical Impedance Spectroscopy, Linear Polarization.

Dedication

To my wife, Mayme Hayes, for her unconditional support.

Acknowledgements

My sincere thanks to Dr. Alberto A. Sagüés for his guidance and encouragement. I am also grateful to Dr. Autar Kaw and Dr Daniel Hess for serving on the committee.

I would also like to thank Kingsley Lau and Dr. Luciano Taveira for their valuable help, and the personnel of the State Structures Laboratory of Florida Department of Transportation for use of the Tendon Test Facility.

This research was supported by the Florida Department of Transportation. The opinions, findings and conclusions expressed here are those of the author and not necessarily those of the supporting agency.

Table of Contents

List of Tables

List of Figures

Practical Vibration Evaluation and Early Warning of Damage in Post-Tensioned Tendons

Jaime Lopez-Sabando

ABSTRACT

Severe corrosion damage and even complete failure was recently discovered in external post-tensioned (PT) tendons of three Florida's pre-cast, segmental bridges over seawater. A key deterioration factor was the formation of large bleed water grout voids at or near the anchorages. Steel corrosion may occur at the grout-void interface or in the air space of the void itself. Since the tendons are critical to the structural integrity of the bridges, reliable and non-intrusive damage detection methods are desirable to manage or prevent future occurrences.

In recent years several indirect non-destructive methods have been developed or improved to evaluate the conditions of the tendons. One of those methods is vibration-based tension measurements, consisting of detecting tendon tension loss by analyzing the tendon's natural frequencies.

Until recently, vibration-based tension measurements were costly and laborious since they required several operators to conduct the tests and complicated analysis through different programs. The first objective of this research is to provide a practical, simplified, user-friendly testing and analysis method for screening tendons by vibration measurements.

Electrochemical Impedance Spectroscopy, Linear Polarization, and Electrical Resistance are alternative methods that could nondestructively detect or monitor corrosion before strand failures occur. The reliability and sensitivity of these conventional monitoring methods in solid or liquid media are well proven. However, few investigations exist on applying these methods to air-space corrosion as it may occur in tendon anchors. The second objective of this research is to establish the feasibility of using the above conventional monitoring methods for detecting air-space corrosion.

In this investigation, two different types of Electrical Resistance probes were designed and evaluated. Also, electrochemical probes were constructed simulating strands conditions in the grout-void interface. Electrochemical Impedance Spectroscopy and Linear Polarization measurements were conducted in the electrochemical probes to calculate their instantaneous corrosion rates. Electrical Resistance and Electrochemical probes results indicate that both methods provide sufficient sensibility to determine the ongoing damage.

Chapter 1

Introduction

Severe corrosion damage and even complete failure was recently discovered in external post-tensioned (PT) tendons of three Florida's pre-cast, PT segmental bridges over seawater. The damage consisted, in each of the three bridges, of a completely separated tendon plus one to several partially detensioned tendons (Figure 1,2). A key deterioration factor was the formation of large bleed water grout voids at or near the anchorages. Steel corrosion may occur at the grout-void interface or in the air space of the void itself. Atmospheric-like air space corrosion may be induced on the bare steel by the high humidity environment inside the grout voids. Since the tendons are critical to the structural integrity of the bridges, reliable and non-intrusive damage detection methods are desirable to manage or prevent future occurrences [1], [2].

The following main characteristics of post-tensioned tendons are noted in the Federal Highway Administration Post-Tensioning Tendon Installation and Grouting Manual [3]. A completely assembled, post-tensioning tendon consists of anchorages, prestressing strands, duct**,** and cementitious grout. The anchorages are embedded in the concrete pier diaphragm. In many applications , including the bridges that experienced corrosion as noted above the duct segments of the tendon are external to the concrete, allowing them to freely vibrate between the

end-span diaphragm and deviation block or between deviation blocks (Figure 3). External segments typically range from 5 to 20 m in length, and their fixity approximates clamped end conditions.

Figure 1. Failed Tendon at Niles Channel Bridge [4]

Figure 2. Failed Tendon at Sunshine Skyway Bridge [5]

The grout provides corrosion protection to the strand and bonds the internal tendon to the concrete structure surrounding the duct. The primary constituent of grout is ordinary Portland cement (Type I or II). Other cementitious material may be added such as fly ash to improve corrosion resistance in aggressive environments or a high range water-reducer (HRWR) to enhance fluidity . There are several commercial grouts approved by the Florida Department of Transportation (FDOT). The relative humidity (RH) inside the void depends on the type of grout being used, and can range from ~75% to ~90% [1].

The duct containing the grout and strands is made of high density polyethylene. The duct size depends on the number of strands inside the tendon "The nominal internal cross sectional area of circular duct should be at least 2.25 times the net area of the post-tensioning strands"[3]. For example, a 11.45cm outer diameter duct with a wall thickness of 0.475cm can encase up to 38 strands of 98.7mm² nominal cross section area, or a 9cm outer diameter duct with a wall thickness of 0.432cm can encase up to 23 strands of 98.7mm² nominal cross section area).

A typical tendon contains from 1 to many strands (e.g. 19,27,etc) made from 7 individual high tensile strength steel wires (A 416), arranged as 6 helically wound outer wires and one center "king" wire. ASTM A- 416 is a special steel alloy that it has been heat treaded to obtain a guaranteed ultimate tensile strength (GUTS) of 1860Mpa (270ksi) [8]. Strands used in PT bridges in Florida are mainly of two nominal sizes, 12.7mm (0.5in) and 15.24mm (0.6in) diameter, with nominal cross sectional areas of 98.7mm^2 and 140mm^2 (0.153 and 0.217

square inches), respectively. After wedge set and relaxation, the terminal stress in post-tensioned strands is on the order of 70% of their GUTS [9]. Therefore, a strand would likely fail if corrosion decreased its cross section area decreased by more than 30%, or even earlier because of stress concentration effects as corrosion is rarely uniform .

A typical anchorage assembly consists of a wedge plate, anchor, trumpet, and wedges (Figure 4)[7]. The wedge plate carries all the strands and bears on the steel anchor. The anchor is typically made of ductile iron (ASTM A27) bearing directly against the concrete. Plastic or galvanized sheet metal trumpets are used to transition from the anchor to the duct. Wedges are of case-hardened, low carbon or alloy steel, and their length is at least 2.5 times the strand diameter [3].

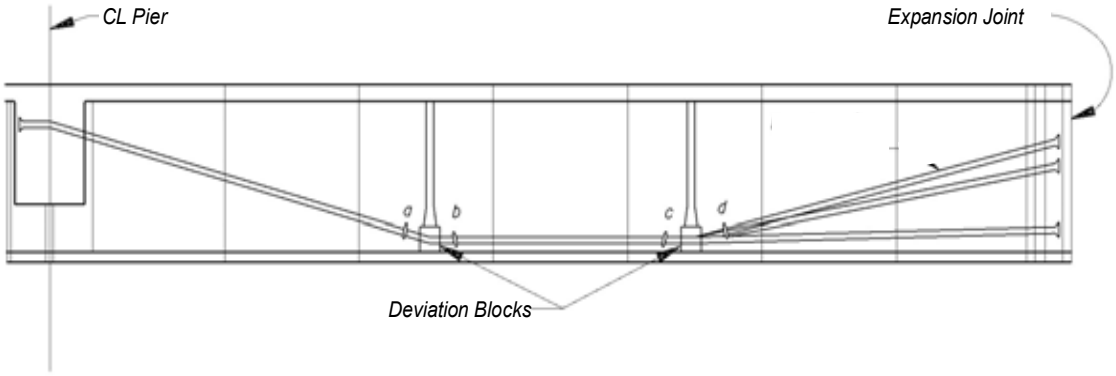

Figure 3. Typical Tendon Configuration [3]

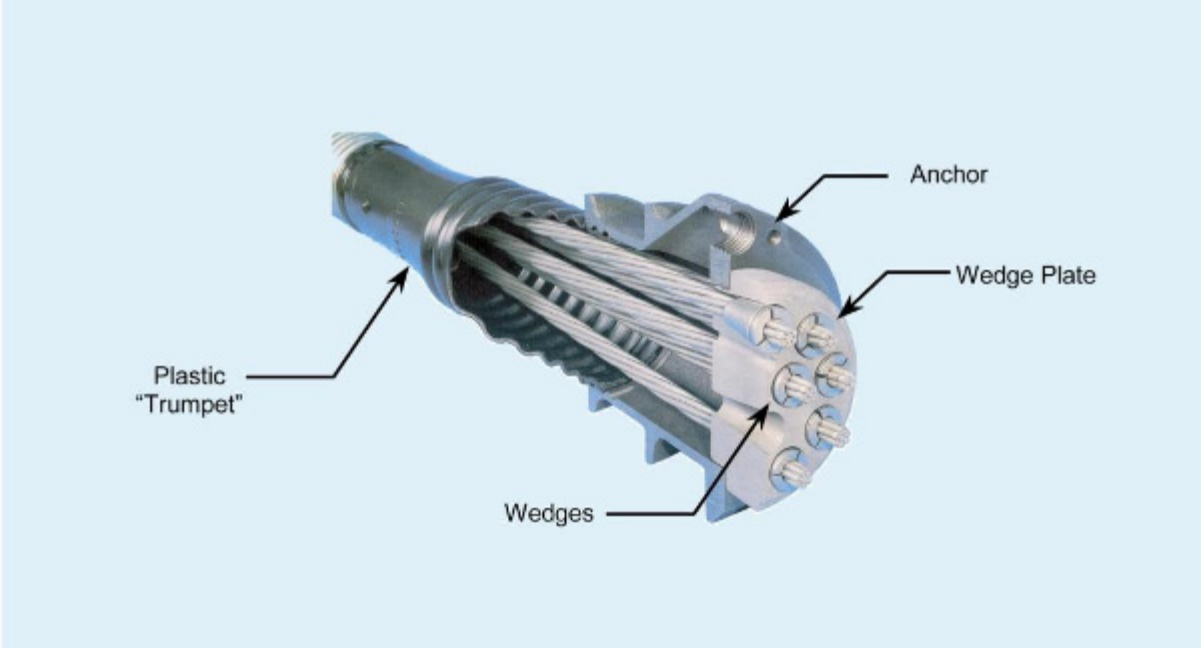

Figure 4. Details of a Typical Anchorage System (Dywidag International)

Direct detection of strand corrosion in the external section is difficult without damaging the tendon since the strands are encased within polyethylene ducts filled with hardened grout. Observation of corrosion in the anchorages is even more difficult unless a grout voids is present, in which case a boroscope may be introduced through a vent hole or unused wedge hole. In recent years several indirect non-destructive methods have been developed or improved to evaluate the conditions of the tendons such as magnetic flux leakage or pulsed eddy current [6]. One of those methods is vibration-based tension measurements, consisting of detecting tendon tension loss by analyzing the natural frequencies of the vibrating external tendon length.

Until recently, vibration-based tension measurements required several operators to conduct the tests and complicated analysis through different programs. Frequent implementation can be costly since Florida has more than

80 major, post-tensioned bridges, which would require a commensurately large need of specialists work hours and funding. The *first objective* of this research is to provide a practical, simplified, user-friendly testing and analysis method for screening tendons by vibration measurements. The research addresses different options of acquiring the tendon frequencies, required the employment of only one operator.

Although the vibration technique can be easy to implement, a drawback is that it would only detect a damaged tendon after at least one of its strands has snapped, since tension loss may result only if a strand has failed and the grout cannot support the resulting transferred load. Electrochemical Impedance Spectroscopy (EIS), Linear Polarization (LP), and Electrical Resistance (ER) are alternative methods that could nondestructively detect or monitor corrosion before strand failures occur. The reliability and sensitivity of these conventional monitoring methods in solid or liquid media are well proven. However, few investigations exist on applying these methods to air-space corrosion as it may occur in tendon anchors. The *second objective* of this research is to establish the feasibility of using the above conventional monitoring methods for detecting air-space corrosion. If these methods prove to be sensitive enough, then they could be used as a supplement to vibration testing for early warning of tendon deterioration.

Chapter 2

Practical Vibration Evaluation Methodology*

Vibration-Based tension measurements consist of measuring the vibrational response of tendons to mechanical excitation, and using the results along other tendon parameters to estimate the tendon tension. A damaged tendon can be detected by comparing its actual estimated tension against prior tension measurements, peer tendons, or by comparing segments tension at each end of the tendon. Conditions for a damaged tendon to be detected are that at least one of its strands has snapped, since tension loss may result only if a strand has failed, and that the grout cannot support the resulting transferred load.

As derived by Morse [2, 11] the vibration frequency (f_n) of modes n = 1,2,… of a stiff bean of length L, mass per unit length mu, flexural stiffness S, tensioned by force T, and clamped at both ends are given by:

$$f_n = n/L \cdot \sqrt{T/mu} \cdot [1/2 + (S/T \cdot L)^{1/2} + (2 + n^2 \cdot \pi^2/4) \cdot (S/T \cdot L)] \qquad [1]$$

If S, L, mu, and f_n are known then T can be found by solving the above equation for T. An independent estimate of T is obtained for each f_n.

* Parts of the work in this chapter have appeared in A. Sagüés, T. Eason, C. Cotrim and J. Lopez-Sabando, "Validation and Practical Procedure for Vibrational Evaluation of Tendons", Project No. BC 353#44, 158 pages, Draft Final Report to Florida Department of Transportation, University of South Florida, Tampa, Fl, December, 2007 [10].

$$T = \left[L^2 \frac{f_n}{n} - \sqrt{\frac{S}{mu} + \frac{1}{n\sqrt{2}}} \cdot \left(\frac{2 f_n^2 \cdot L^4 \cdot mu \cdot \sqrt{\frac{S}{mu} - 6S \cdot n^2 \cdot \sqrt{\frac{S}{mu}} - n^4} \cdot \sqrt{\frac{S}{mu}} \cdot \pi^2 \cdot S - 4L^2 \cdot f_n \cdot S \cdot n}{mu \cdot \sqrt{\frac{S}{mu}}} \right)^{\frac{1}{2}} \right]^2 \cdot \frac{mu}{L^2} \quad [2]$$

2.1 Tension Spreadsheet

As it was explained in the introduction, the first objective of this research is to provide a practical, simplified, user-friendly testing and analysis method for screening tendons by vibration measurements with the employment of only one operator. A spreadsheet called *Tension-Spreadsheet* was prepared in Excel to estimate the tension per strand in a set of 6 tendons, three on each side of a symmetric bridge span, each tendon having external segments terminating at the diaphragm at each end of the span. The *Tension-Spreadsheet* consisted of four worksheets called: *Inputs*, *Calculations*, *Results*, and *Chart*.

The *Inputs* worksheet (Figure 5) asks for the following parameters corresponding to each of the before mentioned tendon segments in a span: mass per unit length (mu), stiffness (S), number of strands, length of the tendon segment (L), and the first two vibration mode frequencies, corresponding to 4 vibration tests (two straight impact and two side impact). The length of the tendon segment is obtained from direct measurements, and the number and type of strands is obtained from construction data. Other parameters estimations are explained in the following sections.

The *Calculations* worksheet estimates the tension per strand for each tendon using equations (1,2) explained in the previous section. The frequency used for each mode is the average of the four vibration tests. The final estimated

tension is the average of the estimated tension for each mode. This worksheet is hidden to make sure the calculations stay uncorrupted by the user.

The *Results* worksheet displays the estimated average tension per strand for each tendon (kN/strand) and the Quality %, or percent difference between the tension estimated from the first and second mode frequencies f_1 and f_2 (Figure 6). The *Chart* worksheet (Figure 7) graphically displays peer tendon tensions to facilitate flagging potentially deficient tendons.

Bridge's Name

Segment	L meters	Strands	mu	S	Test	Mode 1	Mode 2
SWL	18.65	19	19.268	127275	1	8.8	17.6
					2	8.7	17.4
					3	8.8	17.5
					4	8.8	17.6
SWM	13.24	24	26.996	165700	1	12	24.1
					2	12.1	24.1
					3	12.1	24.2
					4	12.1	24.3
SWS	7.852	28	29.641	246875	1	20.7	42.3
					2	20.7	42.3
					3	20.8	42.5
					4	20.8	42.5
SEL	18.641	19	19.268	127275	1	8.8	17.5
					2	8.8	17.4
					3	8.8	17.5
					4	8.8	17.5
SEM	13.258	24	26.996	165700	1	12.1	24.3
					2	12.1	24.3
					3	12	24.5
					4	12.1	24.5
SES	7.879	28	29.641	246875	1	20.6	42.2
					2	20.6	42.2
					3	20.9	43
					4	20.9	43
NWL	18.581	19	19.268	127275	1	8.7	17.4
					2	8.6	17.4
					3	8.7	17.4
					4	8.7	17.5
NWM	13.215	24	26.996	165700	1	12	24
					2	12	24
					3	12	24
					4	12	24
NWS	7.911	28	29.641	246875	1	20	40.9
					2	20.2	40.9
					3	20.2	41.4
					4	20.2	41.4
NEL	18.554	19	19.268	127275	1	8.9	17.7
					2	8.9	17.7
					3	8.9	17.7
					4	8.9	17.7
NEM	13.23	24	26.996	165700	1	12	24
					2	12	24
					3	12.1	24.2
					4	12.1	24.2
NES	7.901	28	29.641	246875	1	20.3	41.6
					2	20.3	41.6
					3	20.5	41.9
					4	20.5	41.9
Segment	L meters	Strands	mu	S	Test	Mode 1	Mode 2

Figure 5. *Input* Worksheet

Results

Segment	Avg Tension (kN/strand)	Quality%
SWL	102.15	0.85
SWM	105.47	0.89
SWS	94.49	0.26
SEL	102.05	2.03
SEM	106.83	1.07
SES	95.83	1.41
NWL	99.56	0.31
NWM	103.55	1.14
NWS	90.04	0.02
NEL	103.58	1.72
NEM	104.72	1.12
NES	92.53	0.57

Figure 6. *Results* Worksheet

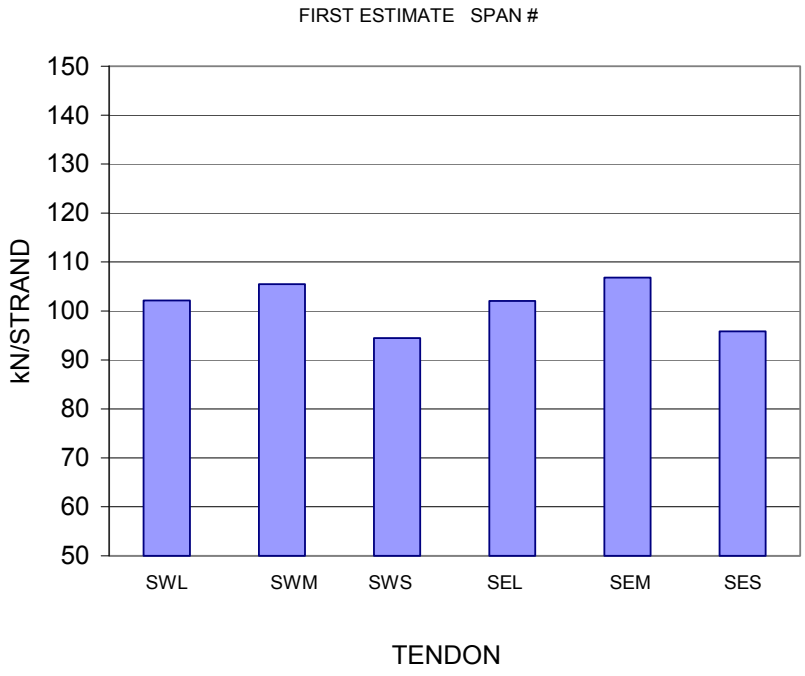

Figure 7. Output Field – Graphic

2.2 Mass per Unit Length (mu)

Prior to testing the operator can calculate the tendon mass per unit length (mu) from design or construction data by using the following equation.

$$mu(^{kg}/_{m}) = 0.1 \cdot [\pi[(d \cdot D - d^2)\rho_p + \frac{(D-2d)^2}{4}\rho_g] + N \cdot A_s \cdot (\rho_s - \rho_g)] \qquad [3]$$

mu = mass/length (kg/m)

D = outer tendon diameter (cm)

D = 8.92 (cm) (“3.51 in” diameter duct)

D = 11.45 (cm) (“4.51 in” diameter duct)

d = polyethylene duct wall thickness (cm)

d = 0.43 (cm) (“3.51 in” diameter duct)

d = 0.48 (cm) (“4.51 in” diameter duct)

N = # of strands

A_s = Area of one strand

A_s = 0.99 (cm²) (“½ in” strand diameter)

A_s = 1.44 (cm²) (“0.6 in” strand diameter)

ρ_p = polyethylene density = 1.0 (g/cm³)

ρ_g = hardened grout density = 1.84 (g/cm³)

ρ_s = steel density = 7.8 (g/cm³)

Example: Tendon of 10cm diameter, 0.6cm duct wall thickness, and 17 strands of type “½ in” diameter, m = 23.04 kg/m.

This value of mu is permanently input to the spreadsheet before conducting the tests. If different types of tendons are tested in the same bridge various values of mu are entered in designated cells.

2.3 Stiffness (S)

Geometric strand arrangement within the tendon cross section is non-uniform. The strands tend to crowd against the inside curvature of the tendon path as it is altered at end span and deviation blocks. As the steel strands contribute the most to the composite flexural stiffness, their non-isotropic distribution provides greater flexure stiffness in the horizontal than in the vertical direction. Thus, different sets of vibration frequencies may be expected for vibration deflection along those two directions [2, 12]. Averaging the two sets of frequencies (peak doublets) for each mode in the tension spreadsheet corrects to some extent the stiffness difference along the tendon. For an ideally bonded, close-packed arrangement of strands and grout the stiffness can be estimated by the following equation (4). This is a rough estimation, since strands distribution along the tendon are not always arranged as bonded and close-packed (Figure 8,9), in which case stiffness can be significantly larger as the strands' moment of inertia increase.

$$S(N.m^2) = \pi/6.4 \cdot [D^4 E_p + (D-2d)^4 (E_g - E_p) + \left(\frac{4 \cdot N \cdot A_s}{\pi}\right)^2 \cdot (E_s - E_g)] \qquad [4]$$

S = Tendon stiffness (N.m²)

D = outer tendon diameter (cm)

D = 8.92 (cm) ("3.51 in" diameter duct)

D = 11.45 (cm) (“4.51 in” diameter duct)

d = polyethylene duct wall thickness (cm)

d = 0.43 (cm) (“3.51 in” diameter duct)

d = 0.48 (cm) (“4.51 in” diameter duct)

N = # of strands

A_s = Area of one strand

A_s = 0.99 (cm²) (“½ in” strand diameter)

A_s = 1.44 (cm²) (“0.6 in” strand diameter)

E_p = polyethylene modulus of elasticity = 1.276 (GPa) [13]

E_g = hardened grout modulus of elasticity = 40 (GPa) [13]

E_s = steel modulus of elasticity = 206.8 (GPa) [13]

Example: A tendon with a “3.51in” diameter duct, and 19 strands of type “½ in” diameter; S = 120kN-m². The average of 19-strand tendon S values observed at Niles Channel Bridge shows order-of-magnitude values of 125kN-m² and 140kN-m² [12], in reasonable agreement with the above estimate.

This value of S is permanently input to the spreadsheet before conducting the tests. If different types of tendons are tested in the same bridge various values of S are entered in designated cells.

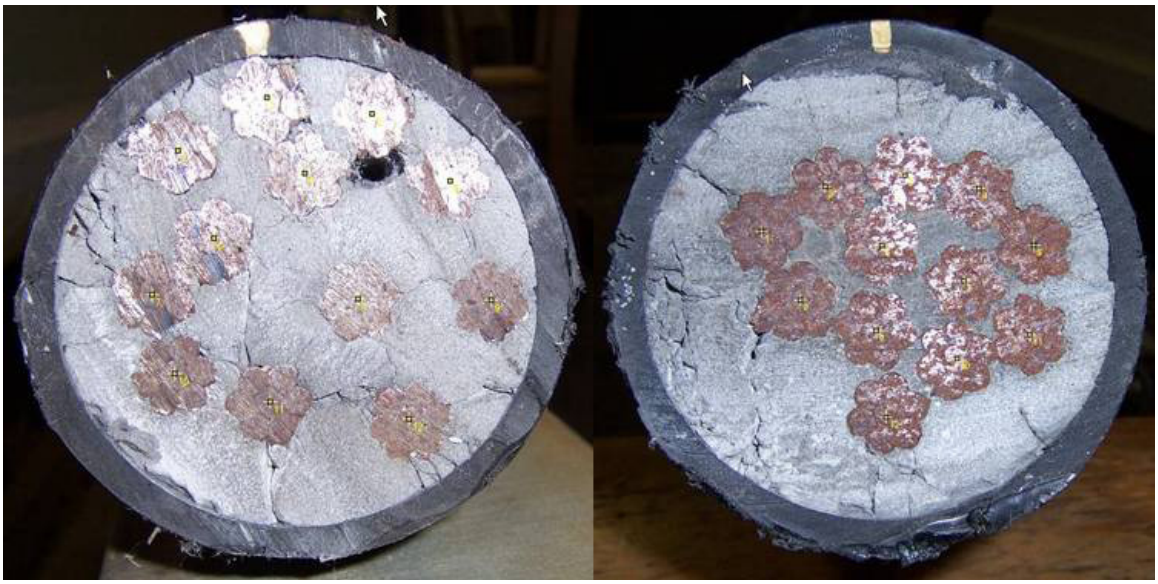

Figure 8. Strands Configuration, Tendon 13A Sloping Section [10]

Figure 9. Strands Configuration; Tendon 13A, Horizontal Section [10]

2.4 Tendon Frequencies

This section addresses different methods of acquiring the first two vibration mode frequencies, requiring only one operator. One of these methods uses the built-in sound card of a computer, another method uses a data-acquisition-board (DAB), and a third method uses a microphone recorder.

Programs were developed in Lab-VIEW™ for each of those methods to analyze and display the processed accelerometer output. Other components used in the data acquisition process are coaxial cables, accelerometer Model PCB 338B34, and signal conditioning amplifier ICP-Model 480E09; all of which are common for the three acquisition methods.

2.4.1 Built-in Sound Card Method

The method using the built-in sound card is based on a Dell Latitude 840 computer operating Windows XP. A Lab VIEW™-based program *Analyzer-M* was developed to manage data acquisition through the Line In port of the 16-bit resolution computer sound card. The program *Analyzer-M* has three Levels (1,2, and 3). Levels 1 and 2 are both graphical interfaces that display screens information. Level 3 is involved in data acquisition, data processing, and graphics.

On Level 1 the first interface screen appears (Figure 10), which displays the University South Florida logo and requests the user to press “F2”. When the user presses the “F2” key, the screen front panel for Level 1 closes and the program opens Level 2. The block diagram of Level 1 is in Appendix 1.

The Level 2 interface displays a screen with copyright information (Figure 11). When the user accepts the conditions of use, the Level 2 modulus opens Level 3, otherwise the screen closes and the program stops . The block diagram of Level 2 is in Appendix 2.

Figure 10. Level 1 Front Panel

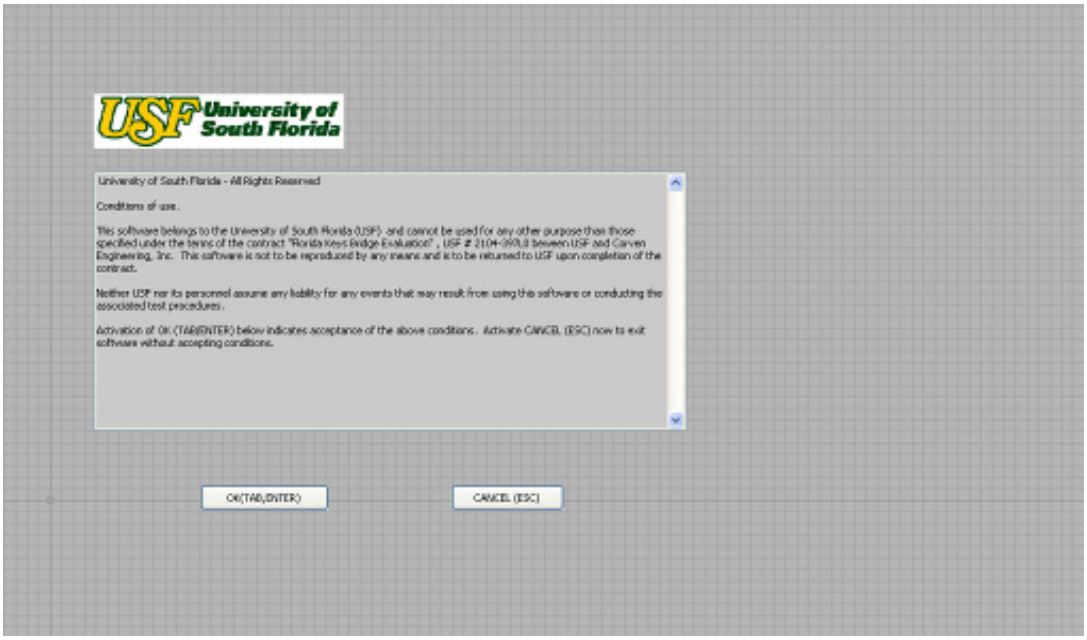

Figure 11. Level 2 Front Panel

Level 3 is the main program which controls data acquisition, creates a *.wav* file of the acquired data, converts the processed accelerometer signal from time domain to frequency domain, and graphically displays both domains. The Level 3 block diagram consists of a sequence structure with two main subdiagrams (0,1).

Subdiagram 0 (Appendix 3) has two sequence structures and one case structure. The first sequence structure specifies the file size in bytes, without the header, to be recorded (2^{18}) and the path to create the file. The number of samples to collect (2^{17}) is half the file size without the header since each sample requires 2 bytes. The time for acquiring the data is 11.8886s for a sampling frequency of 11,025Hz, and the frequency resolution is 0.084Hz.

The second sequence structure contains a *while loop*. The *while loop* terminates if Start or Record is activated, otherwise the *while loop* continues to iterate. The Start key F1 activates the case structure. The case structure contains two *while* loops, the first of which is used to configure the sound input device (computer sound card) with the chosen options of 11,025Hz sampling, monaural sound quality, 16 bits per sample, and 8192 buffer size . The second *while* loop reads data from the buffer and displays it in a chart continuously (Figure 12) until the stop key (F2) is pressed. This function is used to adjust hammer impact.

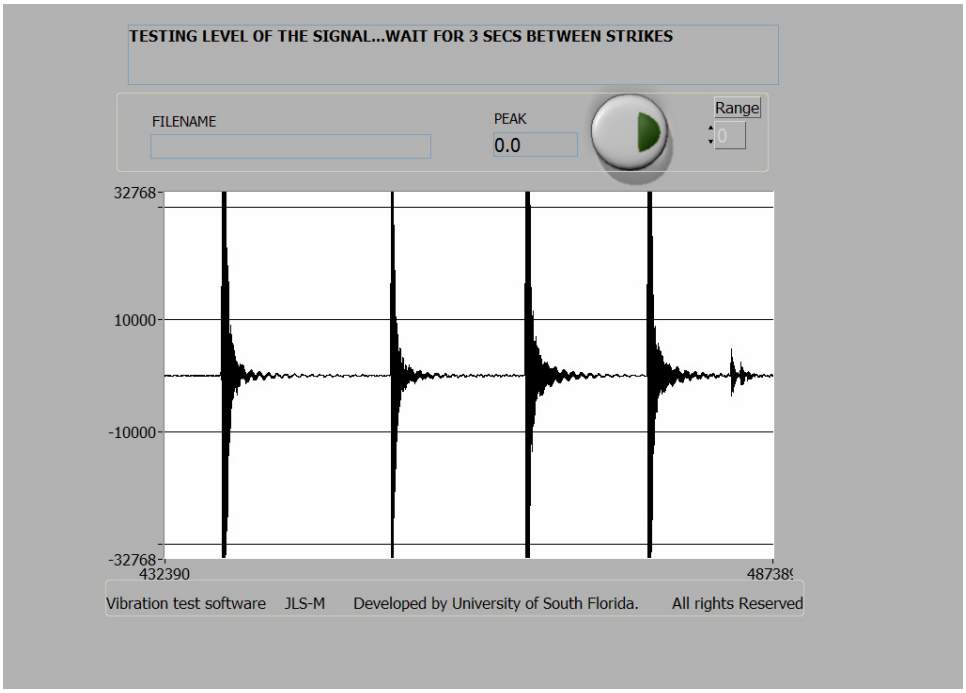

Figure 12. Level 3, Continuous Signal Display

Subdiagram 1 (Appendix 4) is activated when the stop key F2 or the start key F3 is pressed, prompting the user to enter a name for the *.wav* file to be recorded (Figure 13). Subdiagram 1 tasks are acquiring, recording, analyzing, and displaying the data. The first sequence structured deals with initial preparations of acquiring and recording the data such naming the file to be recorded and sound input configuration as subdiagram 0. Once the file is named and accepted the next *while* loop is activated displaying on the front panel in the info box "Hit F3 or the push button to begin recording" (Figure 14). The push button can be actuated by using a wireless presentation remote control such as Targus™ Model PAUM30, which has a distance range of up to 50 feet and thus permits the operator to hit the tendon at the required time without the need of an assistant. This *while loop* is followed by the module *SI Start* which starts the data acquisition once the start button is actuated.

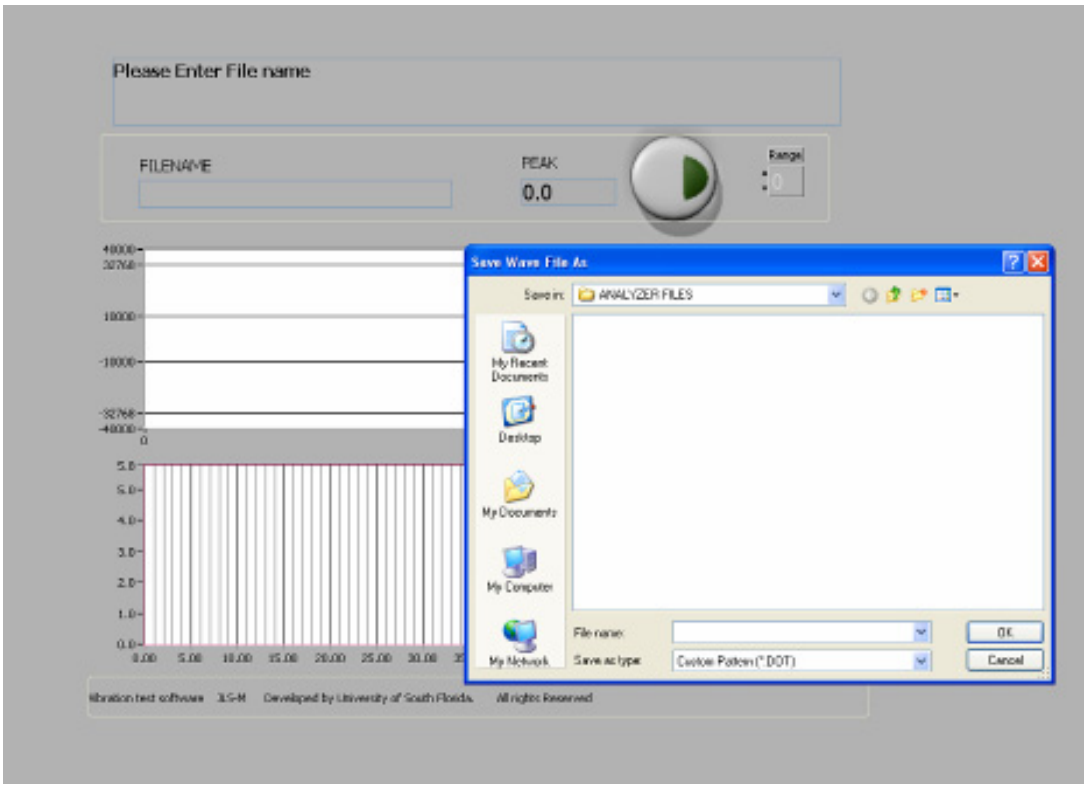

Figure 13. Level 3, File Name Prompt

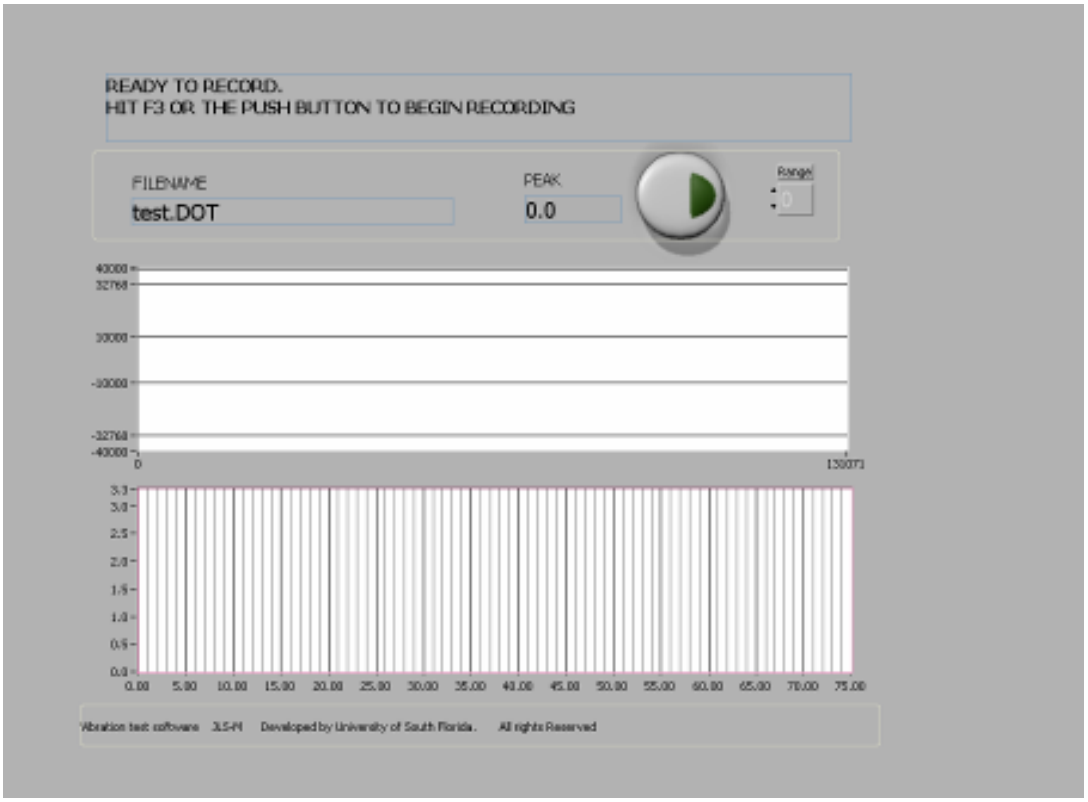

Figure 14. Level 3, Ready to Record Prompt

The next frame is a sequence structure in which the data from the buffer is read, producing a one-dimensional array of 16-bit intergers. A string “TEST IN PROGRESS” is assigned to info to be displayed on the front panel (Figure 15) while the data is being collected for the time assigned in subdiagram 0.

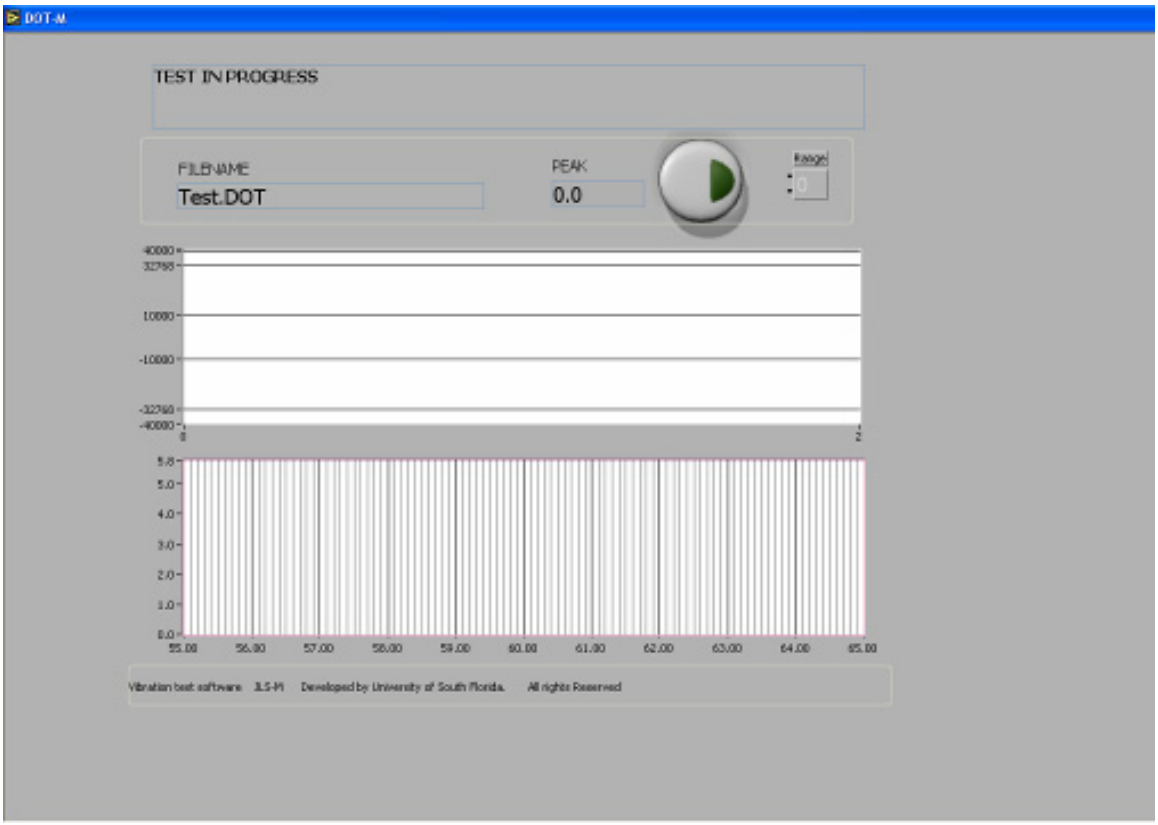

Figure 15. Level 3, Test in Progress Prompt

In the next sequence structure the one dimensional array containing the time domain signal is passed as input to module *F(x)* which computes the real Fast Fourier Transform. The resulting complex number is normalized with respect to the array size and separated into its polar components. The frequency magnitude is displayed on the front panel at a frequency spacing or resolution of ~0.084Hz (Figure 16). The time domain signal is also displayed beside the frequency domain graph for the purpose of quality control. If the data are

acceptable then the one-dimensional array containing the time domain signal is saved as a 257kB 16bit wave file.

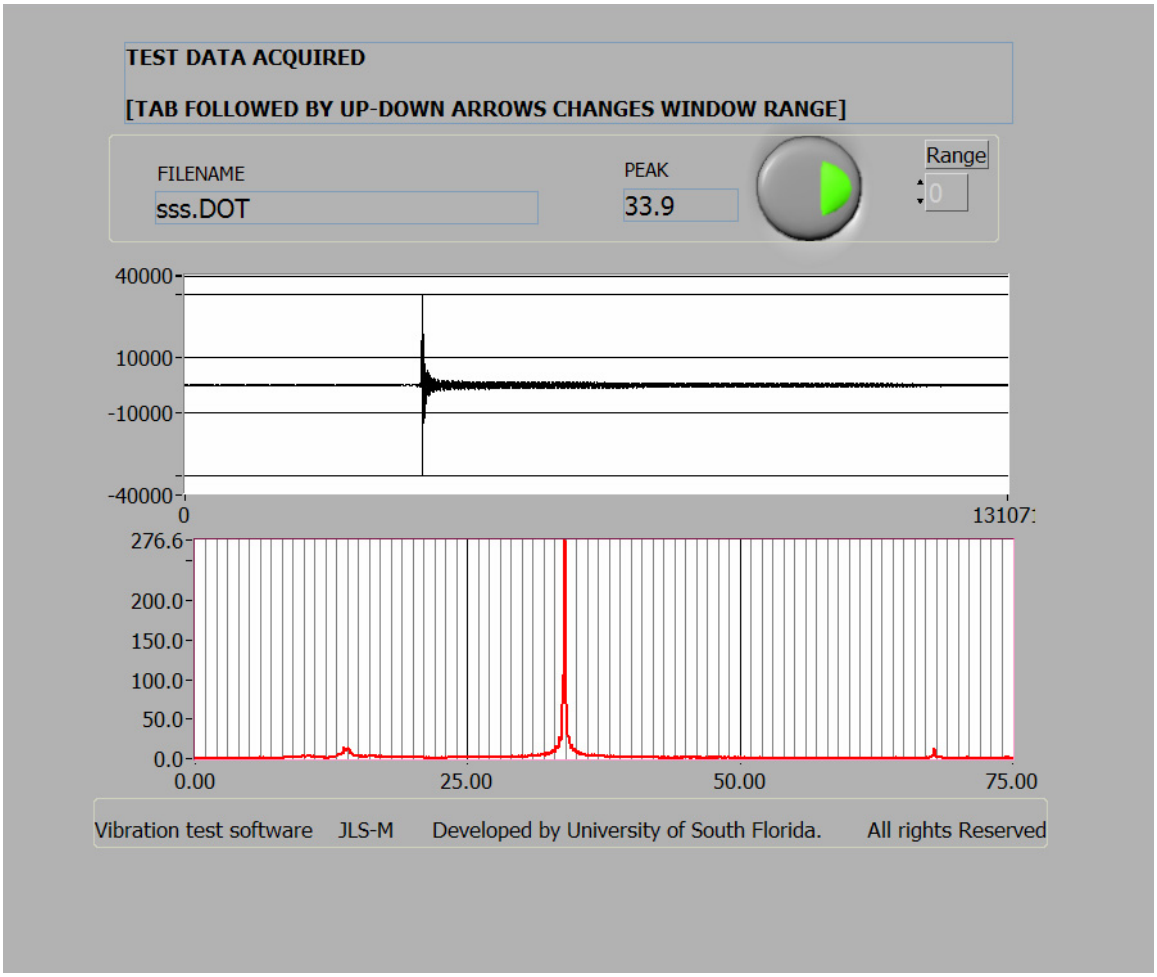

Figure 16. Time and Frequency Domain Graphs

The *Analyzer-M* program was prepared as an executable file. Also, an executable program called *WavePlayer-Mono* (Figure 17) was made to retrieve the data from the wave files that were saved during the vibration tests; its block diagram is in appendix 5. Appendix 6 includes the program installation guide, the Step by Step Procedure to operate equipment and *Analyzer-M* software, and tendon preparation.

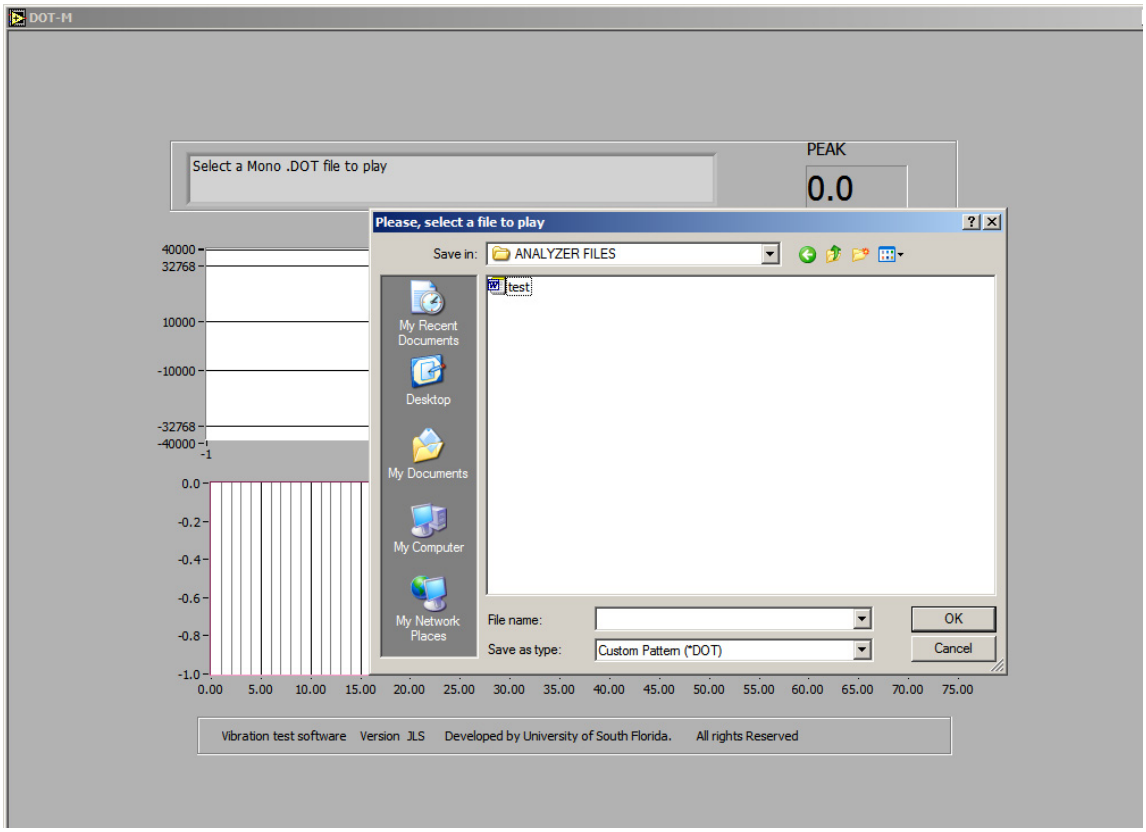

Figure 17. *WavePlayer-Mono* Front Panel

2.4.2 Data Acquisition Board Method

The data acquisition board (DAB) method uses a LabVIEW-based program (*ANALYZER-DAB*) to acquire and analyze data from a 12-bit resolution NI USB-6008 data acquisition board. The program *ANALYZER-DAB* is similar to the program *ANALYZER-M* but several key differences exist in level 3 of the program (Appendix 7). Data acquisition in *ANALYZER-DAB* is controlled by a NI-DAQmx Base 2.0 driver instead of the Sound Input VI used in the *ANALYZER-M*.

The number of samples collected by *ANALYZER-DAB* is 2^{13} and the sampling frequency is 800Hz, therefore it has a frequency resolution of ~0.0977Hz. Also, the collected data are saved as a binary Single Precision Floats (SGL) file which requires 4 bytes per data sample, which is 32kb total file

size. An example of *ANALYZER-DAB* data collection quality is in Figure 18. The installation guide is in Appendix 8. An executable program called *WavePlayer-DAB* was made like the *WavePlayer-MON* to retrieve the data from the SGL files that were saved during the vibration tests; the block diagram of *WavePlayer-DAB* is in Appendix 9.

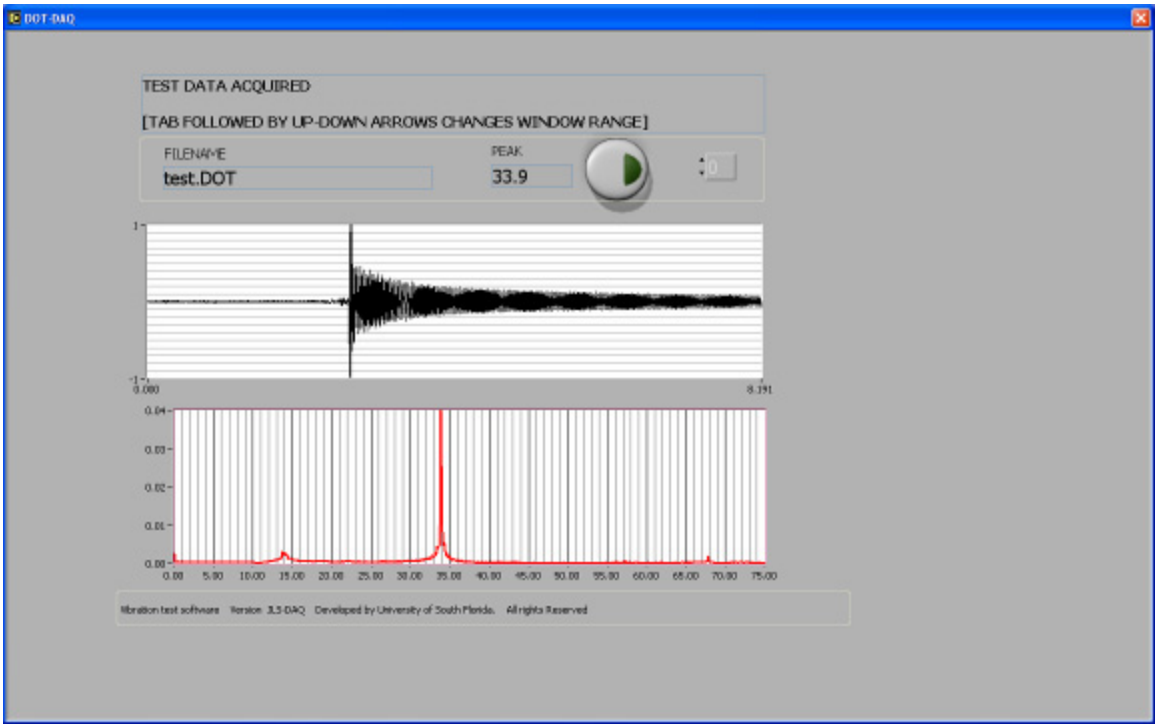

Figure 18. Front Panel *Analyzer-DAB*

2.4.3 Digital Recorder Microphone Method

Another method of acquiring the first fundamental tendon frequencies is by using a digital recorder microphone. Accelerometer, cables, and signal conditioner set up is like that of the previous methods but with the adapter cable coming from the signal conditioner connected to the microphone line input (mic). The digital microphone recorder to be used is a SONY™ ICD-P210. The SONY™ ICD-P210 allows you to save the recorder files in a PC as a 16bit 11000kHz

monaural wave file. The recording files are also easy to identify since their initial assigned names correspond to the microphone folder used, their recording position with respect to the other files, and the date and time of the recording. The recording files can be analyzed by using a Lab VIEW program *Wave Player Micro* which works in a similar way as *WavePlayer-MON*. The block diagram of *Wave Player Micro* is in Appendix 10. A sample of data quality recording and analysis of the microphone method is in Figure19 with microphone sensitivity set to low and recording mode set to HQ.

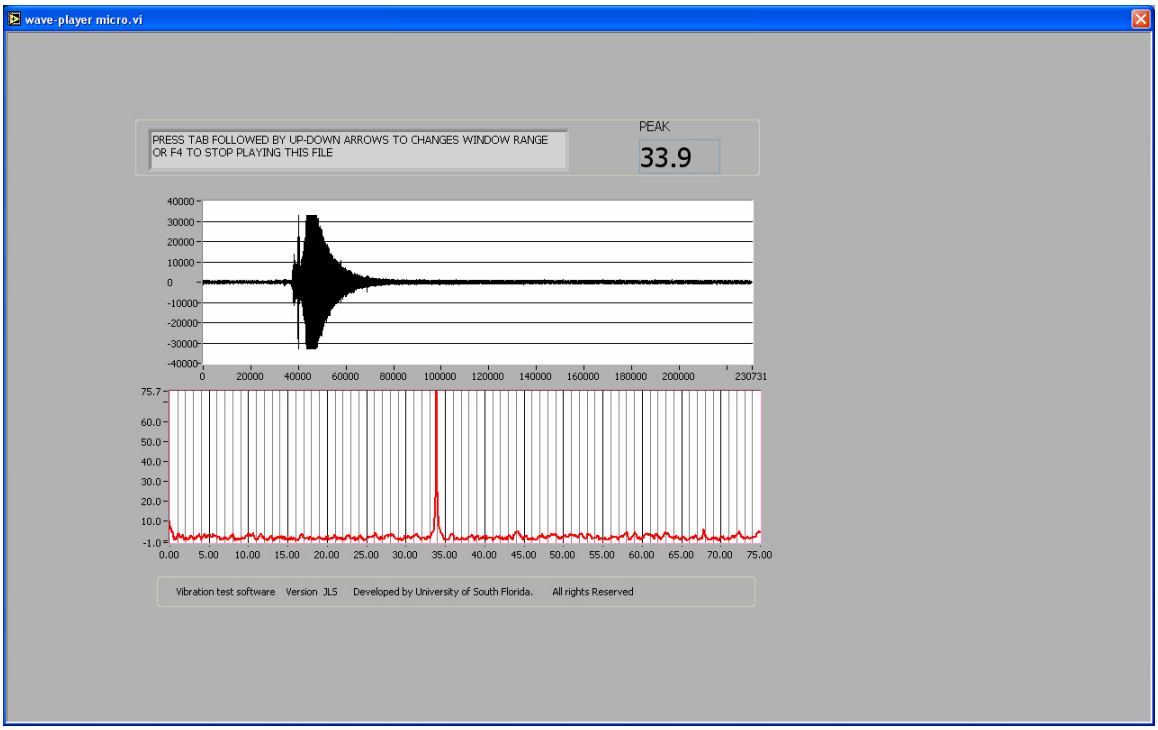

Figure 19. *Wave Player Micro* Front Panel

Chapter 3

Practical Vibration Evaluation Validation*

The practical vibration evaluation explained in chapter 2 to detect tendon tension was validated on nearly full-scale tendons constructed at the FDOT Structures Laboratory as part of an ongoing parallel investigation [10].

A Tendon Test Facility (TTF) was constructed at the FDOT Structures Laboratory (FSL) in Tallahassee, FL. for large-scale model validation tests. The TTF had one fixed reinforced concrete anchor block (South end) and one movable anchor block (North end) with horizontal anchors approximately 9m away. The anchor assemblies were Type E manufactured by VSL. The fixed block had provisions for horizontal anchors at the same elevation as those in the movable block, allowing for straight horizontal tendons with a free length of ~9m (Figure 20). Tension was applied by displacing the movable block by the required amount with hydraulic jacks and than placing stops between the block and the end of the frame. Load cells monitored the tensioning force at the movable block end allowing for precise computation of the force. Two duplicate full length horizontal tendons (0A and 0B) were constructed. Both tendons had twelve one-

* Parts of the work in this chapter have appeared in A. Sagüés, T. Eason, C. Cotrim and J. Lopez-Sabando, "Validation and Practical Procedure for Vibrational Evaluation of Tendons", Project No. BC 353#44, 158 pages, Draft Final Report to Florida Department of Transportation, University of South Florida, Tampa, Fl, December, 2007 [10].

half in low-relaxation seven wire strands per ASTM A416 grade 1860 supplied by VSL.

Figure 20. Tendon Test Facility

The design stretching stress capability was 1800kN, corresponding to 80 % of the Guaranteed Ultimate Tensile Strength (GUTS) but actual stretching stresses were typically 1500kN, (67% GUTS). The strands were contained in a high density polyethylene (HDPE) duct type DR17 3 in NPS (8.9cm outer diameter with a wall thickness of 0.4cm). Galvanized steel pipes 7.62cm internal diameter and 0.48cm wall thickness emerged from the end and deviation blocks and served as attachment points for the polymer duct by means of an 8.9cm inner diameter 15.24cm long Neoprene duct coupler. After stretching the

tendons, they were grouted with QPL-938 grout manufactured by Masters Builders using a colloidal pump. There was no indication of grout voids in any of the tendons constructed. Further details are given in [10].

After a grout setting period of 7 days minimum, vibration testing was conducted on the free length(s) of the tendon. The vibration tests consisted of basic tests as explained in chapter 2, in which the tendon was impacted at a point 1/6 of the free length away from one of the blocks at either end of the free length of the tendon, and the accelerometer was placed at 1/3 of the distance from the same or opposite end of the tendon (Figure 21).

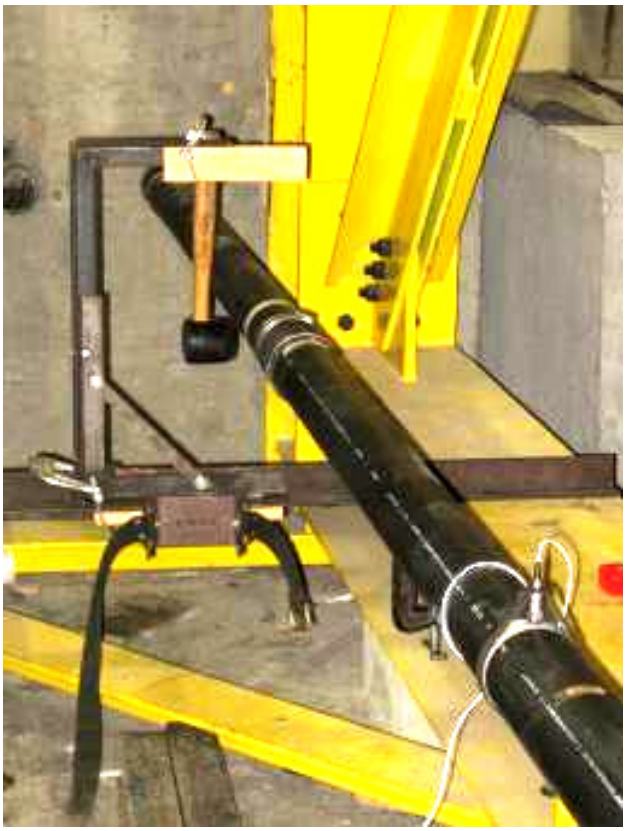

Figure 21. Tendon Test Set Up[10]

Tendon impacts were conducted with a rubber hammer with a total mass of 611 grams. The accelerometer, Model 338B34 by PCB Piezotronics with a

sensitivity of 10.00 mV/g, was placed with its sensing axis attached to 45° from horizontal side of the tendon. A flexible coaxial wire ~0.25cm diameter connected the accelerometer to a Model 480E09 signal conditioning unit by PCB Piezotronics, with a voltage gain set to 10x, resulting in a signal amplitude upon impact typically < 0.6V . The signal was acquired using the Sound Card line input of a Model Latitude C840 computer by Dell and controlled by a LabVIEW™ program similar to *Analyzer-M* which was described in Chapter 2.

Input tendon parameters (Table 1) were obtained as explained in chapter 2. Tendon tension approximation results (Table 2) indicates a small difference with the load cells (less than 4%) for both tendons (0A, 0B) for the experiments chosen for analysis. This result is consistent with the general level of agreement between vibrational and load cell tension estimates obtained in a broader investigation in progress [10], although results from particular test sequences may differ

.

Table 1. Tendon (0A, 0B) Input Parameters

Segment	L meters	Strands	mu	S	Test	Mode 1	Mode 2	Test #
0B-South	9.279	12	17.5759	102477	1	15.65	32.05	0BBASSC
					2	15.65	32.05	0BBASSD
					3	15.65	31.88	0BBATSA
					4	15.65	31.88	0BBATSB
0B-North	9.279	12	17.5759	102477	1	15.65	32.05	0BBASNA
					2	15.65	32.05	0BBASNB
					3	15.65	31.88	0BBATNA
					4	15.65	31.88	0BBATNB
0A-South	9.319	12	17.5759	102477	1	16.16	32.8	0ABASSA
					2	16.16	32.8	0ABASSB
					3	16.35	32.8	0ABATSA
					4	16.41	32.8	0ABATSB
0A-North	9.319	12	17.5759	102477	1	16.24	32.8	0ABNASA
					2	16.24	32.8	0ABNASB
					3	16.24	32.8	0ABNATA
					4	16.24	32.8	0ABNATA

Table 2. Tendon (0A, 0B) Results

Results				
Segment	Avg Tension (kN/strand)	Quality%	Load Cell (kN/strand)	% Difference
0B-South	109.17	1.86	113.14	3.6
0B-North	109.17	1.86	113.2	3.6
0A-South	118.30	0.77	122.28	3.3
0A-North	118.07	0.37	121.8	3.1

Chapter 4

Early Warning Corrosion Probes Methodology*

4.1 Test Environments

Controlled humidity chambers were constructed using lidded glass fish tanks. The dimensions of the glass chamber were 51x31x26cm, total volume of 39000cc.

A 95% RH environment was implemented by adding 266gr of NaCl (common salt) to 3 liters of distilled water at the bottom of the chamber. The concentration of NaCl to water was calculated using equation (5) derived by Cinkotai (1971) [15]. Where Cs=ms/(ms+mw), and ms, mw are the mass of solute and water, respectively.

$$RH = 1 - 0.4867 \times Cs - 1.55 \times Cs^2 \qquad (5)$$

This steady state RH should be stable over the experiment's length even if the lid of the chamber is removed for short periods of time. The mass of water vapor present in the air inside the chamber at 95% RH and 23° Celsius was calculated to be 0.81g [16]. The latter is an insignificant amount compared with the 3000g total mass of water in the chamber so lost water can be replenished by

* Parts of the work in this chapter have appeared in L. Taveira, A. Sagüés, J.Lopez-Sabando, and B. Joseph, "Detection of Corrosion of Post-Tensioned Strands in Grouted Assemblies", Project No. BD544-08, 71 pages, Final Report to Florida Department of Transportation, University of South Florida, Tampa, Fl, October 31, 2007 [14].

evaporation without substantial change in the solution composition. The above estimation is based on the following equations:

$$m = \frac{V}{v_{vapor}} \qquad v_{vapor} = \frac{R \times T}{P_v} \qquad P_v = RH \times P_g \qquad (6)$$

Where m is the mass of water vapor, V is the volume of air, v_{vapor} is the saturated vapor specific volume, R is the water gas constant (461.5J/(kg K), T is the temperature in Kelvin, P_v is the partial pressure of water vapor, RH is the relative humidity, and P_g is the saturated water pressure at 23° Celsius (2.82kPa).

The 75% relative humidity was accomplished by introducing inside the chamber 1.0 liter of water saturated with sodium chloride (NaCl) [17].

4.2 Electrochemical Probes

An atmospheric corrosion electrochemical test array was designed and constructed using a methodology inspired by that of Mansfeld and Kenkel [18]. The probes consist of two 5mm diameter steel wires extracted from an ASTM A416M-98 high strength strand. The wires were 0.508cm diameter and 10.5cm long. Both wires were attached parallel to each other, with a gap between them of 0.6mm. Plastic spacers at the end of the probes kept the two wires electronically isolated from each other. A thin, stainless steel wire <1mm diameter was spot welded to the end of the each wire probe to permit external measurements. Two probes with the afore mentioned characteristics were made and immersed in fluid, 0.42 water/cement ratio grout (type 1 Portland cement) and then lifted, forming upon curing a thin grout layer on the surface and across the gap. The length of the probes covered with grout was 9.0cm, with the

extremes of the wires uncovered by grout [Figures 22, 23]. Another two probes were made three days later with similar characteristics but with a gap between the wires of 1.0 mm, and a thicker layer of grout covering the wires.

The grouted probes were cured in a 100% RH glass chamber for a day and inserted afterwards into the 95% RH chamber at a temperature of 23±2°C. Holes were made and then caulked in the lid of the chamber for the stainless steel wires attached to the probes to allow external measurements of the probes without disturbing the corroding conditions inside the chamber.

Figure 22. Electrochemical Probe Before Grouting

Figure 23. Grouted Electrochemical Probe

4.3. Electrical Resistance Probes

The Electrical Resistance (ER) method is another corrosion monitoring approach. ER probes use the simple principle of an increase in electrical resistance produced by a decrease in the section thickness of the metal as it corrodes. Two different ER probes were developed in this study. The first

generation ER probe contained two identical plain low carbon steel rebar tie wires 120cm long and 1.60mm diameter, in the “as-received” condition (dark mill scale on the metal surface). One of the wires, the working element, was exposed to the corrosive atmosphere inside the chamber. The other, the reference element, was protected by sealing it inside the probe body (pvc pipe) from the corrosive medium. The covered wire provided a reference for evaluating changes in the uncovered wire and also served to compensate for the effects of temperature changes on resistance (Figure 24). The latter can be an important source of error, as the resistivity of steel varies roughly by 0.3% for every 1°C change near ambient temperature [19].

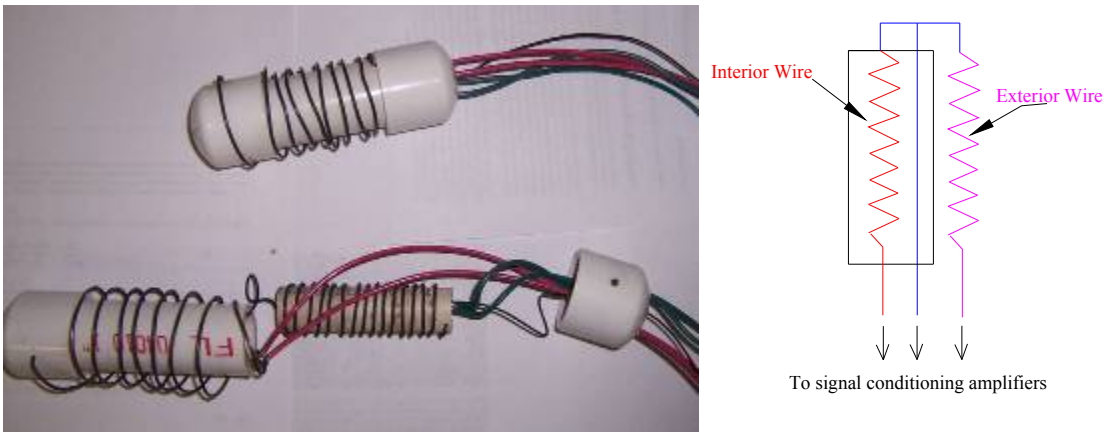

Figure 24. ER Probe Interior Design

The corrosion rate ($Corr_{rate}$) of ER probes can be determined by the radius change of the corroding wire (Δr) over its exposed time in days (t) and multiplied by 365(days/year):

$$Corr_{rate} = \Delta r \cdot 365/t \qquad (7)$$

A 60Hz AC, 80mA excitation current was created with a 21V output transformer in series with a 260Ω resistor and the probe. The resistance of each wire was ~0.8Ω, resulting on only ~10mW total probe power dissipation, a negligible amount of heat production rate considering the dimensions of the probe. Two 100X amplifiers and a 0.1mV A.C resolution multimeter were used to measure the potential drop across wires. The sensitivity of this probe was calculated to be 1/1428 parts (0.6μm) of the corroding wire radius. The above estimation is based on the following equations:

$$\text{Probe sensitivity} = r_{corr}/r_o \tag{8a}$$

$$r_{corr} = r_o - r_f \tag{8b}$$

$$E = I \cdot L \cdot \rho \cdot \left[\frac{1}{\left(\pi \cdot r_f^{\,2}\right)} - \frac{1}{\left(\pi \cdot r_o^{\,2}\right)} \right] \tag{8c}$$

where E is the minimum drop in potential that can be detected (0.05mV), I is the current in the circuit, L is the length of the wires, ρ is the resistivity of steel, r_o is the original radius, r_f is the final radius after corroding, and r_{corr} is the change in radius due to corrosion that can be detected.

Two ER probes with the above mentioned characteristics were tested only in the low RH (75%) insulated glass chamber at a temperature of 23°±2°C, mainly to check operation at the electronic signal acquisition system as corrosion rates were very low in that environment.

A second generation of ER probes was later designed to simplify measurements and improve sensitivity. A potentiometer was added to the earlier design to create a bridge as a way of measuring the change in the resistance of the corroding wire [Figure 25]. The bridge was initially balanced (V_{out} = 0) by adjusting the potentiometer, so the resistance ratio of the probe wires was the same as that of the potentiometer. The initial resistance ratio, R_{out} / R_{in} (see Figure 25), of the probe was nearly 1. From that initial condition, when the wire corrodes the resistance increases by a factor of (1+P). P is a function of the input voltage (V_{in}) and output voltage (V_{out}), according with the relationship below (equation developed in appendix 11).

$$P = \frac{4 \cdot V_{out}}{V_{in} - 2 \cdot V_{out}} \qquad (9)$$

The corroding wire radius (r_{corr}) can be calculated by the following equation:

$$r_{corr} = r_o \cdot \sqrt{1/(1+P)} \qquad (10)$$

Where r_o is the original radius of the wire, Equation (10) is derived in Appendix 12.

For a constant supply voltage from the transformer, the input voltage shouldn't change over time since the increase in the resistance of the corroding wire is negligible in comparison with the resistance of the whole assembly. If the input voltage is known a priori, P can be calculated by just measuring the bridge output voltage.

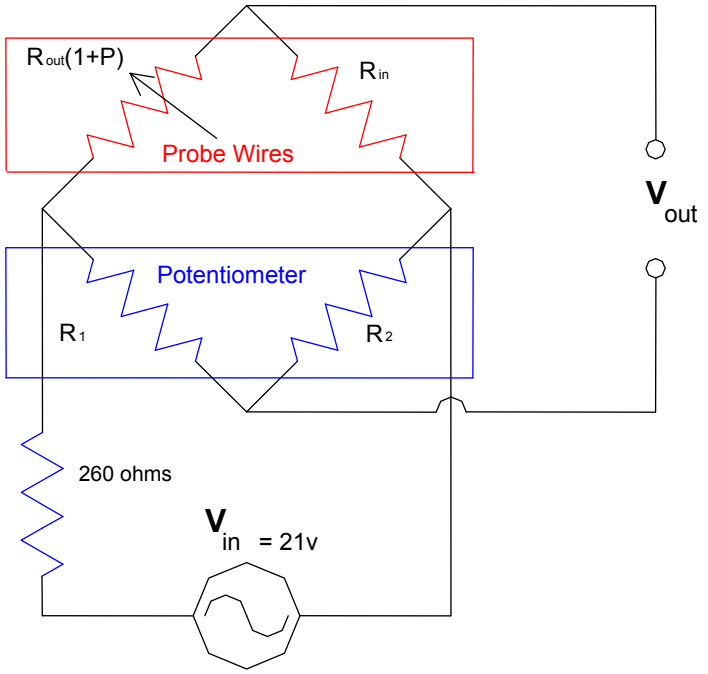

I.C.

$$@\, V_{out} = 0 \Rightarrow P = 0$$

$$\frac{R_{out}}{R_{in}} = \frac{R_1}{R_2} \approx 1$$

$$P = \frac{4 \cdot V_{out}}{V_{in} - 2 \cdot V_{out}}$$

Figure 25. Schematic of ER Probe.
A 0.03μF capacitor was placed across R2 to minimize phase shift.

Since the input voltage is not constant, because of fluctuation in the power grid, input and output voltages need to be measured at the same time for an accurate calculation of P. To measure simultaneously the input and output AC voltage across the bridge, a Lab View™ program *P-Measurements* was developed. Other components of the data acquisition system are: a data acquisition board (DAB) and a 100-gain amplifier to condition the signal between the bridge voltage divider and the acquisition board.

The block diagram developed to measure the bridge input and output voltage is shown in the Appendix 13. The *P-Measurements* program consists of three parts, the first part configures the DAB and converts binary counts to engineering units, the second part performs voltage measurements, and the third

part analyzes the data and calculates P. The front panel of the *P-Measurements* program (Figure 26) lets you choose the voltage range and displays the RMS, average voltage peaks and P.

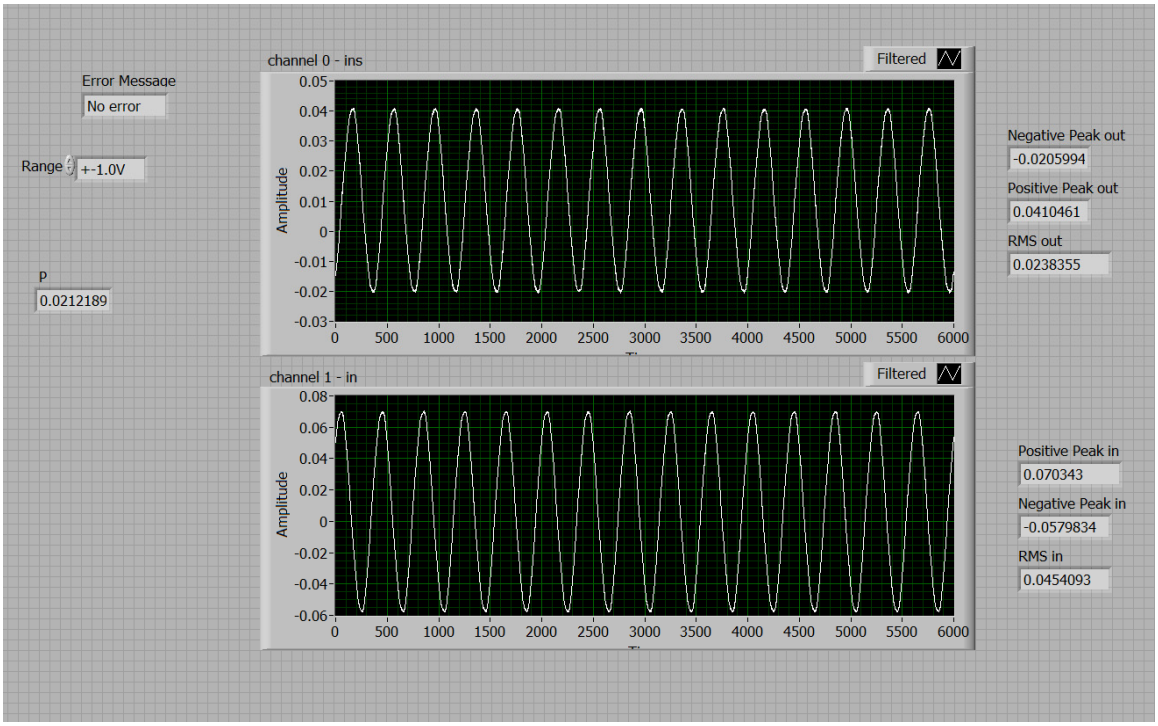

Figure 26. Front Panel of The *P-Measurements* Program

The data acquisition board used for this task was an USB-1608FS from Measurement Computing, with a 16-bit precision (0.03mV resolution error). The sampling rate was set to 24000Hz and the number of samples was 6000.

Another improvement was placing a ~0.03μF capacitor (value selected by trial and error) across the potentiometer arm R2 until there was nearly zero phase shift across the V_{out} terminals. Without that capacitor a small phase shift, due to the mutual inductance of the internal and external coiled wires and the magnetic properties of steel, was present which prevented obtaining a sharp null during initial adjustment. The probes were made with counter turn coils to

minimize induction effects, but the capacitor was still needed for improved compensation. The resulting system imbalance sensitivity was ~0.005mV, corresponding to a detectable change of corroding wire radius in the order of 1 part in 4000 (0.2μm).

Four of this second generation ER probes were made and placed in the 95% RH glass chamber described earlier for the Electochemical probes. Two of the ER probes were dipped in grout as described earlier for the Electrochemical probes.

4.4 Probe Materials Characterization

Metallographic examination of the strand wires (ASTM A416) and the steel tie wires cross sections was conducted to reveal and compare their microstructures. The specimens were mounted metallographically, ground, fine polished to a 0.05μm alumina suspension finish, and etched with 2% nital solution. The micrographs in Figure 27 reveal the fine eutectoid pearlitic microstructure of the high strength PT wires, and the nearly all ferrite (low carbon) microstructure of the softer steel tie wires These structures were as expected and the tests served to confirm the identity of the probe materials.

4.5 Gravimetric Measurements

Gravimetric measurements were conducted to compare against the results of the Electrochemical and ER probes to verify their reliability. The weight loss experiments were conducted with bare and dip-grouted wires. The tests included 20 helically shaped outer wires extracted from actual 7-wire steel strands from the same stock used for the Electrochemical probes, and 8 low

carbon steel tie wires with mill scale as used for the ER probes. The specimens grouted by dipping were processed as for the other tests, and cured for 2 days inside a 100% RH chamber before introducing in the 95% RH chamber.

The helically shaped wires were 0.508cm in diameter and 35cm long; the steel tie wires were 0.16cm in diameter and 46cm long. Before and after the test, the strand and tie wire specimens were cleaned per ASTM G1 and then weighed to 10^{-3} and 10^{-5} grams precision respectively.

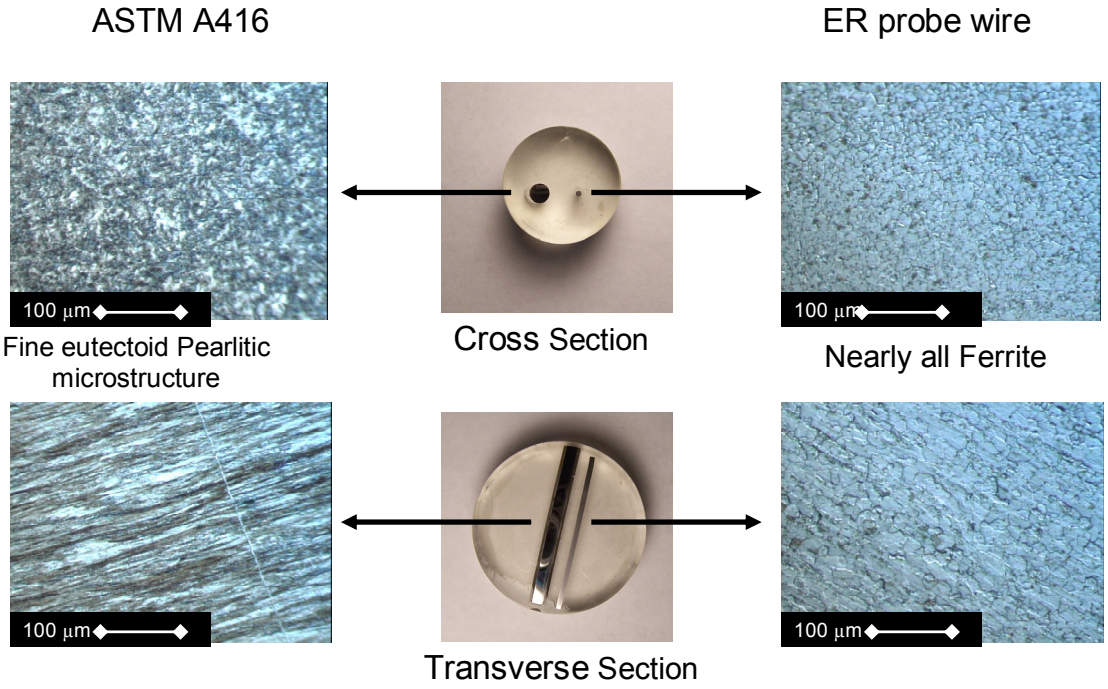

Microstructure of High-Strength PT Wire (Eutectoid) and Steel Tie Wire ER Probe Wire (Low carbon steel).

Figure 27. Probe Materials Characterization

Chapter 5

Early Warning Corrosion Probes Results and Discussion*

5.1 Electrochemical Probes

The Electrochemical probe system, illustrated in cross section in Figure 28 can be approximated as behaving as the equivalent circuit in Figure 29.

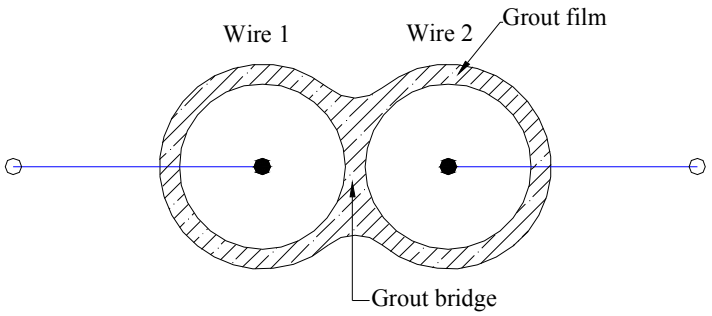

Figure 28. Schematic of Electrochemical Probe Cross-Section

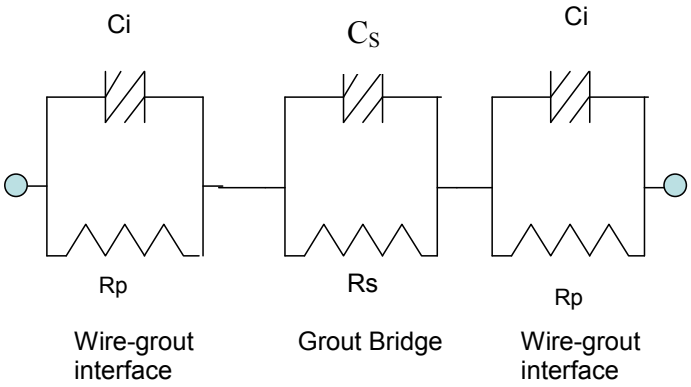

Figure 29. Electrochemical Probe Equivalent Circuit

* Parts of the work in this chapter have appeared in L. Taveira, A. Sagüés, J.Lopez-Sabando, and B. Joseph, "Detection of Corrosion of Post-Tensioned Strands in Grouted Assemblies", Project No. BD544-08, 71 pages, Final Report to Florida Department of Transportation, University of South Florida, Tampa, Fl, October 31, 2007.[14].

C_i are constant phase angle elements, of admittance $Y = Y_{0i} (j2\pi f)^n$, representing the interfacial capacitance of the metal-grout interface of each wire (Y_{0i} and n are the constant phase angle element parameters [20],[21]), R_P is the polarization resistance of that interface, and C_S and R_S represent, respectively, the dielectric capacitance and ohmic resistance of the grout bridge, the former of which was found to be not negligible for the system and frequency range examined. For simplicity the two metal-grout interfaces were assumed to behave similarly. Thus, the measured impedance could be represented by a single C_m-R_m parallel combination (where $R_m=2R_P$, and C_m is a constant phase element with parameters $Y_{0m}=Y_{0i}/2$ and n) in series with the C_S - R_S parallel combination as shown in Figure 30.

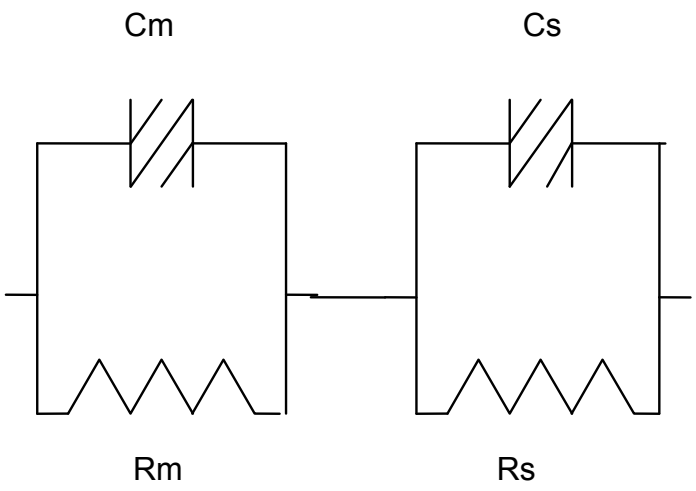

Figure 30. Simplified Equivalent Circuit for the Electrochemical Probe

EIS measurements of the Electrochemical probes were carried out at the open circuit potential (OCP) with 10mV RMS amplitude in the frequency range

from 100kHz to 10mHz, to determine polarization resistance and corrosion currents of the probes. The experiments were performed periodically during 264 days. Both experiments were performed using Parstat™ 2263 from Princeton Applied Research, Oak Ridge, U.S.A. and Gamry™ PCI-4 from Gamry Instruments, Warminster, U.S.A. potentiostats. The electrochemical parameters were estimated by using the programs Gamry Echem Analyst™ from Gamry Instruments, Warminster, U.S.A or Zview2™ from Scribner Associates, Inc., Southern Pines, U.S.A. The reference and counter-electrode were connected to one wire of the probe and the working electrode to the other one, so the impedance measured corresponded to the wire-grout-wire series combination. Other records were temperature and relative humidity inside the chamber.

Examples of EIS results for 1mm and 0.6mm gap electrochemical probes exposed to the 95% RH environment are shown in Figure 31. Two depressed semicircles can be distinguished. The first semicircle corresponds to R_S and C_S, while the second is related to R_m and C_m as discussed above and illustrated in Figure 32. Because the grout resistance-capacitance component has a very short time constant, the analysis to determine the circuit parameters relevant to the polarization of the corrosion reactions was limited to the frequency interval 10mHz to 1Hz, where the effect of C_s is small. Thus, the equivalent circuit used for the actual EIS data analysis had R_S, R_m and C_m as the only fit parameters and the results in the following are discussed in terms of the parameter values for one of the interfaces.

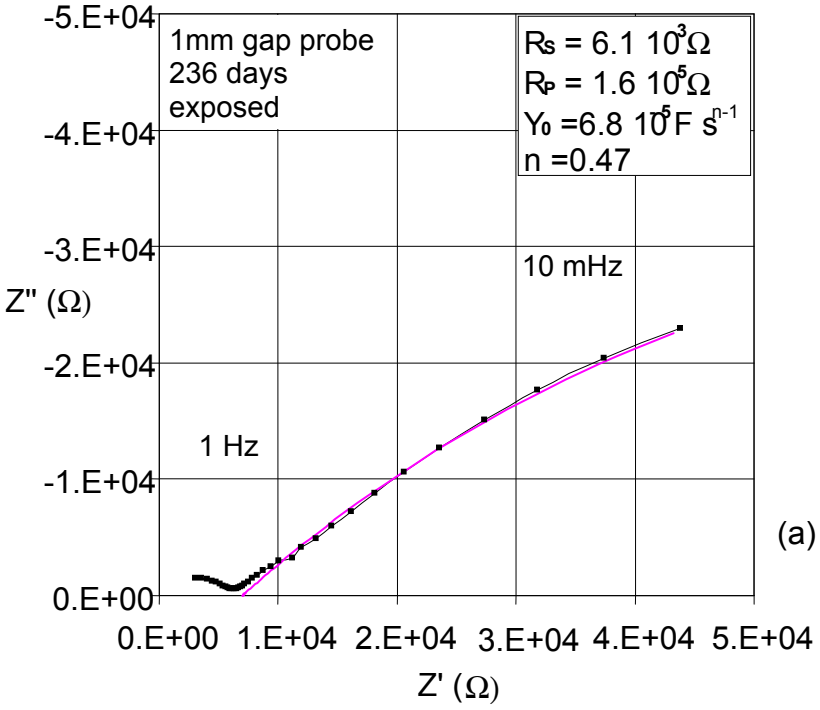

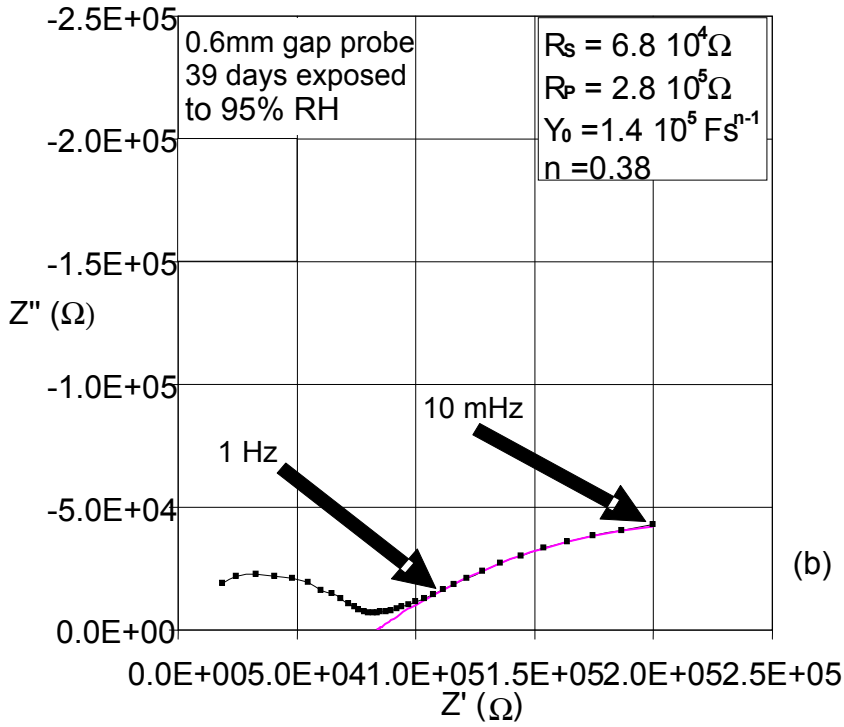

Figure 31. EIS Behavior of (a) 1mm Gap and (b) 0.6mm Gap Probes. The solid line indicates the model fitting.

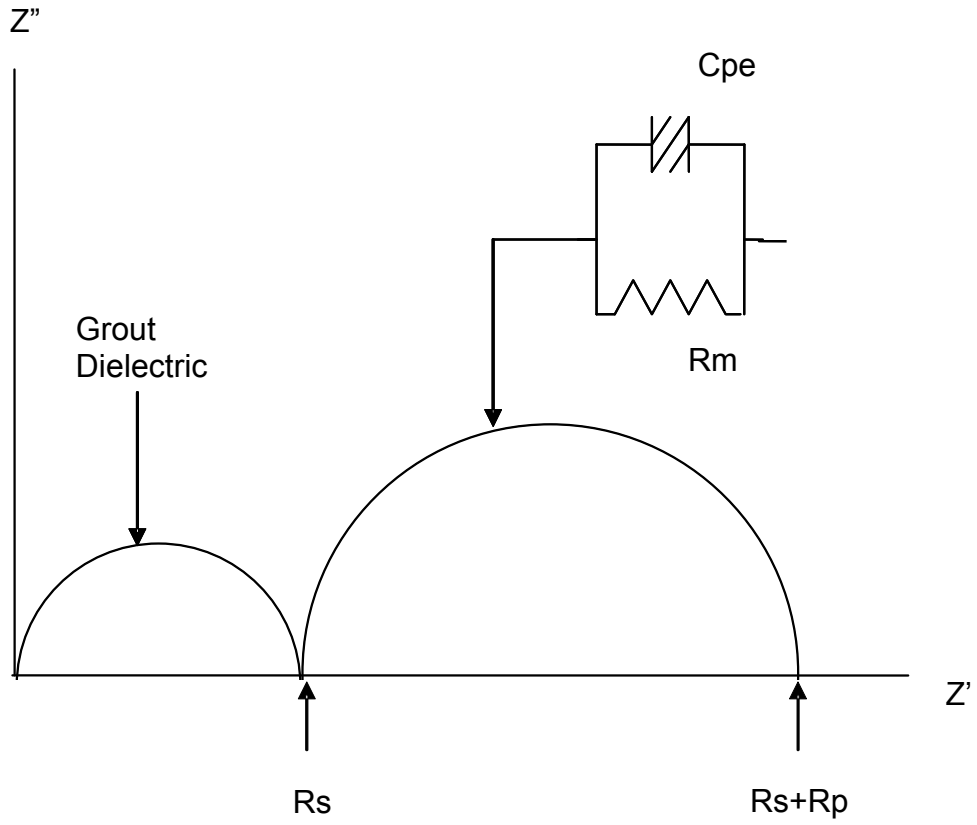

Figure 32. EIS Interpretation

Treating the reactions in the system as if they were under simple activation polarization, the corrosion rate can be estimated by the Stearn-Geary relationship (equation 11) between R_P and the corrosion current density (i_{corr}).

$$I_{corr} = \frac{\beta}{R_P} \qquad \beta = \frac{\beta a \times \beta c}{2.303 \cdot (\beta a + \beta c)} \qquad (11)$$

where βa and βc are the Tafel slopes ~ 0.12V [20],[22].

Another important parameter is the solution resistance (R_S). The solution resistance or grout resistance (equation 12) is on first approximation proportional to the resistivity of the grout (ρ), the cross section area of the grout between wires (A), and the distance between wires (d).

$$Rs = \rho \times \frac{d}{A} \qquad (12)$$

The actual system is more complicated (Figure 28), but for a fixed effective distance between wires, the resistivity of the grout can be determined if an effective area is known, and vice versa. For probes with similar grout, distance, and conditions such as RH and temperature, their solution resistance can be assumed to be equal to the inverse of their effective contact areas multiplied by a constant.

The R_S and the R_P trends for the 1mm gap electrochemical probes exposed to 95% RH environment are shown in Figure 33. Upon initial exposure to 95% RH the R_S and the R_P values were small, but then increased drastically tending to stabilize after ~50 days. The increase in R_s likely reflects the establishment of a less interconnected pore network in the grout as curing matures. Other factors that can alter the resistivity of the grout are temperature and the relative humidity. Figure 34 shows that the values for R_P in the 0.6mm probes were in the same order as those for the 1mm probes, but not as stable. The values of R_s were about one order of magnitude greater than those for the 1mm gap probes and less stable as well.

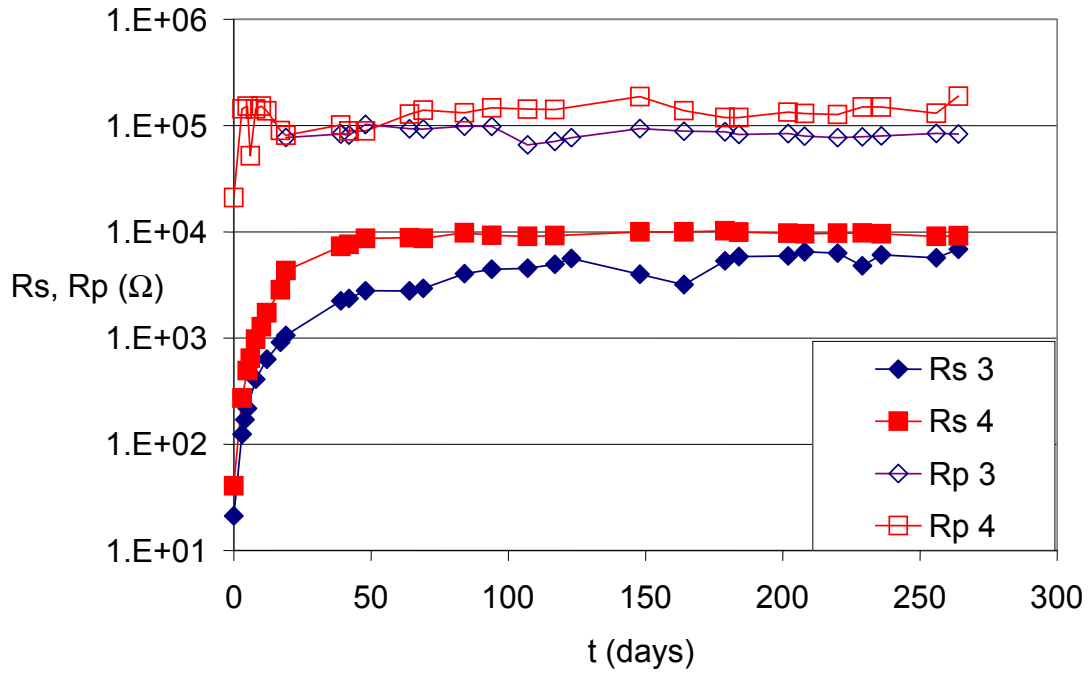

Figure 33. R_S and R_P Trends for Duplicate (No.3 and 4) 1mm Gap Electrochemical Probes

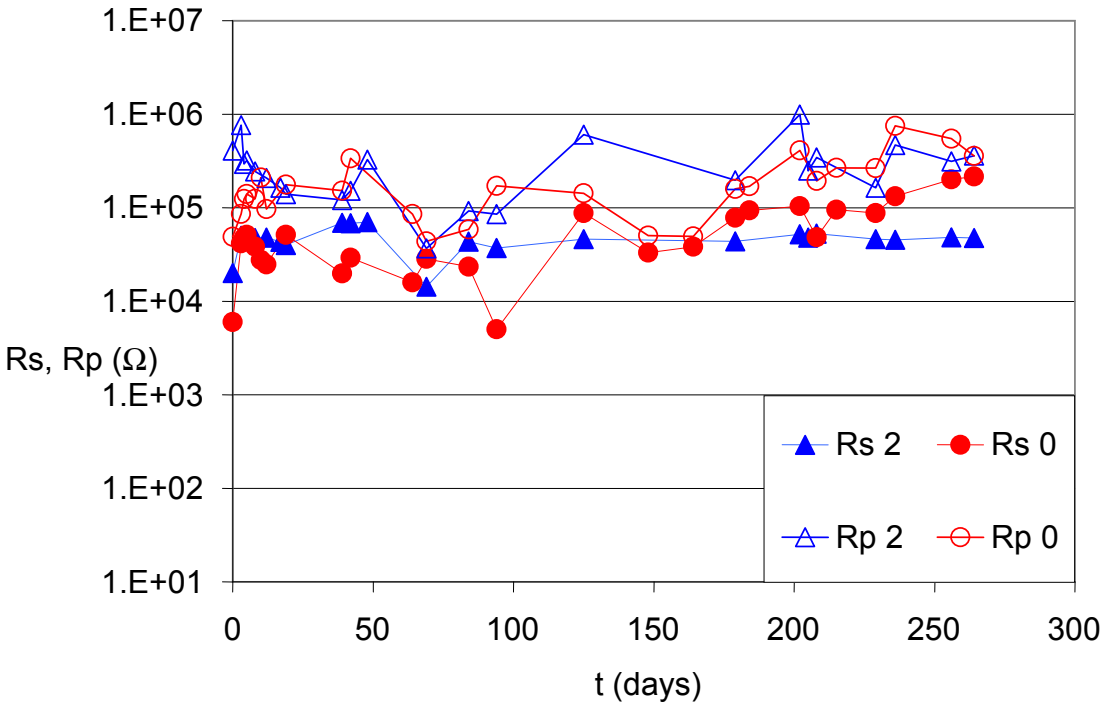

Figure 34. R_S and R_P Trends for Duplicate (No.2 and 0) 1mm Gap Electrochemical Probes

Polarization resistance can also be determined by the linear polarization resistance (LPR) technique. The LPR method is based on the relationship between small amplitude applied polarization potentials and the corresponding polarization current of a corroding system. The LPR experiments were conducted using the Gamry PCI-4 Potentiostat at 0.1mV/s, starting from the OCP to an overpotential of 10mV in the cathodic direction. A typical LPR potential-current curve of a 1mm gap electrochemical probe is shown in Figure 35. The results of the LPR measurements are not straightforward since the experimental arrangement to measure the polarization resistance can only directly sense the values of the total voltage and the total applied current without distinction of the current demanded by any element of the system [23]. Therefore, to determine the corrosion currents values a refined R_P (LPR-R_P) value was calculated. The LPR-R_P values were compensated for R_S and for the presence of interfacial CPE behavior using the corresponding parameters obtained from the EIS measurements. The compensation was made by first subtracting an amount equal to $I \cdot R_s$ from the potential V at each point of the measured current (I) - V curve obtained in the LPR test, thus obtaining an ohmic resistance-compensated curve I-V_{comp}. The correction for the current demanded by the CPE used the following relationship [20, 23]:

$$R_{ap} = [1/R_p + Y_o \cdot S^n \cdot V_{\max}^{-n} / \Gamma(1-n)]^{-1} \qquad (13)$$

where V_{max} is the maximum compensated potential applied, S is the scan rate (0.1mV/s), Γ is the Euler´s Gamma function, and R_{ap} is the apparent R_P determined by the slope at V=V_{max} of the I-V_{comp} curve, and Y_0 and n are the CPE

parameters obtained from an impedance experiment performed shortly before or after the test. It is noted that the correction represents only a first approximation as it does not take into consideration the convolution resulting from the simultaneous presence of the R_S and the CPE [20],[23].

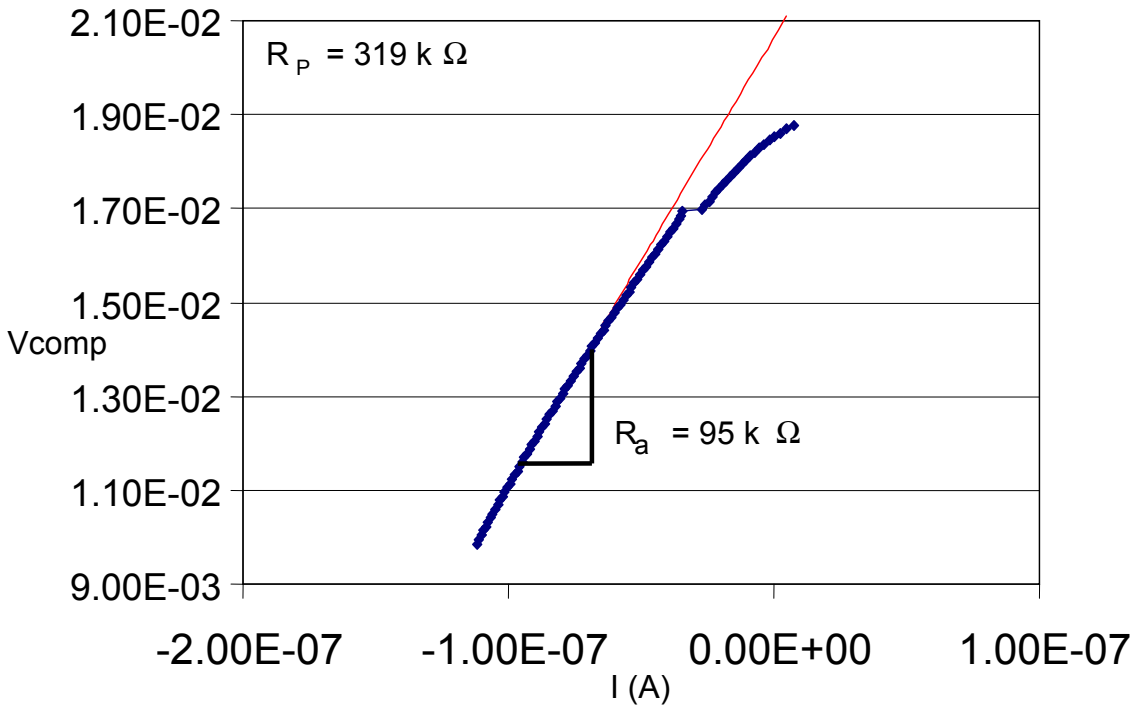

Figure 35. *I*-V_{comp} Curve of 1mm Gap Electrochemical Probe

Figures 36 and 37 show comparable relative trends for the R_P values estimated by LPR and EIS methods for both the 1mm and 0.6mm gap probes, but the R_P obtained from LPR tended to be lower than those ones from EIS (EIS-R_P) by about a factor of 2.

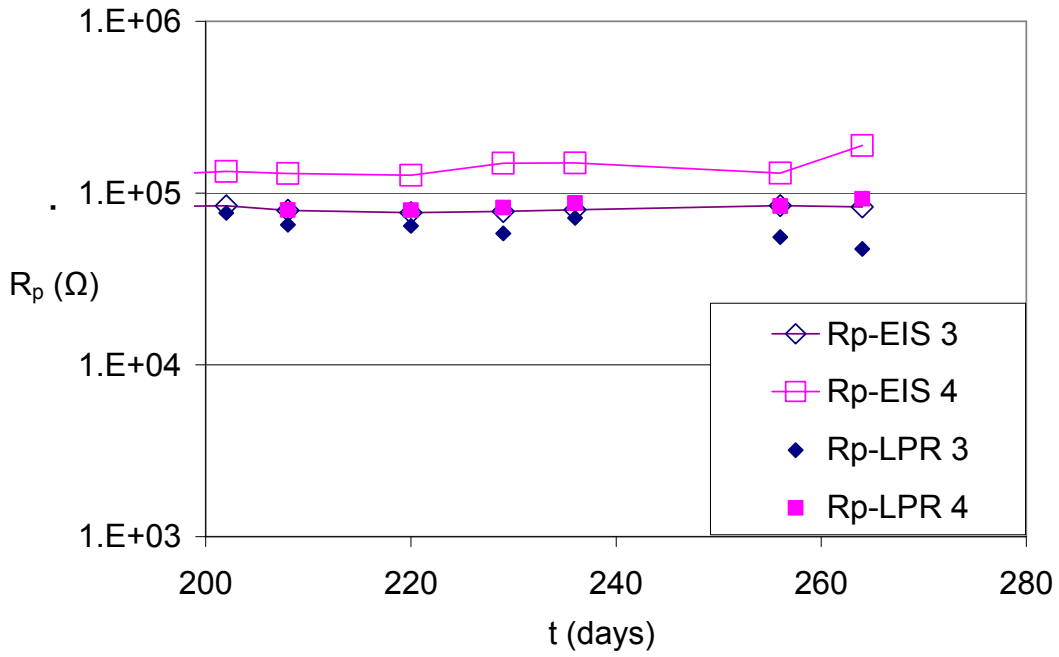

Figure 36. R_P Values Estimated by LPR and EIS Methods for Duplicate Probes with 1.0mm Gap

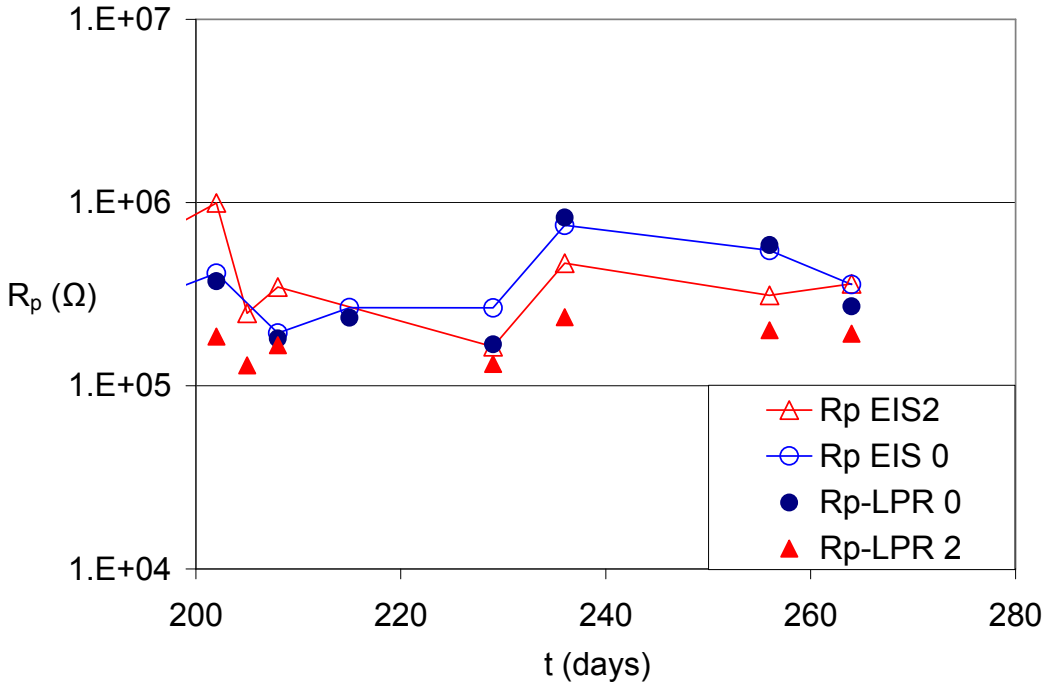

Figure 37. R_P Values Estimated by LPR and EIS Methods for Duplicate Probes with 0.6mm Gap

Corrosion current I_{corr} values were calculated by the Stearn-Geary relationship (equation 11), assuming that both wires were corroding equally. The corresponding nominal corrosion rates were estimated per equation (14) assuming an area of 8cm^2 for the metal in effective contact with grout on each of the probe wires. That area value was estimated by making the rough assumption that all the excitation current flows through the one-half of the wire perimeter facing the other wire. The time evolution of I_{corr} for both types of electrochemical probes is shown in Figure 38 and 39. The I_{corr} values were, in general, larger in the first days of exposure but after several days decreased to ~0.3μA and ~0.1μA for 1mm and 0.6mm gap probes, respectively. The I_{corr} for 0.6mm gap probes were less stable than those of the 1mm gap probes, reflecting the instability of the estimated R_P values noted before.

The instantaneous corrosion rate was calculated by the Stearn-Geary relationship introduced earlier (Equation 11) and by the Faradaic conversion formula (equation 14).

$$\frac{dW}{dt} = I_{corr} \cdot M /(n \cdot F \cdot A) \qquad (14)$$

where W is the mass lost of the corroding metal in g/cm^2, t is the time in seconds, M is the atomic mass of iron 55,845g/mol, A is the effective area, n is the valence of iron (2), and F is the Faraday's constant 96,485C/mol. The result is converted to cm/y (later expressed as μm/y) by dividing the mass by the density of iron 7.87g/cm^3. While there is considerable uncertainty in the effective area of these

specimens and from the other simplifying assumptions used, the results suggest that corrosion rates estimated by this method were in the order of ~0.3μm/y.

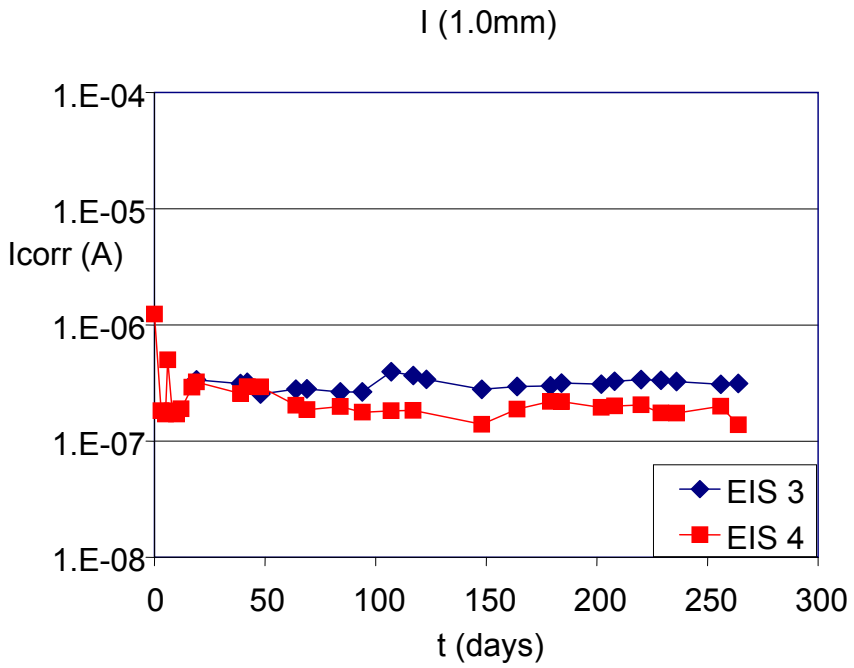

Figure 38. I_{corr} Trends of Electrochemical Probes with 1.0mm Gap

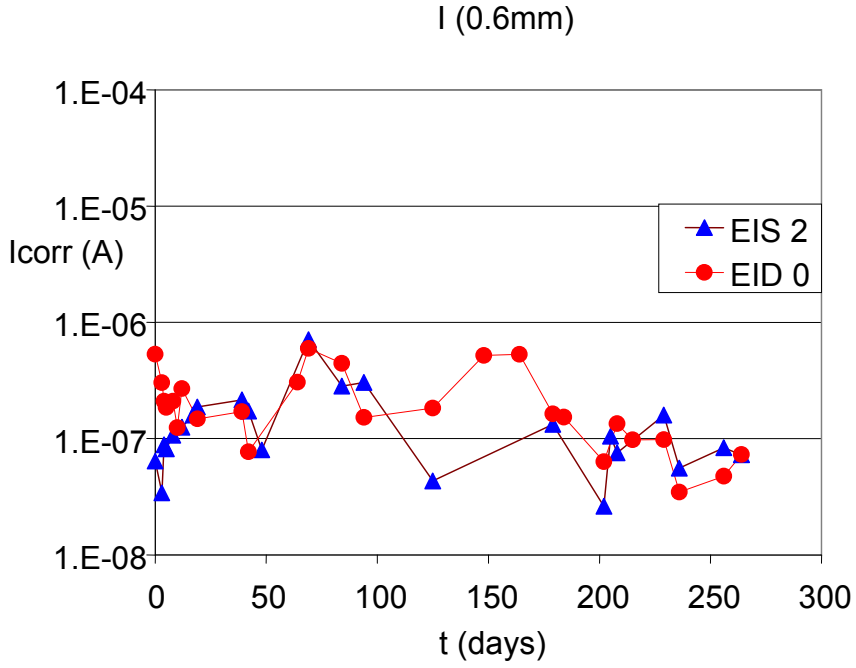

Figure 39. I_{corr} Trends of Electrochemical Probes with 0.6mm Gap

5.2 Electrical Resistance Probes

The cumulative (i.e. averaged from the beginning of exposure until an exposure time *t*) corrosion rate of ER probes in μm/year was determined by:

$$CR = \Delta r \cdot 365/t \qquad (7)$$

where Δr is the radius change of the corroding wire in μm ($r_{initial}$ - r_{corr}) and *t* is the exposure time in days.

An instantaneous (actually short interval) corrosion rate can be calculated by evaluating equations (10) and (7) using the short interval Δt between two measurements, and using the first measurement as the initial condition.

The instantaneous and cumulative corrosion rate trends for grouted and bare ER probes exposed to the 95% RH environment are shown in the Figures 40 and 41. Higher corrosion rates were observed in the first days of exposure especially for the bare steel probes but after 50 days the rates for both conditions reached a plateau of ~5μm/y. The fluctuations of the instantaneous corrosion rate may be attributed to the resolution of the individual measurements and/or minor temperature and RH fluctuations. The cumulative corrosion rates for ER probes had comparable decreasing trends. After 98 days the cumulative corrosion rates were 12μm/y and 24μm/y for grouted and bare ER probes respectively, reaching, after 196 days, 8μm/y and 15μm/y.

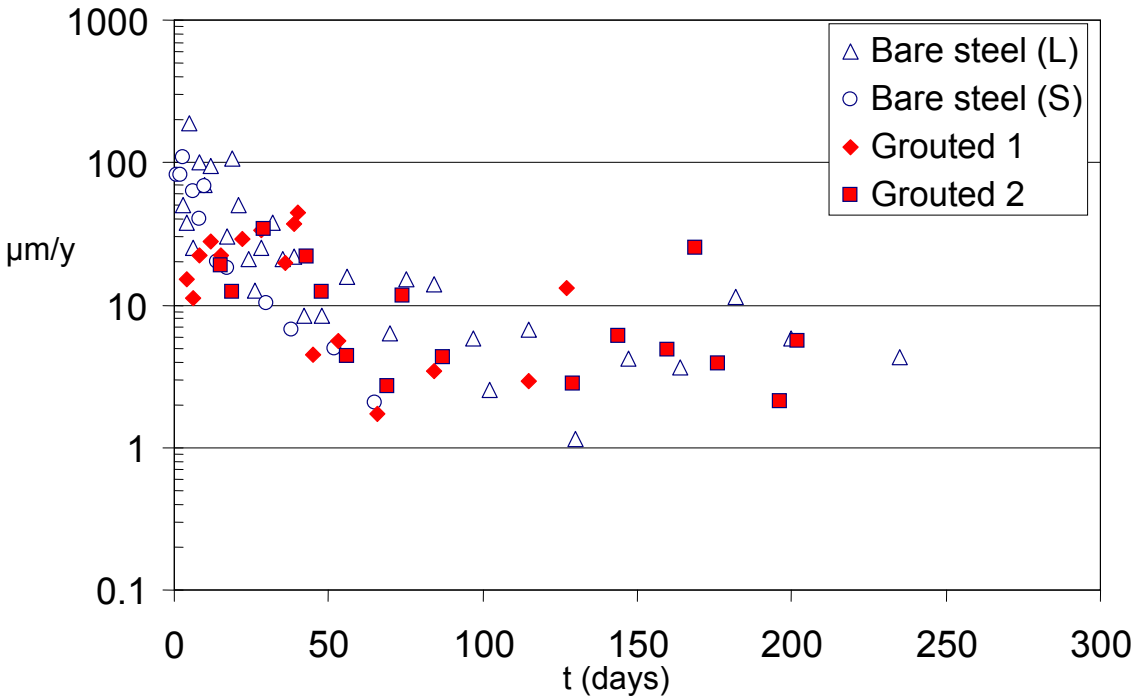

Figure 40. ER Probes Instantaneous Corrosion Rate

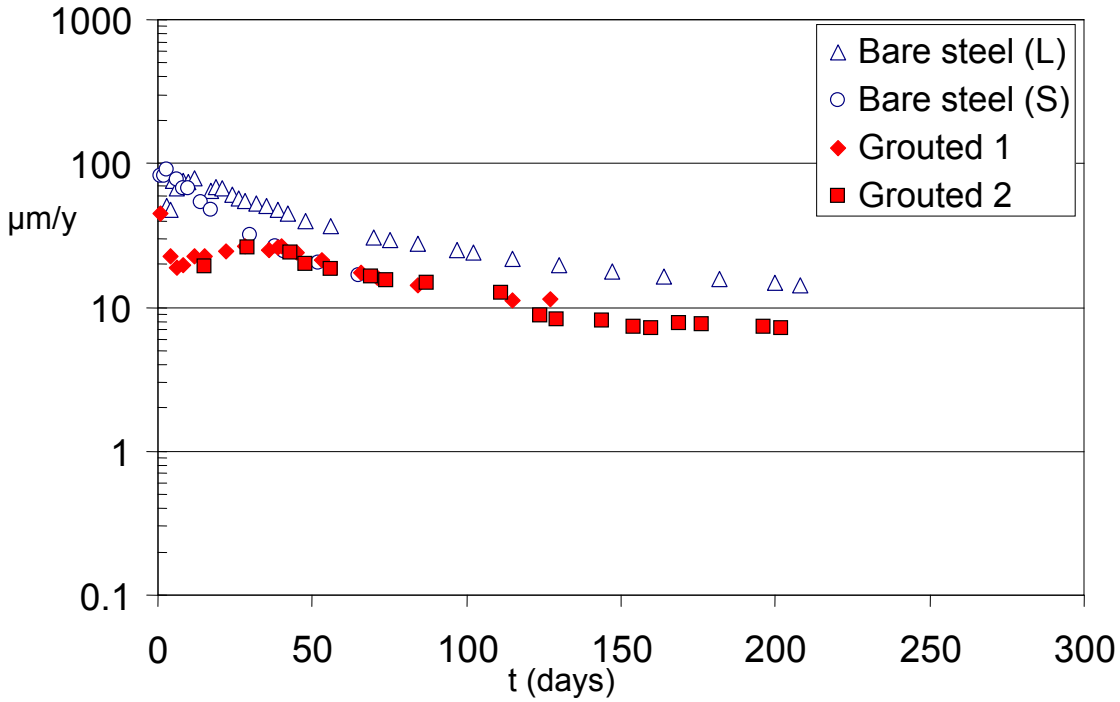

Figure 41. ER Probes Cumulative Corrosion Rate

In the 75% RH chamber none of the specimens examined experienced measurable corrosion rates, so that condition served as a baseline control. The result is consistent with the expectation that exposure at 75% RH does not meet the conditions necessary to trigger atmospheric corrosion. For bare metals that condition is typically encountered above 85% RH [24], consistent with the present results.

5.3 Gravimetric Measurements

The weight loss measurements yielded results comparable to those of the ER probes as illustrated in Figure 42. After 98 days of exposure the average corrosion rate for grouted and bare helically shaped wires were 11μm/y and 12μm/y respectively, and 10μm/y and 11μm/y after 196 days. The average corrosion rate for bare steel tie wires was ~ 13μm/y after 98 and 196 days of exposure.

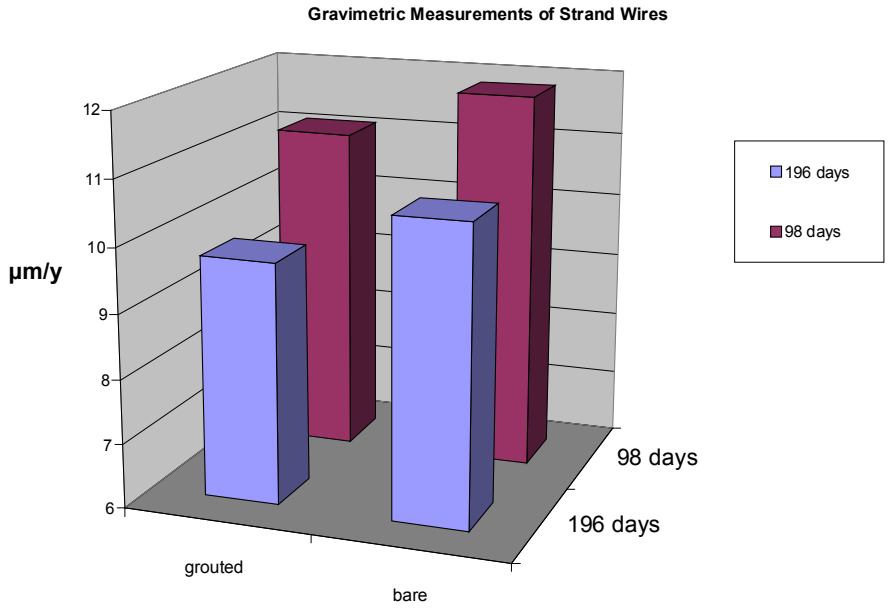

Figure 42. Corrosion Rate of Grouted and Bare Steel Strands Exposed to a 95% RH, Estimated by Weight Loss Measurement

5.4 Early Warning Probes Discussion

The observation of rust on some electrochemical probe wires clearly indicated that significant corrosion was taking place in the 95% RH chamber. However, the electrochemical probe apparent corrosion rates were one order of magnitude lower than those obtained by ER or weight loss. This discrepancy may be attributed in part to uncertainty in estimating the effective probe area in contact with grout. That area may be much less than the nominal assumed value because of cracks in the grout or disbondment at the grout-metal interface, thus greatly underestimating the actual rates over the remaining area of contact. Another likely cause of insensitivity would be that the assumption of equal electrochemical behavior at the two metal-grout interfaces in a probe is wrong. If corrosion were to start at only one of the interfaces with the other largely in the passive condition, then the total series impedance would still be very large and the corresponding apparent current density would stay low until both wires are simultaneously in the active condition.

The ER probes and weight loss measurements showed evidence that at 95% RH the corrosion rates were considerably high. That rate was expected from the relatively thin effective electrolyte layer present on the metal surface in the air space case. The grout film was not particularly protective, as shown by similar corrosion rates in the bare steel and grouted specimens. Tests, after long exposure times, with pH paper and sprayed phenolphthalein on the grout film on probes in the 95% RH chamber indicated a near neutral pH, meaning that the thin layer of hardened grout had eventually carbonated in the chamber

environment. Thus, the grout no longer had passivating properties to the steel and it is not surprising that measurable corrosion was taking place. This was further confirmed by direct observation of rusting on ER, weight loss and even some of the electrochemical probe wires.

The worst-case surface-averaged corrosion rate values observed in the high humidity chamber (about 10μm/y), if sustained over 10 years would correspond to an average loss of diameter of 200μm, or about 8% reduction in cross-sectional area in a 5 mm diameter wire. Such a loss may already be considered of concern even if it were uniform, considering that one decade is a relatively short time compared to typical design life goals (e.g. 75years). As corrosion is likely to show some degree of localization, critical loss of strength could occur even earlier. Thus, these findings highlight air space corrosion as a potential cause of strand failure.

Chapter 7

Conclusions

A simplified test and analysis procedure for rapid screening of structures with commonly encountered tendon configurations was developed and validated on nearly full-scale tendons constructed at the FDOT Structures Laboratory.

The developed practical vibration tendon tension approximation was validated against nearly full-scale tendons, showing less than 4% difference between the tension obtained by the simplified vibration method and independent measurements from load cells.

Electrical Resistance (ER) probes customized for PT anchor air space conditions were constructed and their operation with readily available electronic instrumentation was demonstrated. The probes showed adequate sensitivity to detect the corrosion rates of interest, and the results were validated against direct gravimetric measurements.

Electrochemical probes for EIS and LPR measurements in PT anchor air space conditions were constructed and their operation with readily available electronic instrumentation was demonstrated. However, sensitivity may be low and the interpretation of the electrochemical probe results needs to be refined to better assess their usefulness.

There was good correlation between EIS and LPR measurements showing that the latter, simpler method has good potential for practical implementation.

Simulated air-space corrosion experiments showed that an aggressive environment may evolve in the grout void even on strand wires covered with a residual hardened grout layer, resulting in corrosion rates that may have damaging effects in a relatively short service time.

References

[1] H. Wang, A.A. Sagüés; “Corrosion of Post-Tensioning Strands,” Final Report to Florida Department of Transportation BC353-33, Florida, November 1, 2005.

[2] A.A. Sagüés, S.C. Kranc, and T.G. Eason; “Vibrational Tension Measurement of External Tendons in Segmental Posttensioned Bridges” Journal of Bridge Engineering, Vol. 11, No. 5, September/October 2006, pp. 582-589.

[3] J.Corven, A. Moreton; ” Post-Tensioning Tendon Installation and Grouting Manual” Federal Highway Administration, U.S. Department of Transportation, May 2004.

[4] A.A. Sagüés, R.G. Powers, and H. Wang; Corrosion/2003, Paper No. 03312, NACE International, Houston, 2003.

[5] H. Wang, A.A. Sagüés, and R.G. Powers; “Corrosion of the Strand-Anchorage System in Post-Tensioned Grouted Assemblies”, Corrosion/2005, Paper No. 05266, NACE International, Houston, 2005.

[6] A.T. Ciolko and H. Tabatabai; “Nondestructive Methods for Condition Evaluation of Prestressing Steel Strands in Concrete Bridges” Final Report to Transportation Research Board National Research Council NCHRP Project 10-53, 1999.

[7] DYWIDAG Bonded Post-Tensioning Systems (Brochure) DYWIDAG-Systems International, 2005.

[8] B. Pielstick, and G. Peterson; “Grouting of Bridge Post-Tensioning Tendons Training Manual” Florida Department of Transportation, Federal Highway Administration, July 2002

[9] A. Naaman, and J. Bren; “External Prestressing in Bridges”, American Concrete Institute, ACI SP-120, Detroit, 1990.

[10] A. A. Sagüés,T. Eason,C. Cotrim,J. Lopez-Sabando “Validation and Practical Procedure for Vibrational Evaluation of Tendons”, Draft Final Report to Florida Department of transportation BC 353#44, Florida, December, 2007.

[11] P.M Morse; *Vibration and Sound*, Mc.Graw Hill, N.Y., 1948.

[12] A.A. Sagüés, S.C. Kranc, and R.H. Hoehne, “Initial Development of Methods for Assessing Condition of Post-Tensioned Tendons of Segmental Bridges’, Final Report to Florida Department of Transportation BC374, Florida, September 1999.

[13] A.A. Sagüés, C. Cotrim, V.Balakrishna, “Vibrational Evaluation of Tendons in Segmental Sections of Sunshine Skyway Bridge Main Spans”, Final Report to Florida Department of Transportation BD544, Florida, August 1, 2005.

[14] L. Taveira, A. Sagüés, J.Lopez-Sabando, and B. Joseph, “Detection of Corrosion of Post-Tensioned Strands in Grouted Assemblies”, Project No. BD544-08, 71 pages, Final Report to Florida Department of Transportation, University of South Florida, Tampa, Fl, October 31, 2007 .

[15] F.F. Cinkotai. “The Behavior of Sodium Chloride Particles in Moist Air”, J. Aerosol Sci. Vol 2, 1971, pp 325–329.

[16] M.J. Moran, and H.N. Shapiro. *Fundamentals of Engineering Thermodynamics*, 5th Edition. John Wiley & Sons, Danvers, 2004.

[17] J.F. Young. “Humidity control in the laboratory using salt solutions, A. Review”, J. Appl. Chem. Vol 17, 1967, pp 241-245.

[18] F. Mansfeld, and J.V. Kenkel. “Electrochemical Monitoring of Atmospheric Corrosion Phenomena”, Corrosion Sci., Vol 16, 1976, pp.111-122.

[19] D.C. Giancoli, *Physics for Scientists & Engineers*, Third Edition. Prentice Hall, New Jersey, 2000.

[20] A.A. Sagüés, “Lectures Notes on Electrochemical Impedance Spectroscopy for Corrosion Testing”, University of South Florida, 2006.

[21] R. Coelho; *Physics of Dielectrics for the Engineer*, Elsevier, N.Y., 1979.

[22] A. Bentur, S. Diamond, and N.S Berke. *Steel Corrosion in Concrete*, London: E&FN Spon, 1997. pp 77.

[23] A.A. Sagüés, S.C. Kranc, and E. Moreno. "The Time-Domain Response of a Corroding System with Constant Phase Angle Interfacial Component: Application to Steel in Concrete" Corrosion Science, Vol 37, 1995, pp 1097.

[24] R.B. Griffin, “Corrosion in Marine Atmospheres,” in Corrosion: Environments and Industries, ASM Handbook Vol. 13c, Materials Park: ASM International, 2006, pp. 42-60.

Appendices

Appendix 1: Level 1 Block Diagram of *Analyzer-M*

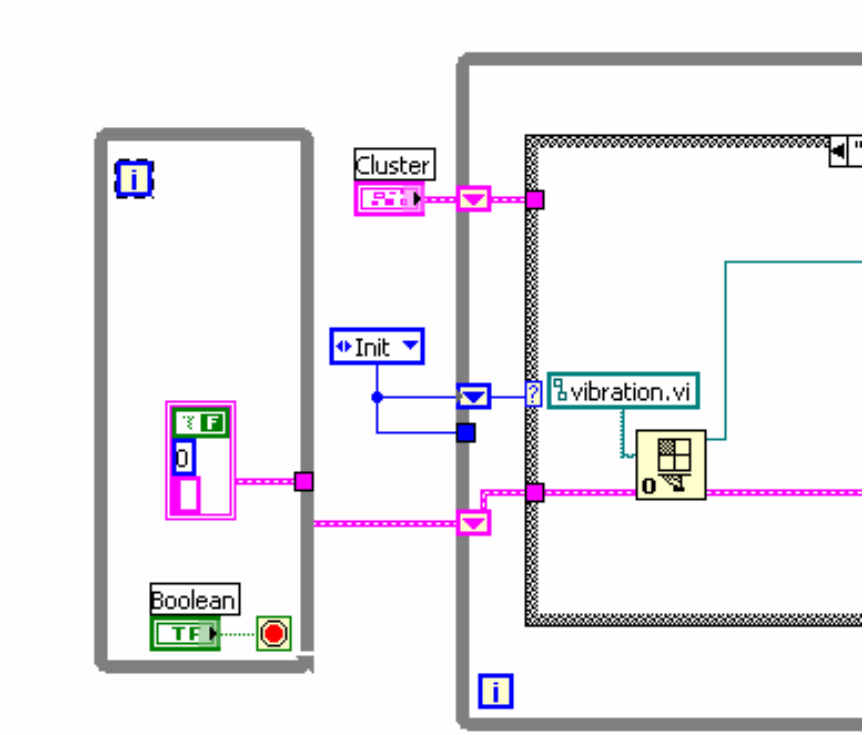

Figure 43. *Analyzer-M* Level 1Block Diagram A

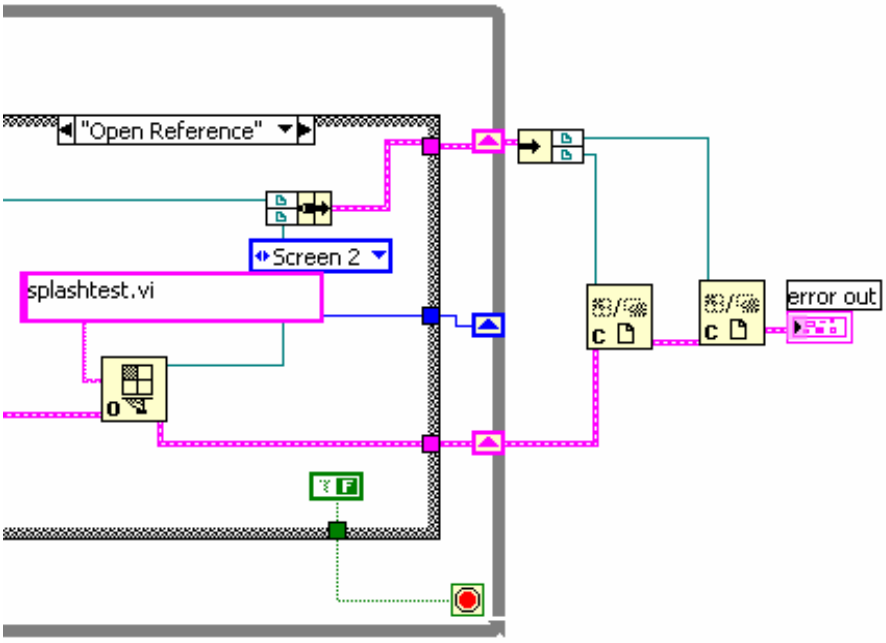

Figure 44. *Analyzer-M* Level 1Block Diagram B

Appendix 2: Level 2 Block Diagram of *Analyzer-M*

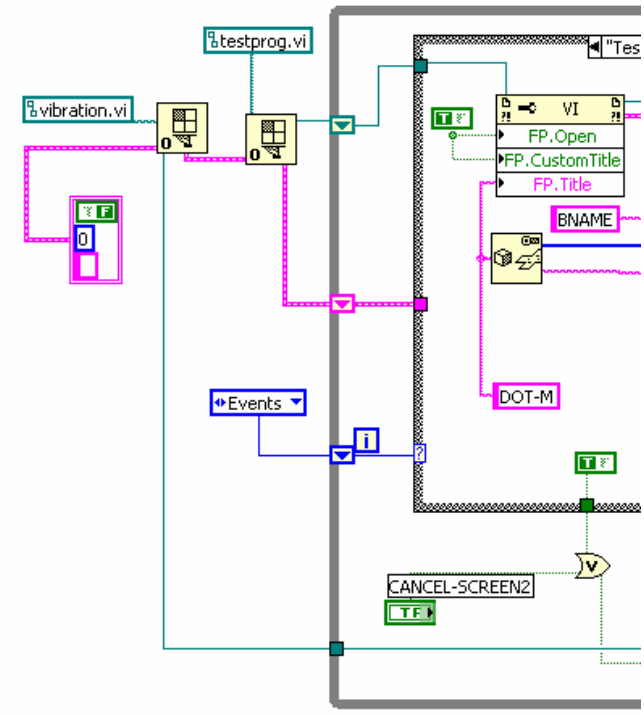

Figure 45. *Analyzer-M* Level 2 Block Diagram A

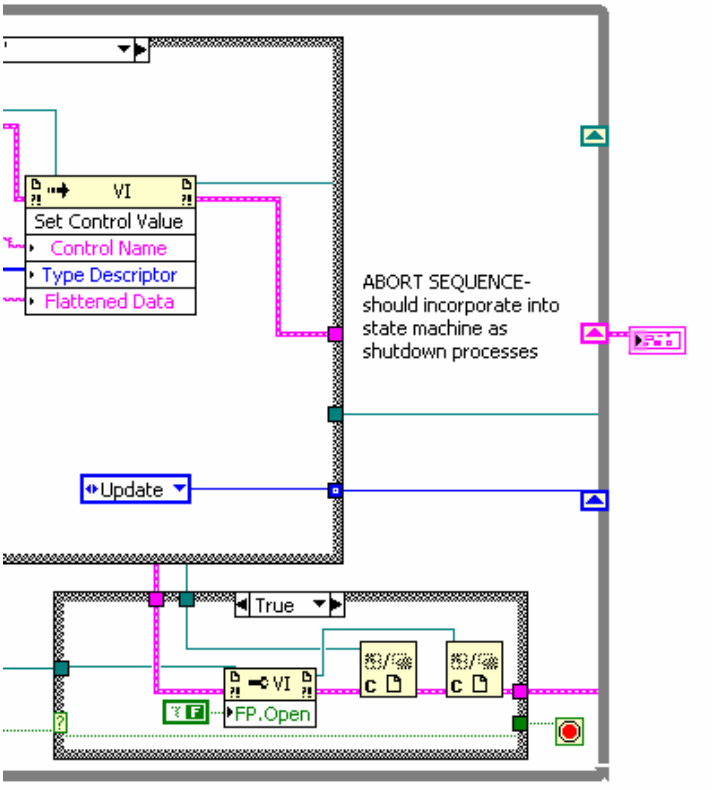

Figure 46. *Analyzer-M* Level 2 Block Diagram B

Appendix 3: Level 3 Subdiagram 0 of *Analyzer-M*

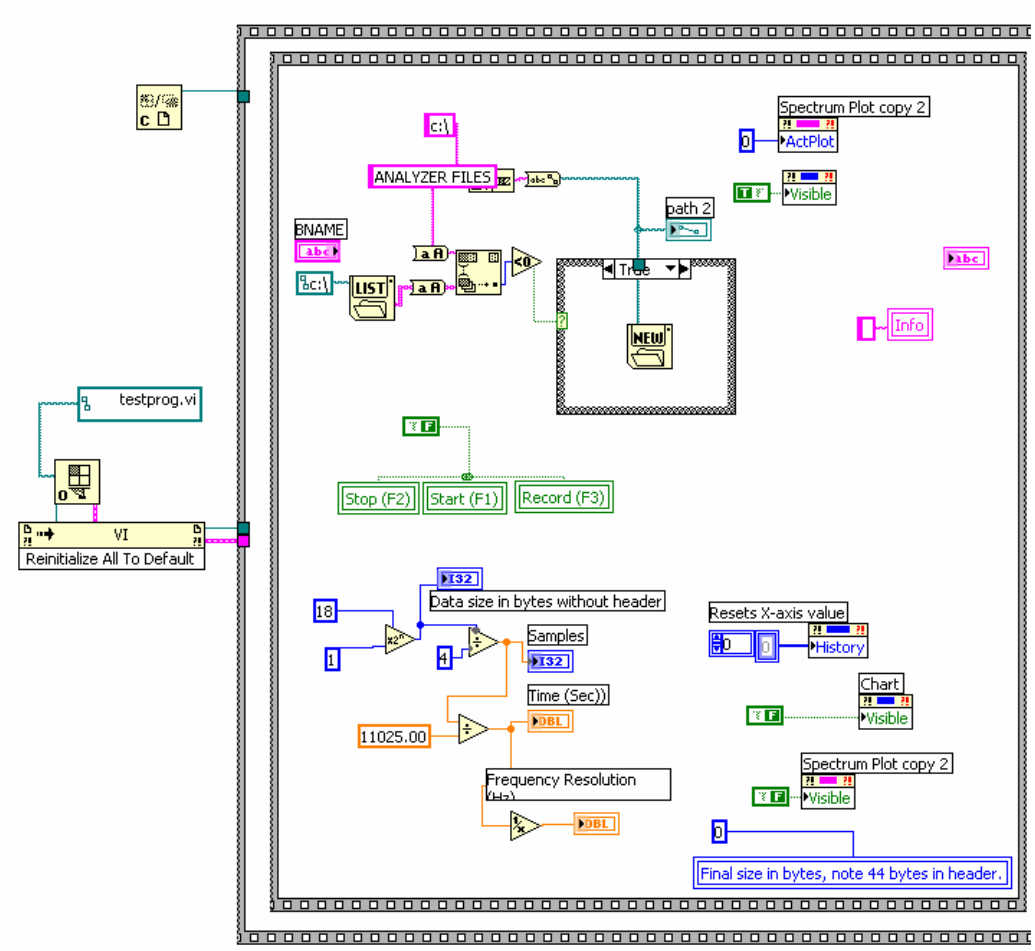

Figure 47. *Analyzer-M* Level 3 Subdiagram 0 Block Diagram A

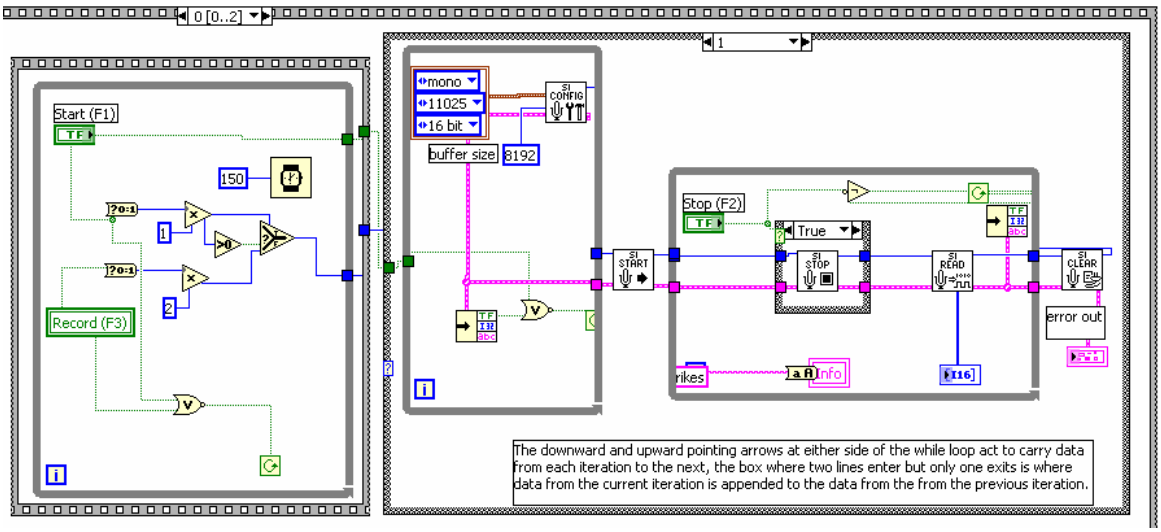

Figure 48. *Analyzer-M* Level 3 Subdiagram 0 Block Diagram B

Appendix 4: Level 3 Subdiagram 1 of *Analyzer-M*

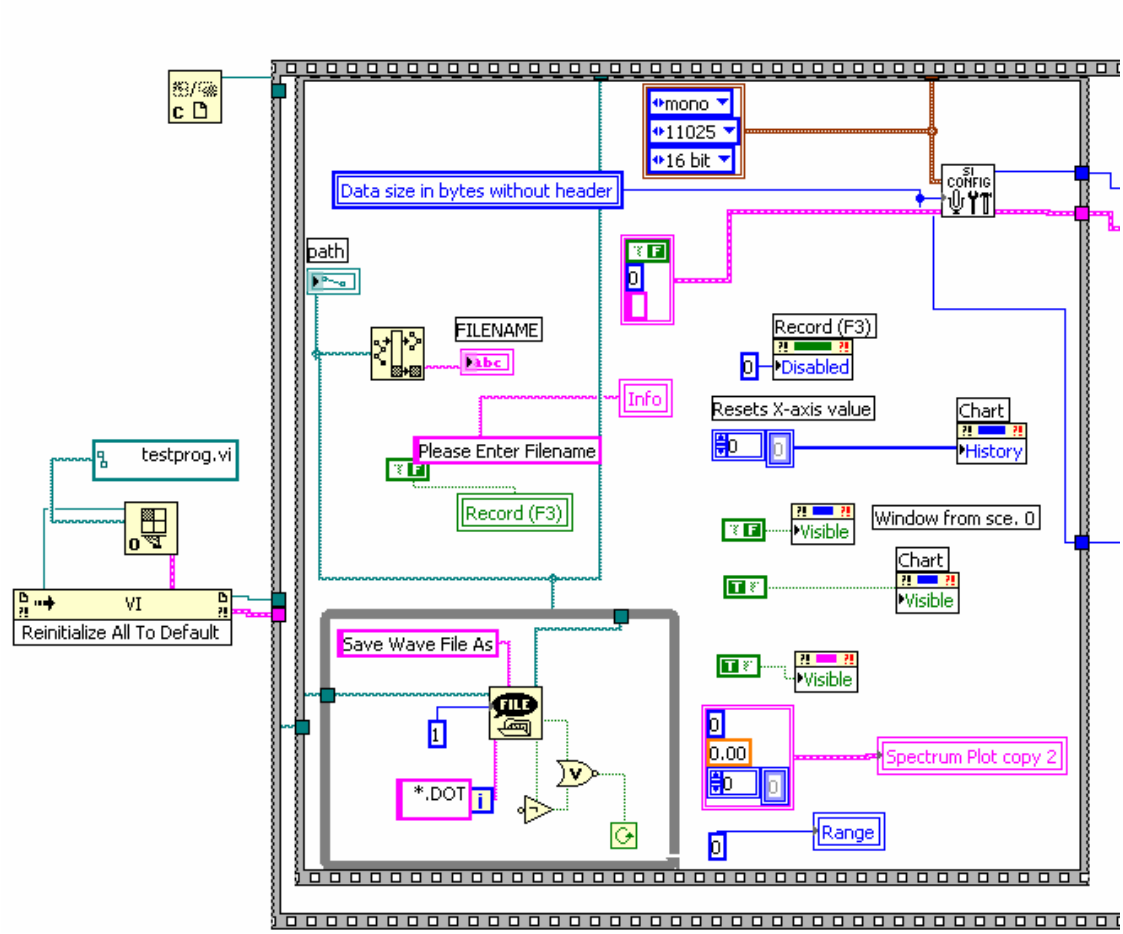

Figure 49. *Analyzer-M* Level 3 Subdiagram 1 Block Diagram A

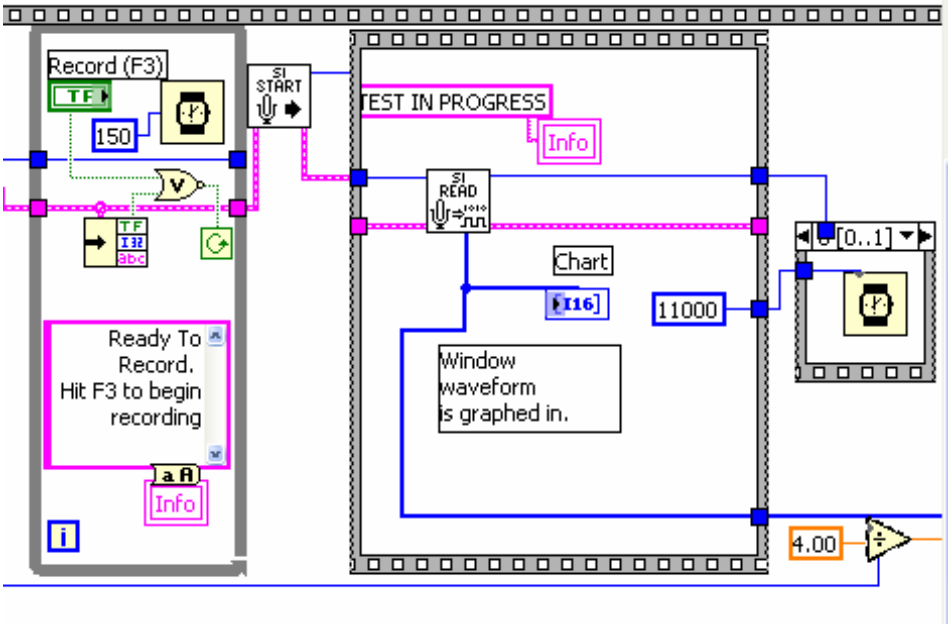

Figure 50. *Analyzer-M* Level 3 Subdiagram 1 Block Diagram B

Appendix 4:(Continued)

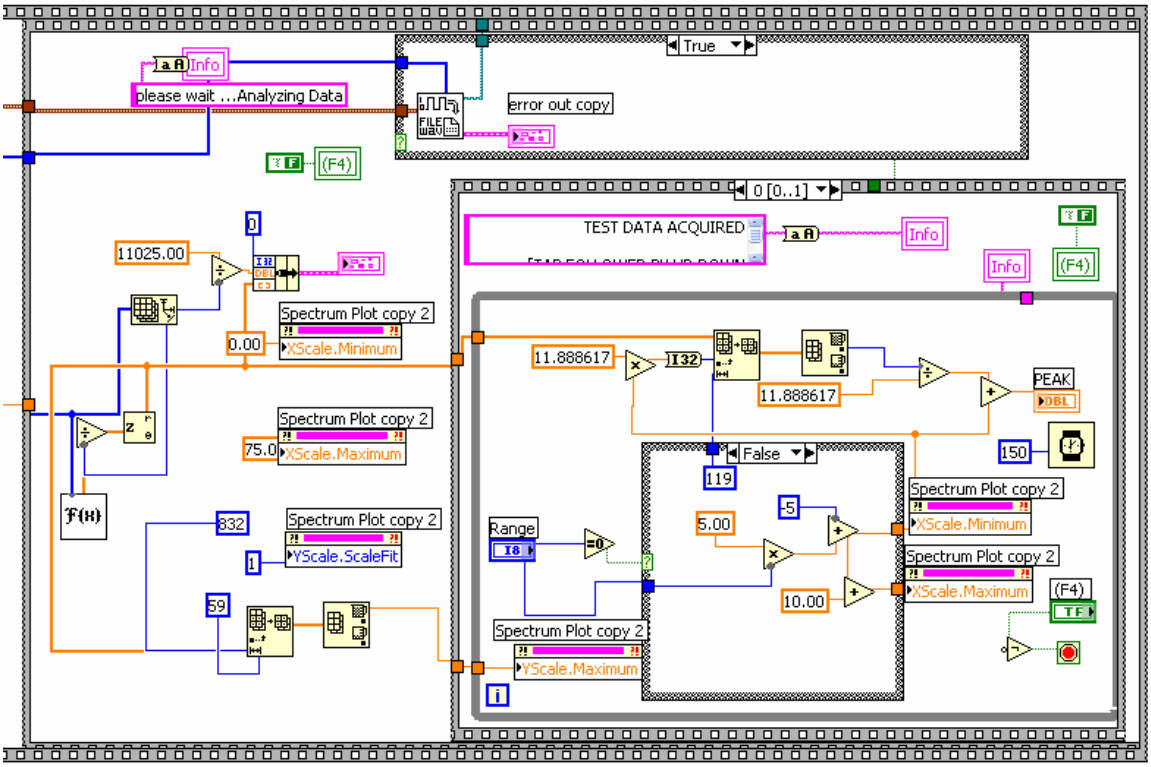

Figure 51. *Analyzer-M* Level 3 Subdiagram 1 Block Diagram C

Appendix 5: *WavePlayer-Mono* block Diagram

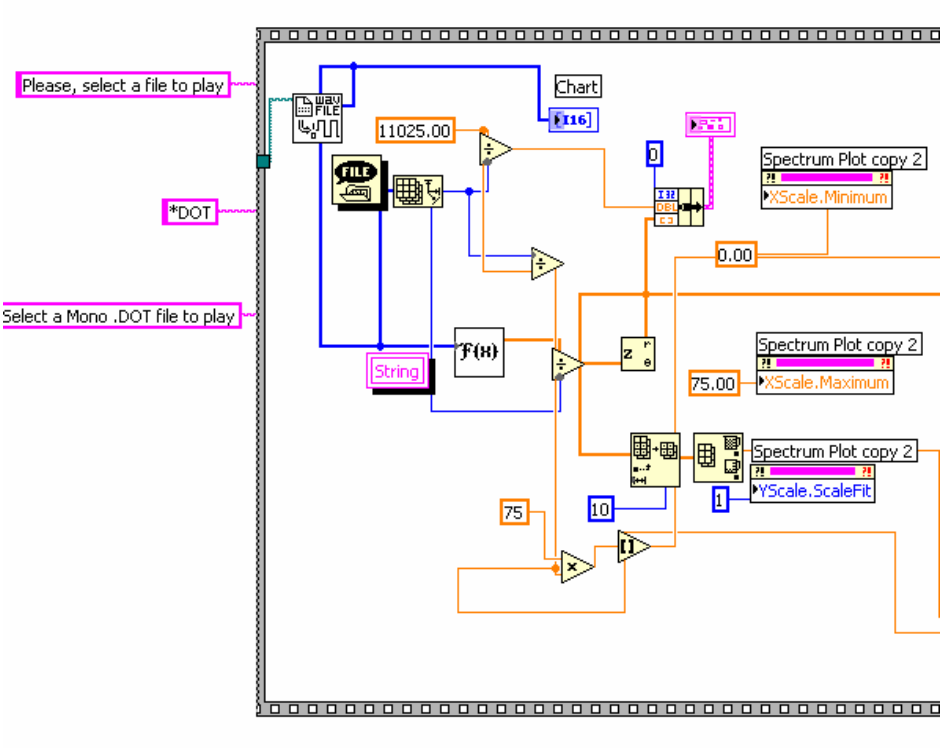

Figure 52. *WavePlayer-Mono* block Diagram A

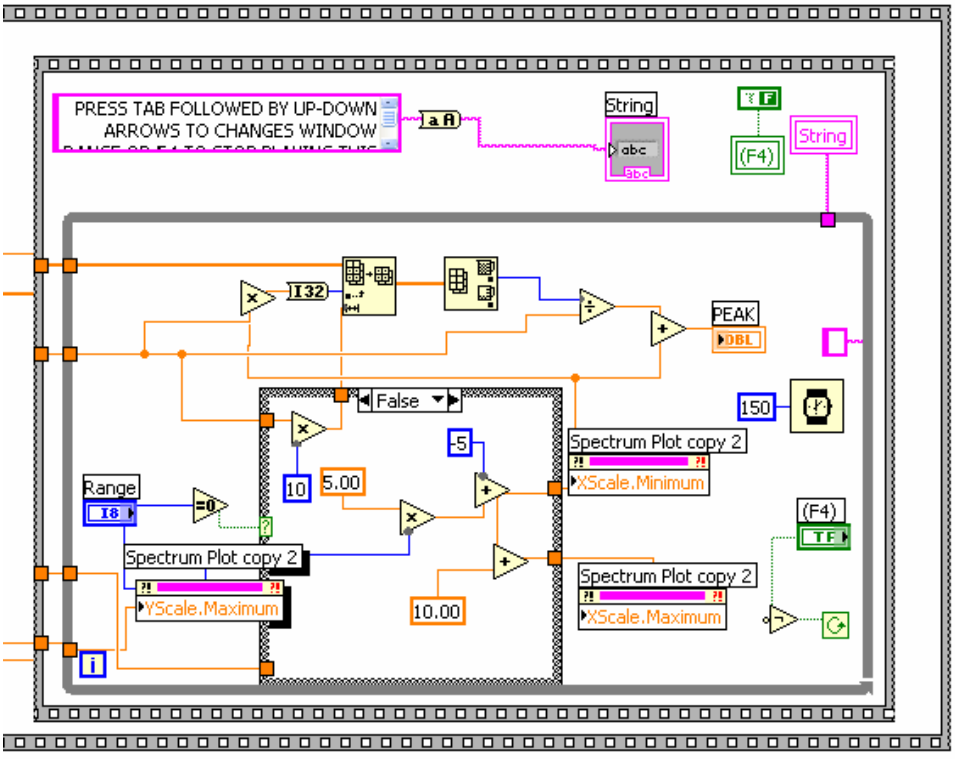

Figure 53. *WavePlayer-Mono* block Diagram B

Appendix 6: *Analyzer-M* Instructions [10]

INSTRUCTIONS FOR INSTALLATION / UN-INSTALLATION OF ANALYZER-M.EXE

Install:

1. If Windows Explorer is not already configured to show file extensions, configure your Windows Explorer to always show file extensions.
2. Install LabVIEW Run-time Engine 7.1 if LabVIEW 7.1 or higher is not installed in the computer.
3. Go to M-remote folder in the Installation CD.
4. Navigate to the Installer folder inside M-remote folder.
5. Click on install.msi and follow the instructions in the WIZARD.

    i. During the installation process, the setup will display the location where the program will be installed. The "Destination Folder" item should display *EXACTLY* "c:\ANALYZER-M" (and NOTHING ELSE) as the path for the destination of the program. If it does not, navigate to the folder "c:\ANALYZER-M" using the "Browse" button located on the right hand side of the setup window.

6. After installation is complete, locate the file ANALYZER-M.EXE (it should be located in the folder "c:\programs\ANALYZER-M" or go to the start menu and choose programs) and create a shortcut for that file on the desktop.
7. A simplify way to install the program would be to copy the file ANALYZER-M.EXE from the M-remote folder and paste on the desktop.

Un-Install:

1. In the Installation CD, navigate to M-remote\Installer folder, click on install.msi
2. Follow the instructions in the wizard.

Imp. Note: In the un-installation process, the wizard should indicate that the process is indeed un-installation, not an installation.

Run-Time Engine installation

From the installation CD run LVRunTimeEng 7.1.exe to install the LabVIEW 7.1 Run-Time Engine.

Appendix 6:(Continued)

TENDON VIBRATIONAL TESTING STEP-BY-STEP PROCEDURE

A. EQUIPMENT AND SETUP FOR ANALYZER-M

Minimum items required:

1. Laptop DELL LATITUDE 840 computer with *Analyzer-M* software
2. Memory stick with at least 1GB of empty space for "drag and drop" operation.
3. 110 V 60Hz AC Power Source adequate for computer
4. Thermometer to record ambient temperature
5. Long (100 ft) and accurate measuring tape
6. Log Form binder/clipboard/ballpoint pens.
7. Accelerometer Kit Box containing
   - 7a. Accelerometer (PCB 338B34)
   - 7b. Accelerometer Extension Cable
   - 7c. Sensor Signal Conditioner (ICP – Model 480E09)
   - 7d. Stereo Adapter Cable
   - 7e. Spare 9V Alkaline Batteries (bag of 3)
8. BNC Black Extension Cable (2 50-ft sections with 2 Female-Female couplers)
9. Hammer
10. Tuning Fork
11. Wireless presentation remote (Targus, model PAUM30).
12. Card Table and Stool - essential for accurate work.
13. Adequate lighting

Note: Items 1,7 and 8 must be on site in duplicate to provide full spare backup.

Physical arrangement (see Figure 1):

a) Set up Card Table centrally in the Test Station area chosen, so the computer screen is within easy view from the impact position .

b) Set up power source outlet next to Card Table.

c) Ensure that accelerometer wiring can run unobstructed to each of the accelerometer locations in the Test Station. *Ensure that operator movement does not result in tripping over wires or equipment falling down.*

d) Place DELL Computer and Log Form on Card Table. Leave space also for tuning fork. A comfortable working space is essential for reliable operation and record keeping.

Appendix 6:(Continued)

e) Make sure that cooling fan in computer is not obstructed.

Equipment is now ready for operation. Proceed To Part B, System Startup and Pre-Test Steps.

B. SYSTEM STARTUP AND PRE-TEST STEPS

READ EACH STEP COMPLETELY BEFORE ACTING

Step 0. Span and tendon segment ID and preparatory measurements

See ADDENDUM 1 for ID procedures and preparatory work.

Step 1. Set up computer:

1.1 Write down Test Station number (for example 07) on Log Form.

1.2 Power up and boot up computer. Record on Log Form designation of computer being used.

1.3 Perform audio input setup check:

Perform once at beginning of shift. Perform also if machine was operated by others during shift or if abnormal test results are observed.

On desktop, double click Volume Control icon
Ensure Mute All is selected.
Ensure Line In Volume is all the way up and not muted.
Click Options, Properties.
Click Recording, then OK.
Ensure Stereo Mix Volume is all the way up.
Ensure Stereo Mix Select is clicked.
Ensure nothing else is selected.
Close window.

1.4 Double-click *ANALYZER-M* icon on desktop. After Logo appears, press F2 and choose OK or Cancel conditions. If OK is chosen, the operating panel shows up on screen. Turn Caps Lock on.

Step 2. Wire accelerometer, Sensor Signal Conditioner, and connection to computer. Check/replace Sensor Signal Conditioner batteries:

Appendix 6:(Continued)

Remove from Accelerometer Kit Box #1 the Accelerometer. [Use parts in spare Kit Box #2 only if parts in #1 fail]. Record on Log Form Serial Number (SN) of

accelerometer being used. The Accelerometer is a precision instrument. Handle it gently and do not drop.

Connect Accelerometer to white Accelerometer Extension Cable . Turn "floating clamp nut", never the accelerometer as that may damage connector pin. Do not kink or stress Accelerometer Extension Cable.

Connect Accelerometer Extension Cable to BNC Black Extension Cable with provided adaptor. If only one 50-ft length is sufficient, store away the other 50-ft length. *Do not use cables to pull on or hold equipment!*

2.2 Connect other end of BNC Black Extension Cable to XDCR jack on Sensor Signal Conditioner. Verify that Sensor Signal Conditioner controls are as follows:

Gain:	10
Red Rocker:	Press right side (ON) and let go.

2.3 Connect Stereo Adapter Cable to SCOPE on Sensor Signal Conditioner #1.

2.4 Connect other end of Stereo Adapter Cable to LINE INPUT of computer. *MAKE SURE NOT TO USE THE MICROPHONE INPUT*. For easier identification, the LINE INPUT has been marked by a white ring.

2.5 Check batteries by momentarily pressing right side Red Rocker in Sensor Signal Conditioner all the way down. Meter should point to the "BATT OK" region. If it doesn't, replace all three batteries (open box by loosening Phillips-head screw on back).

2.6 After verifying the batteries are OK, check that needle in Sensor Signal Conditioner is in green region. If it isn't, check cables, accelerometer and connectors and reconnect/replace until condition is remedied.

Step 3. Place accelerometer on Tuning Fork 3:

Attach accelerometer with wax securely and precisely between scribe marks on Tuning Fork 3. Route Accelerometer Extension Cable loosely

Appendix 6:(Continued)

through the back of the tuning fork so cable does not touch vibrating beams or interferes with accelerometer motion.

Step 4. *Run Tendon Test program section and acquire Tuning Fork vibration data. Examine response:*

4.1 Press (CTRL+R). Press F3. A File Save window appears on screen. Type XXT (where XX is the Test Station designation, for example 07 and the letter T indicates Tuning Fork test). DO NOT ENTER ANY FILE EXTENSIONS OR ALTER THIS PROCEDURE IN ANY WAY. Press ENTER.

Note: this does not cause a file to be saved yet. It only prepares the system to save the result of the test under the file name chosen, if the test is completed successfully.

4.2 Gently place 1/2 inch dowel crosswise just inside Tuning Fork end until dowel touches stop screw.

4.3 Press F3 or use the wireless remote to press the PUSH BOTTON display on the computer screen ("TEST IN PROGRESS" appears on screen). Immediately start counting: one-thousand-one, one-thousand-two, so as to have a 2-second wait. Immediately following, pull dowel straight out (along main axis of tuning fork) in one quick motion and without introducing torque. The data acquisition stops automatically 12 seconds after pressing F3.

Do not touch anything while the "TEST IN PROGRESS" message shows.

A short while later the test output will appear on the screen.

4.4 a) The frequency plot should show a clear peak at about 33 Hz (electric noise may also cause another peak near 60 Hz; ignore it).
b) Press TAB repeating as needed to select RANGE box. Pressing the UP or DOWN keys causes the spectrum to zoom into a 10 Hz wide window that shifts in 5 Hz steps (window cycles to full width after multiple steps). Move the zoom until it includes the peak near 33 Hz. Read the peak frequency as shown in the "Peak" box. Peak frequency for Tuning Fork 3 should be a value from 33.8 Hz to 34.0 Hz.
c) Read the peak height, as indicated in the vertical axis. Height for Tuning Fork should be between 200 to 500 units.

Appendix 6:(Continued)

Note 1: The "Peak" box always shows the frequency of the highest point in the window. Read the box only when the near-33 Hz peak is the only one showing in the 10 Hz wide window.

Note 2: Since the windows move only in short steps, the peak near 33 Hz will appear in two consecutive windows. The "Peak" reading in those two windows may differ by 0.1 Hz. That small variation is normal; in such case record only one of those values.

Step 5. *If Tuning Fork response is adequate, save data and proceed to Step 7:*

If response is as indicated in each of 4.4 (a), (b) and (c), Press F4, press ENTER (to select "Yes"), and the machine saves the results of the Tuning Fork test under the file name selected earlier. A confirmation message appears (see note after Step 16). The system is now ready for testing the tendons. Write down Peak frequency and Height in Log Form Supplementary Information section and proceed to Step 7.

Otherwise, proceed to Step 6.

Step 6. *If Tuning Fork response is inadequate, check all settings and connections, and proceed to Step 4:*

If response fails to result in any one of 4.4 (a), (b) or (c), the test response is inadequate, indicating a problem. Press F4 and then TAB (to select "No") and then ENTER. This resets the program. Check everything (including that accelerometer is firmly attached to tuning fork, connections, switch positions, etc.) and repeat test starting at Step 4.

Step 7. *Record ambient temperature and Span test start time:*

Enter operator initials, temperature and date/time information on Log Form.

Always use ball-point pen. If there are any entry errors, strike over and write correct entry on the side - do not attempt to write over old entry.

Testing system is now ready to operate. Proceed to Part C.

Appendix 6:(Continued)

C. TEST EXECUTION STEPS

Step 8. Select tendon to test, measure length, mark positions for accelerometer and hammer impact, and place accelerometer:

8.1. Tendon segment designations, segment length measurement and accelerometer placement position.

8.2 Select tendon segments to be tested in the order indicated in the Log Form for the appropriate Test Station. Special procedures for tendon segments obstructed from free vibration will be provided in a separate document.

8.3 Attaching accelerometer to tendon:

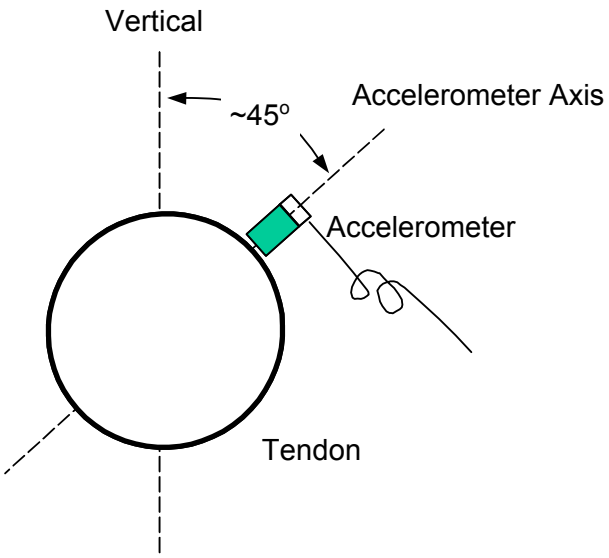

Figure 54. Accelerometer Orientation

The accelerometer is to be placed, with its axis on a plane approximately 45° from vertical, on the plastic duct as shown in Figure 2. Use mounting wax, cleaning any dust first. Avoid dropping accelerometer. If accelerometer is dropped make a note of it on Log Form Supplementary Information section.
Loose accelerometers are major source of rejected data. If necessary, further secure the accelerometer to the duct using adhesive tape or a Velcro strap.

Appendix 6:(Continued)

10.1 Route Accelerometer Extension Cable so that it does not rattle against tendon during vibration. Cable may be lightly wrapped around the next tendon to avoid accidental yanking and to restrain accelerometer fall.

8.4 Hammer impact is to be always applied on a direction perpendicular to the axis of the tendon, at a point approximately halfway between accelerometer and the deviation saddle end of the tendon. Impact will be applied in two manners: Straight and Side. In Straight impact the direction of the blow is contained in a vertical plane. In Side impact the direction of the blow is in a horizontal plane.

Step 9. Run Hammer Practice program section and practice to deliver adequate hammer blow strength. SKIP STEP IF ALREADY TRAINED:

9.1 Ensure that Steps 1 through 8 are completed.

9.2 Using the designated hammer, impact (Straight) the tendon. See ADDENDUM 2 for important Notice and Disclaimer. For this operation screen must be within easy view from impact position.

Hammer hitting:

Adjust impact to obtain desired amplitude as detailed in instructions below.

If duct is not tightly filled with grout at impact point (as indicated by unusual sound), change impact position to a point a few inches to the right or left of initial position)

9.3 Press (CTRL+R). Press F1 and hit tendon repeatedly, waiting about 3 seconds between hits. Watch signal display. Signal trace at impact should go well beyond inner lines but should not cross the outer lines. Train yourself to adjust Straight impact strength until signal stays within limits. With display still running, switch impact direction to Side and train for it similarly.

Press F2 when operation within limits is achieved in both directions and stop hitting tendon. The Save Wave File window will appear; do not attempt to close it.

Training is complete. Wait about 20 seconds before next action.

Appendix 6:(Continued)

Step 10. Run Tendon Test program section and acquire vibration data:

Ensure that Steps 1 through 8 are completed and that operator has already been trained to deliver adequate impact strength. Each tendon is tested 2 times with Straight impact (tests 1 and 2) and 2 times with Side impact (tests 3 and 4).

10.2 Press F3 if the Save Wave File window is not already on screen.

Type the file name (ALL CAPITALS) for the tendon segment to be tested and press ENTER. The file name is the same as tendon segment designation (see ADDENDUM 1) but with the number 1 appended for the first test performed for the tendon segment, 2 for the second test, etc.

Example: File for 1st test on tendon segment 116209NE is named 116209NE1 . File for 3rd test is named 116209NE3. If a test is a repeat of a test that was not acceptable (due to implementation of Step 11), repeat the same file name used in the failed test (the failed test file will be written over). DO NOT ENTER ANY FILE EXTENSIONS OR ALTER THIS PROCEDURE IN ANY WAY.

Note: this does not cause a file to be saved yet. It only prepares the system to save the result of the test under the file name chosen, if the test is completed successfully.

Have operator standby with hammer ready to hit (Straight for tests 1 and 2, Side for tests 3 and 4) when directed.

10.3 Press F3 or the PUSH BOTTON ("TEST IN PROGRESS" appears on screen). Immediately start counting: one-thousand-one, one-thousand-two, so as to have a 2-second wait. Immediately following, direct operator to hit tendon only once. The data acquisition stops automatically 12 seconds after pressing F3.

Do not touch the tendon, accelerometer or anything else in the equipment while the "TEST IN PROGRESS" message shows.

About 20 seconds later the test output appears on the screen. Signal analysis by the computer is now complete.

Step 11.Check to see If data are adequate or not:

Appendix 6:(Continued)

a) Examine strip record of top channel. Is signal in top chart within limits described in step 9.3 ?

b) Examine the spectrum record in the lower chart. A distinct peak should appear near the left end of the chart. That is the Mode 1 peak . An overtone peak (Mode 2) should be visible at about twice the frequency of Mode 1. Higher overtones may be visible at about three or four times the frequency of Mode 1. Also, the line between the peaks should be relatively smooth with few jagged regions.

The signal in the top chart should be relatively symmetric and showing a gentle decay. See Figure 3 for examples of “good” and “bad “signals and spectra.

Do signal and spectrum have the "good' appearance shown in Figure 3?

c) If answers to both (a) and (b) are YES, *go to Step 12.*

d) If answer to (a) is NO, too low or too high impact has been applied. Press F4 and then TAB (to select “No”) and then ENTER. Check equipment and *go to Step 9* for hammer practice.

e) If answer to (a) is YES but answer to (b) is NO, test needs to be rerun. “Bad” signals and spectra are often due to a loose accelerometer, obstructions in the tendon motion, or abnormal hammer impact. Check for those problems as well as equipment and connections. Correct deficiencies. Press F4 and then TAB (to select “No”) and then ENTER. Press (CTRL+R). This resets the program. *Go to Step 10* to repeat test.

Note: If a “bad” spectrum or signal persists after a few tries, complete the tests anyway, make a note of the problem, and proceed to the next tendon. Repeated difficulties in subsequent tendons may indicate equipment malfunction.

Step 12. *Identify and record peak frequencies:*

12.1 Press TAB and select RANGE box. Afterwards, pressing the UP or DOWN keys causes the spectrum to zoom into a 10 Hz wide window that shifts in 5 Hz steps. Shift the window until it includes the Mode 1 peak. Read the peak frequency as shown in the “Peak” box and enter in Log Form. Repeat for Mode 2 peak.

Note 1: The “Peak” box always shows the frequency of the highest point in the window. Read the box only when the desired Mode is the

Appendix 6:(Continued)

main feature showing in the 10 Hz wide window. Some peaks may be split into two closely spaced peaks; record only the tallest.

Note 2: Since the windows move only in short steps, each desired mode may appear in two consecutive windows. The "Peak" reading in those two windows may differ by 0.1 Hz. That small variation is normal; in such case record only one of those values for the Mode. The approximate Mode 1 frequencies expected are listed in Table 1 (rough estimates - actual behavior may be substantially different).

Step 13. Save file:

Press F4, press ENTER. The machine saves the results. A confirmation message appears (see note after Step 16). Press CTRL+R.

Step 14. Conduct second, third or fourth test of the tendon segment. (Steps 10 - 13):

If the previous test was not the fourth successful test for this tendon segment, repeat Steps (10) through (13). Otherwise, go to Step (15).

Step 15. Proceed to next tendon segment in span starting at step (8):

After the 4th successful test for this tendon segment is concluded, go to Step (8). Continue until all tendon segments in the Test Station are tested. Then go to Step (16).

Step 16. After the last segment in the span is tested, record temperature, copy data to CDRW drive, and prepare for next Span:

Press left side of Red Rocker switch of Sensor Signal Conditioner to the OFF position.

Exit *Analyzer-M* program by pressing (ALT+F4).

Read temperature and record temperature and time in Log File.

The files from all tendon tests plus the Tuning Fork test file for this Test Station have been stored in the Folder named ANALYZER FILES in the C drive (folder ANALYZER FILES accumulates all the data from all the Test Stations). Copy all the files for this Test Station to a folder named STATION## (where ## is the Test Station designation) onto the formatted

Appendix 6:(Continued)

CDRW disk that is in the CD drive. That CDRW disk has been formatted to act as if it were a hard drive. Copy into the same folder also any other files that may have originated for this Test Station (for example, from extra tests).

Go through Windows Shut Down sequence and turn off computer.

Preparations

Procedure for identifying tendon segments, measuring and recording lengths, and marking for accelerometer and impact location.

1. Tendon segment designations

Use following order: Span number, direction, position along span, position across span, length of the sloping segment, creating an eight-character name FFFGGHIJ. The values that each of the characters can take are per Table 1.

FFFGGHIJ

Table 3. Eight-Character Tendon Segment Designation

Span Designation		Position Along Span	Position Across Span	Length of Sloping Segment
Span Number FFF	Direction GG	 H	 I	 J
088 to 105 or 117 to 134	SB: Southbound NB: Northbound	S: South End N: North End	W: West Side E: East Side	L: Longest M: Medium S: Shortest

Appendix 6:(Continued)

2. Measuring and recording length.

a. For each tendon segment to be tested, clear any obstructions or debris that may prevent tendon from vibrating freely. Note: If the tendon is obstructed by unremovable obstacles (e.g, contact with walls or with other tendons), frets will need to be installed. Procedures for fret placement and associated testing will be indicated in a supplementary guide.

b. On each tendon segment, measure and record in Log Form the clear concrete-to-concrete distance. Make a note of any unusual details such as uneven concrete surface.

If available, use a metric tape and write result with 1 mm precision (if only English-units tape is available, write result in inches with 1/8 inch precision). If any other device [e.g. Laser unit] is used instead of tape, ensure first that device is accurate by making independent tape and device measurements in at least 12 different segments in actual field conditions. Send table of results for USF where statistical analysis of results will be conducted for verification.

- If using tape, ensure that an accurate, stretch-free tape is used. Do not pull on tape excessively. Replace kinked or damaged tape.

- Make sure that any folding tabs at end of tape are properly positioned.

- If concrete face is irregular, refer distance to main plane representing surface.

3. Marking accelerometer and impact positions

a. Mark with tape or bright marker position where accelerometer is to be placed. See Figure A1 (if end points are not against a bulkhead or a deviation saddle, measure distances from lowest point). Position is at

distance L_A from low end, where L_A is ~1/3 of the tendon segment length.

The value of this distance is not critical but once chosen it must be recorded.

b. Mark with tape or bright marker position where impact is to be made. See Figure A1. Position is at distance L_I from low end, where L_I is ~1/6 of the tendon segment length. The value of this distance is not critical but once chosen it must be recorded.

Appendix 6:(Continued)

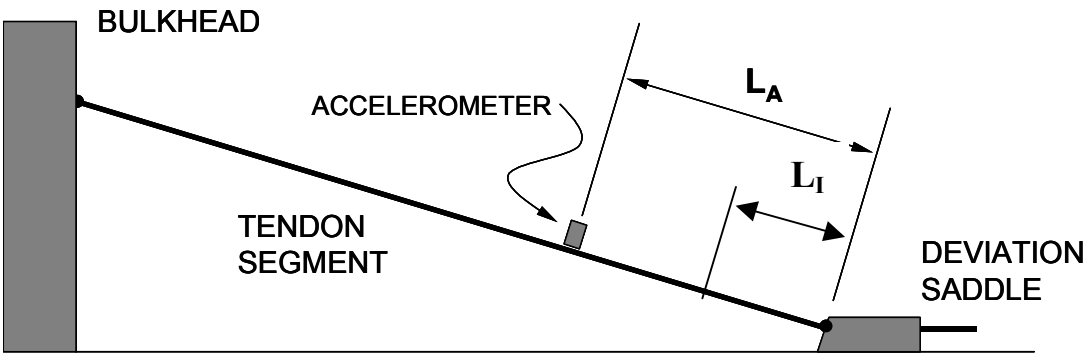

Figure 55. Accelerometer Position

SPREADSHEET FOR TENSION COMPUTATION.

Tension.xls Spreadsheet Instructions

1 - Open the Excel Workbook called “Tension.xls”.

2 - In the Worksheet called “Inputs” enter the following data in their corresponding cells:

-Bridge’s name.

-Length L (meters) and Mode Frequencies f (Hz) for each of the tendon segments tested, from the Log Form.

- Number of strands Strands from bridge construction data.

- Mass mu per unit length (kg/meter), and stiffness S of the tendon (N-m^2), from the Estimation Tables for each tendon segment of being analyzed. The Estimation Tables use as input the number of strands and the tendon diameter, the latter to be measured in situ for each tendon.

3 - The calculated Tension per strand (kN/strand), in each of the bridge segments, appears on the “Results” Worksheet.

Appendix 7: *ANALYZER-DAB* Level 3 Block Diagram

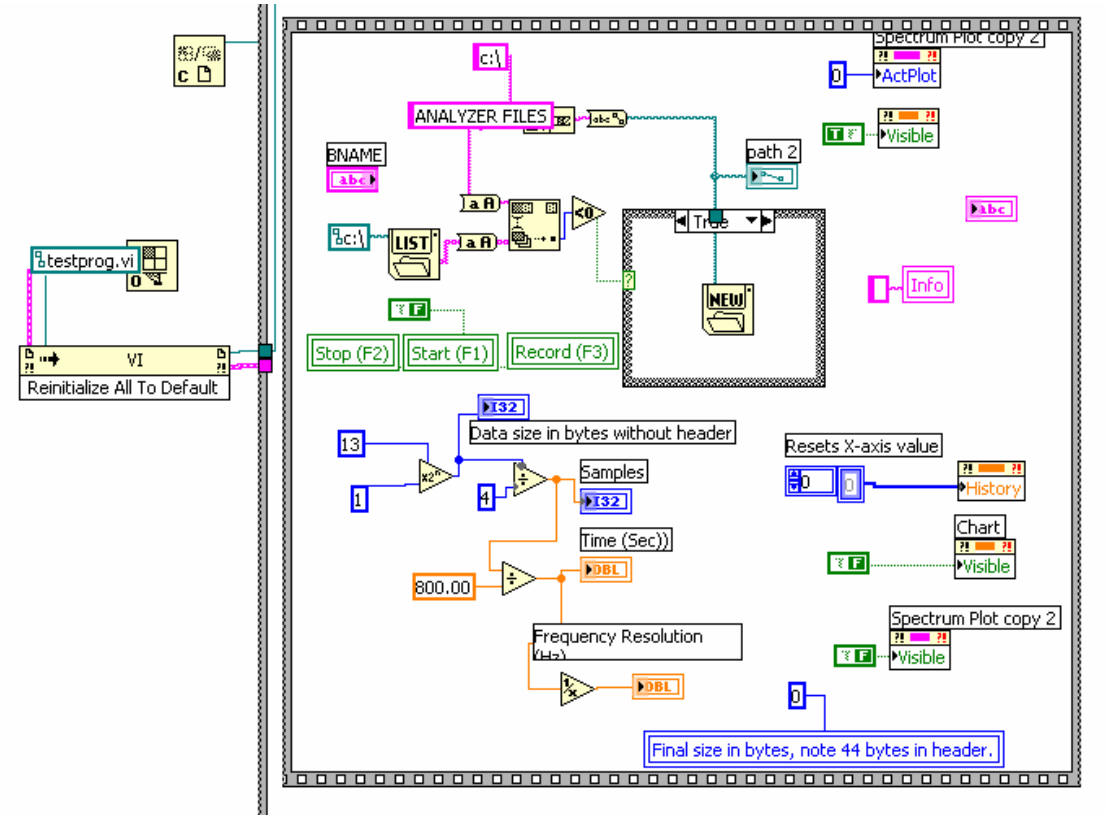

Figure 56. *ANALYZER-DAB* Level 3 Subdiagram 0-A

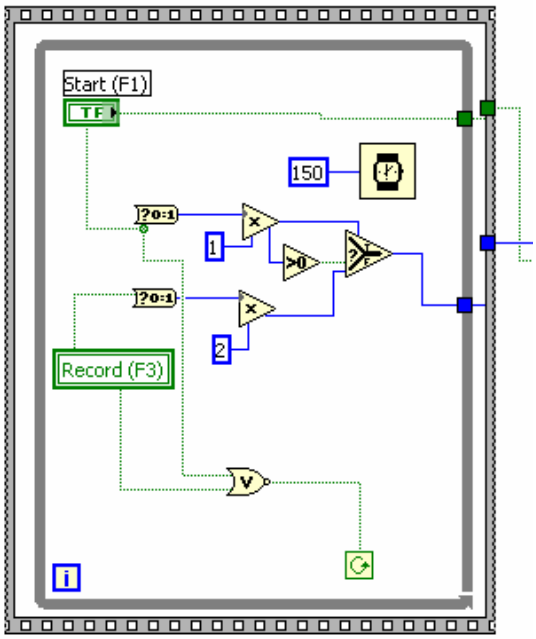

Figure 57. *ANALYZER-DAB* Level 3 Subdiagram 0-B

Appendix 7:(Continued)

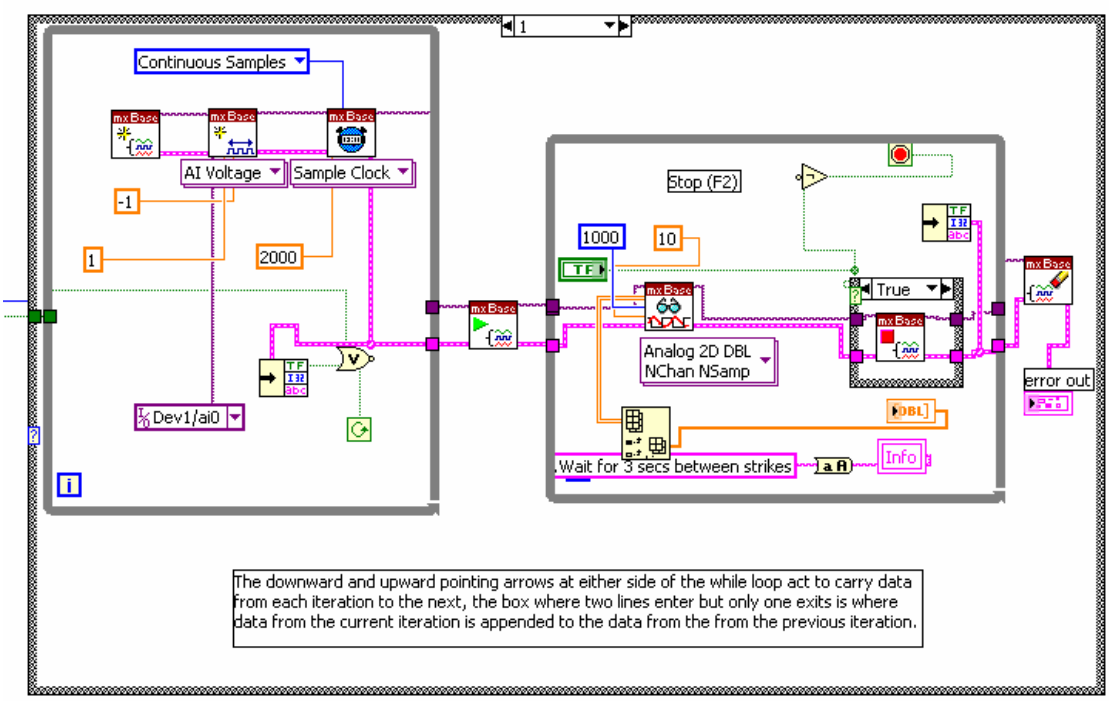

Figure 58. *ANALYZER-DAB* Level 3 Subdiagram 0-C

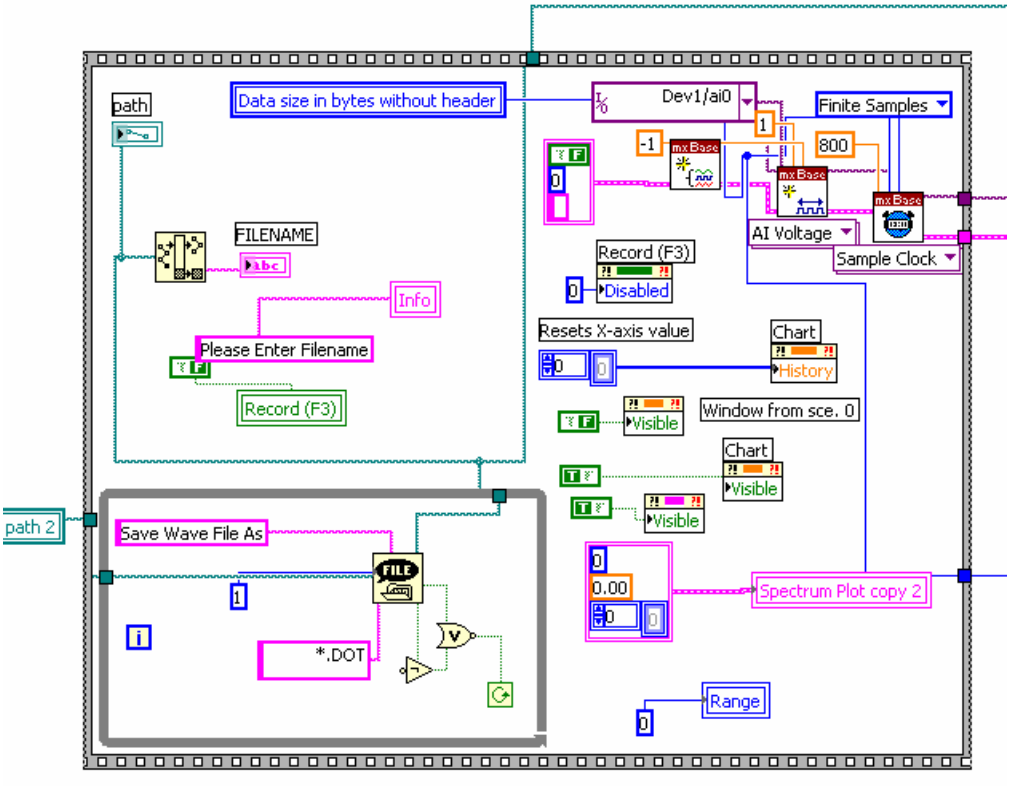

Figure 59. *ANALYZER-DAB* Level 3 Subdiagram 1-A

Appendix 7:(Continued)

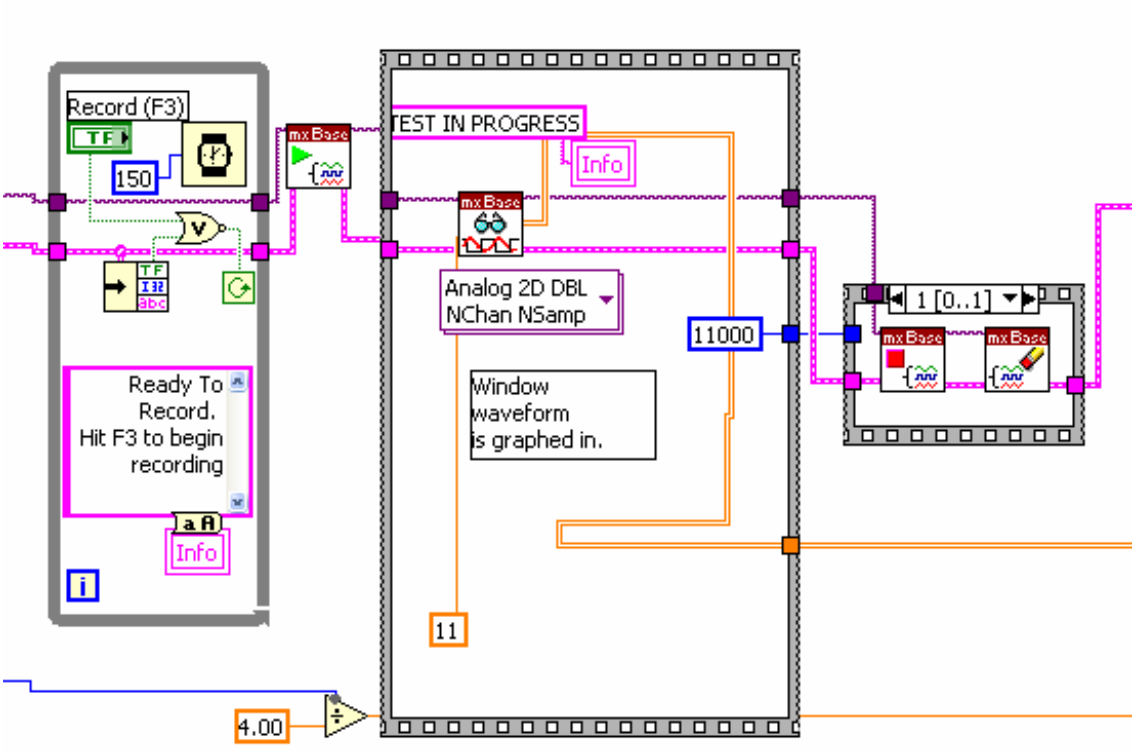

Figure 60. *ANALYZER-DAB* Level 3 Subdiagram 1-B

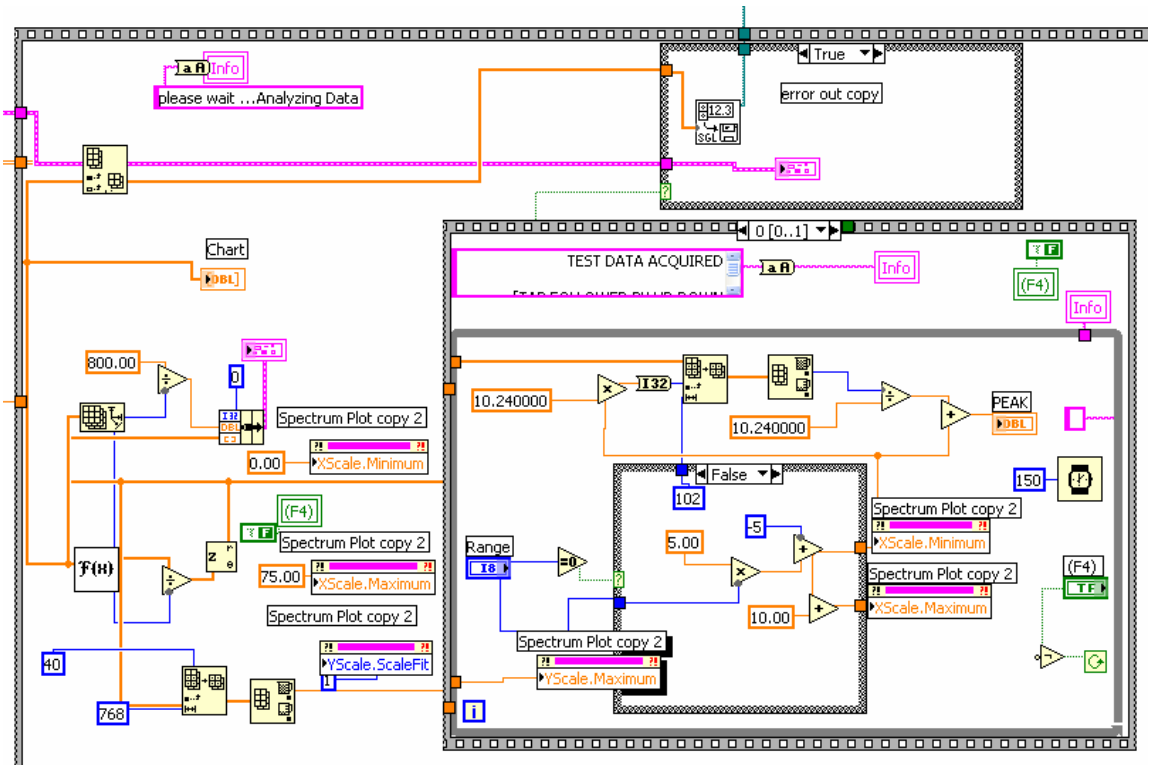

Figure 61. *ANALYZER-DAB* Level 3 Subdiagram 1-C

Appendix 8: *ANALYZER-DAB* Installation Guide

INSTRUCTIONS FOR INSTALLATION / UN-INSTALLATION OF ANALYZER-DAB.EXE

Install:

1. If Windows Explorer is not already configured to show file extensions, configure your Windows Explorer to always show file extensions.
2. Install LabVIEW Run-time Engine 7.1 if LabVIEW 7.1 or higher is not installed in the computer.
3. Install NI-DAQmx Base Version 2.0 for Windows 2000/XP.
4. Go to DAQ-remote folder in the Installation CD.
5. Navigate to the Installer folder inside DAQ-remote folder.
6. Click on install.msi and follow the instructions in the WIZARD.

   During the installation process, the setup will display the location where the program will be installed. The "Destination Folder" item should display EXACTLY "c:*ANALYZER-DAQ*" (and NOTHING ELSE) as the path for the destination of the program. If it does not, navigate to the folder "c:*ANALYZER-DAQ*" using the "Browse" button located on the right hand side of the setup window.

7. After installation is complete, locate the file *ANALYZER-M.EXE* (it should be located in the folder "c:\programs*ANALYZER-DAQ"* or go to the start menu and choose programs) and create a shortcut for that file on the desktop.
8. A simplify way to install the program would be to copy the file *ANALYZER-DAQ.EXE* from the DAQ-remote folder and paste on the desktop.

Un-Install:

3. In the Installation CD, navigate to DAQ-remote\Installer folder, click on install.msi
4. Follow the instructions in the wizard.

Imp. Note: In the un-installation process, the wizard should indicate that the process is indeed un-installation, not an installation.

Wave-Player DAQ.EXE installation

Follow same instructions as for *ANALYZER-DAQ.EXE* but taking into consideration that the files should be under wave-player DAQ folder.

Run-Time Engine installation

From the installation CD run *LVRunTimeEng 7.1.exe* to install the *LabVIEW 7.1 Run-Time Engine*.

Appendix 8:(Continued)

NI-DAQmx Base Version 2.0 installation

1. Create a temporary folder on your local hard drive.
2. Extract the *NIDAQmxBase200.zip* file into the folder created in Step 1. This will create the installation files necessary for installing *NI-DAQmx* Base.
3. To launch the *NI-DAQmx* Base installer, run setup.exe from the folder created in Step 1.

Appendix 9: Block Diagram of *WavePlayer-DAB*

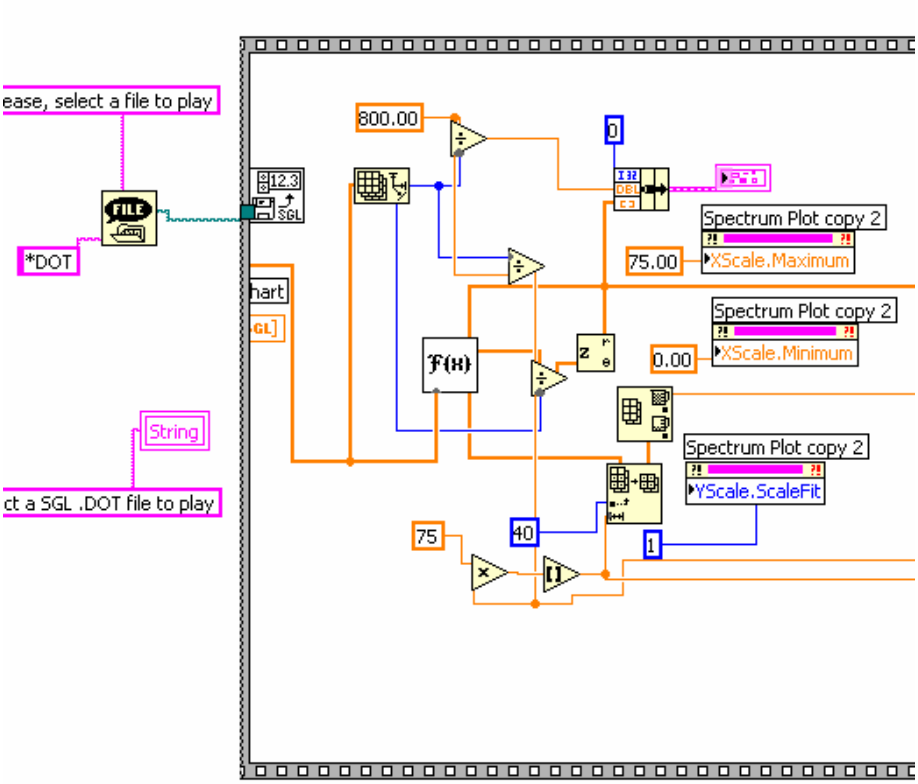

Figure 62. *WavePlayer-DAB Block Diagram A*

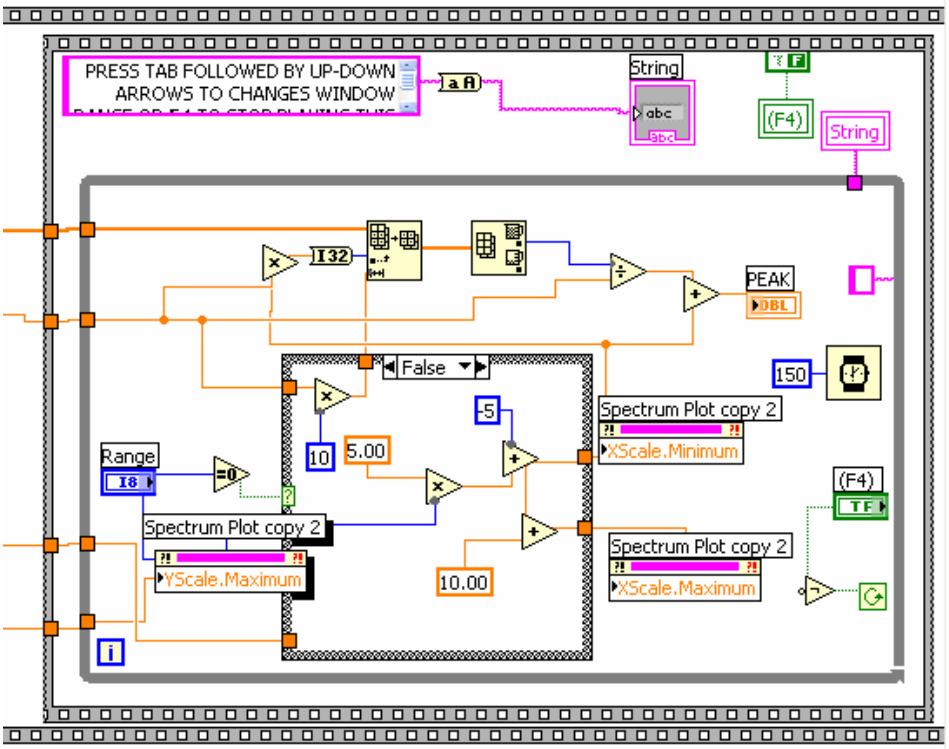

Figure 63. *WavePlayer-DAB Block Diagram B*

Appendix 10: *Wave Player Micro* Block Diagram

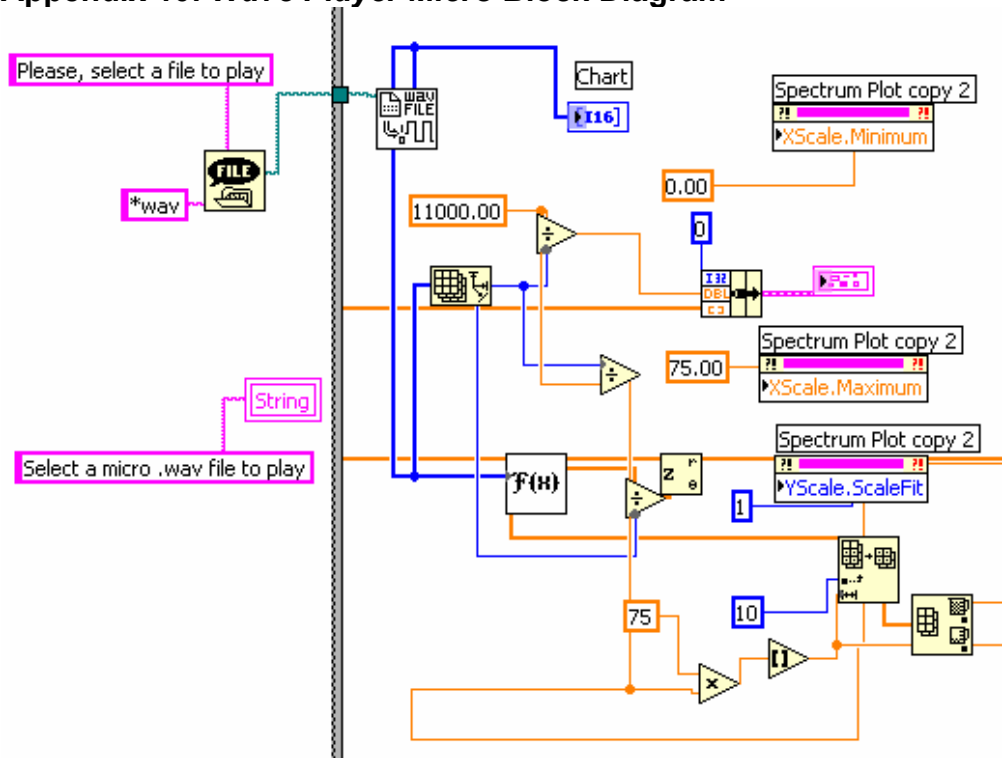

Figure 64. *Wave Player Micro* Block Diagram A

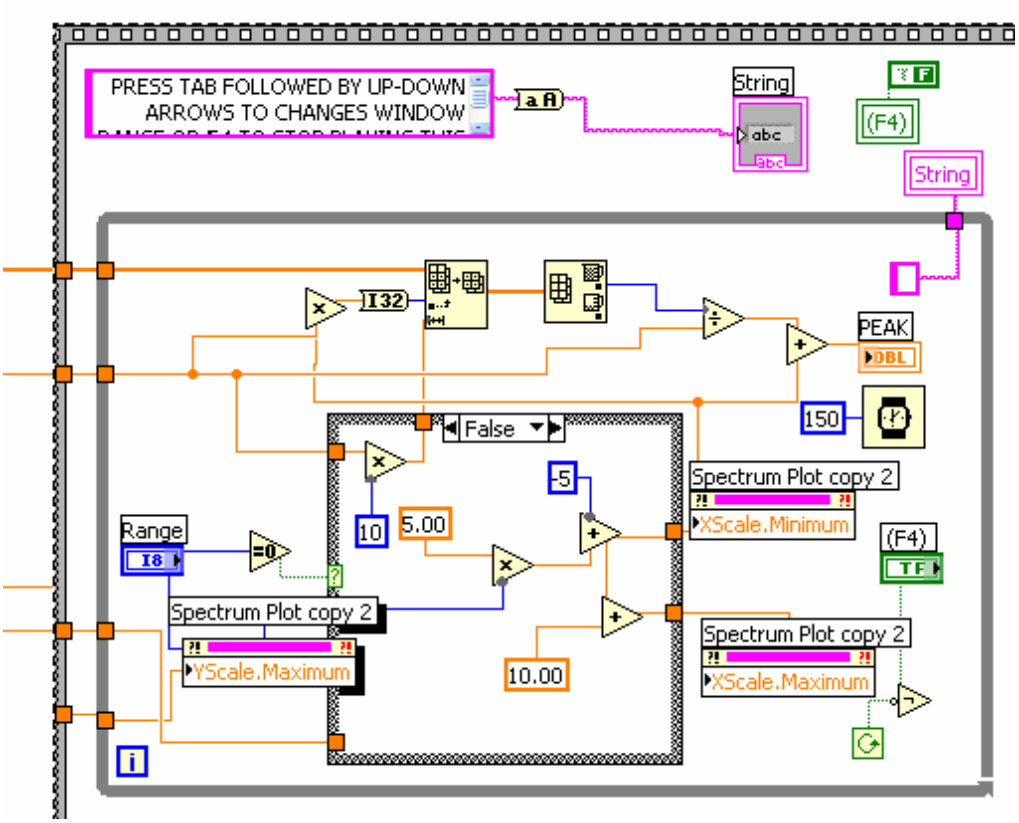

Figure 65. *Wave Player Micro* Block Diagram B

Appendix 11: Derivation of Equation to obtain "P"

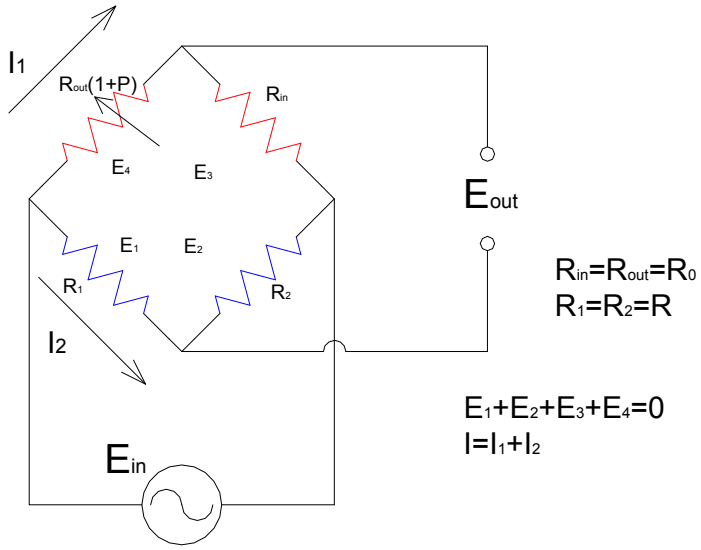

Figure 66. Schematic ER Probe Initial Conditions

$$E_1 + E_2 + E_3 + E_4 = 0$$
$$I_1 \cdot R_o(2+P) - I_2(2R) = 0$$
$$I_2 = I_1 \cdot \frac{R_o(2+P)}{2R}$$

$$R_T = [\frac{1}{R_o(2+P)} + \frac{1}{2R}]^{-1}$$
$$R_T = \frac{R \cdot R_o(4+2P)}{2R + R_o(2+P)}$$

$$I = I_1 + I_2$$
$$\frac{E_{in}}{R_T} = I_1 + I_1 \cdot \frac{R_o(2+P)}{2R}$$
$$I_1 = \frac{E_{in}}{\frac{R \cdot R_o(4+2P)}{2R + R_o(2+P)} \cdot \frac{1}{1 + \frac{R_o(2+P)}{2R}}}$$
$$I_1 = \frac{E_{in}}{R_o(2+P)}$$

$$E_{out} = E_4 - E_1$$
$$E_{out} = I_1 \cdot R_o(1+P) - I_2 \cdot R$$
$$E_{out} = I_1 \cdot R_o(1+P) - (I_1 \cdot \frac{R_o(2+P)}{2R}) \cdot R$$
$$E_{out} = I_1 \cdot R_o \cdot \frac{P}{2}$$

$$E_{out} = I_1 \cdot R_o \cdot \frac{P}{2}$$
$$E_{out} = \frac{E_{in}}{R_o(2+P)} \cdot R_o \cdot \frac{P}{2}$$
$$P = \frac{4 \cdot E_{out}}{E_{in} - 2E_{out}}$$

Appendix 12: Derivation of Equation to Obtain "Rcorr"

$R = \frac{L \cdot \rho}{A}$ where R is the resistance of the wire in ohms, L is the length of the wire, ρ is the resistivity of the steel, and A is the cross section area of the wire.

$A = \pi \cdot r^2$, where r is the radius of the wire.

$\frac{R_o}{R_{corr}} = \frac{L \cdot \rho / (\pi \cdot r_o^2)}{L \cdot \rho / (\pi \cdot r_{corr}^2)}$ where R_o is the original resistance of the wire, R_{corr} is the Resistance of the wire after it corroded, r_o is the original radius of the wire, and r_{corr} is the radius of the wire after it has corroded.

Simplifying the above equation.

$r_{corr} = r_o \cdot \sqrt{R_o / R_{corr}}$

Since $R_{corr} = R_o \cdot (1 + P)$

$r_{corr} = r_o \cdot \sqrt{R_o / R_o \cdot (1 + P)}$

$r_{corr} = r_o \cdot \sqrt{1/(1 + P)}$

Appendix 13: Block Diagram *P-Measurements*

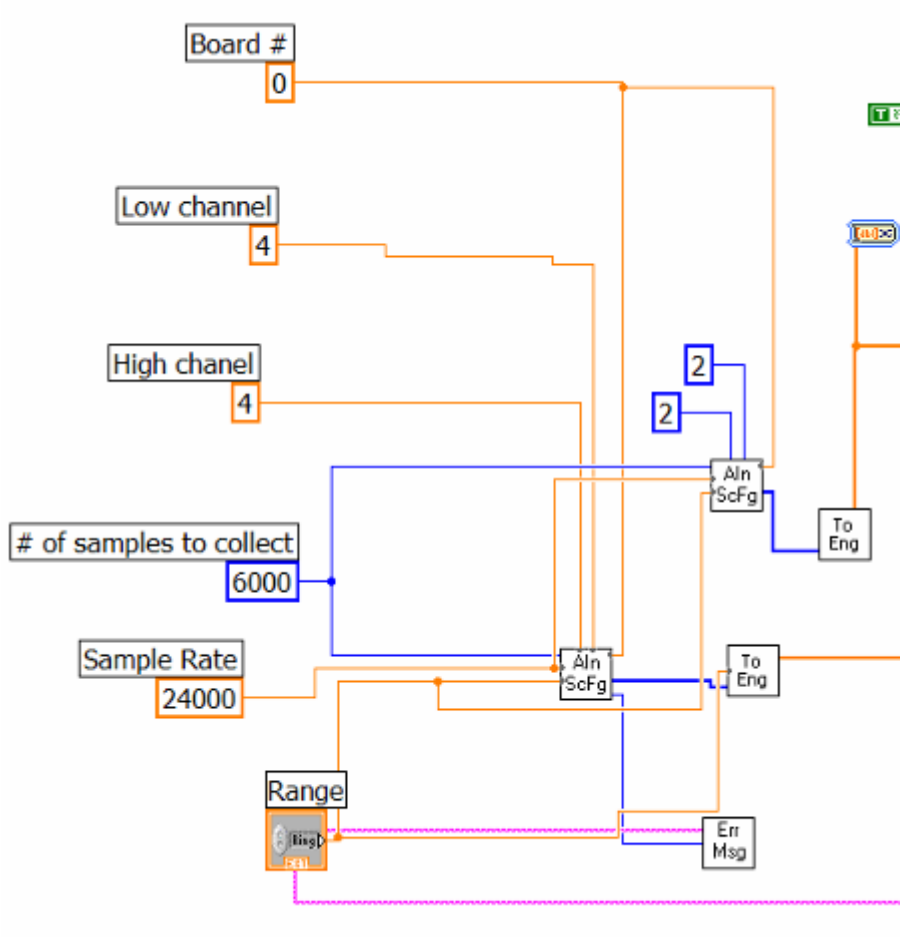

Figure 67. Block Diagram *P-Measurements* A

Appendix 13:(Continued)

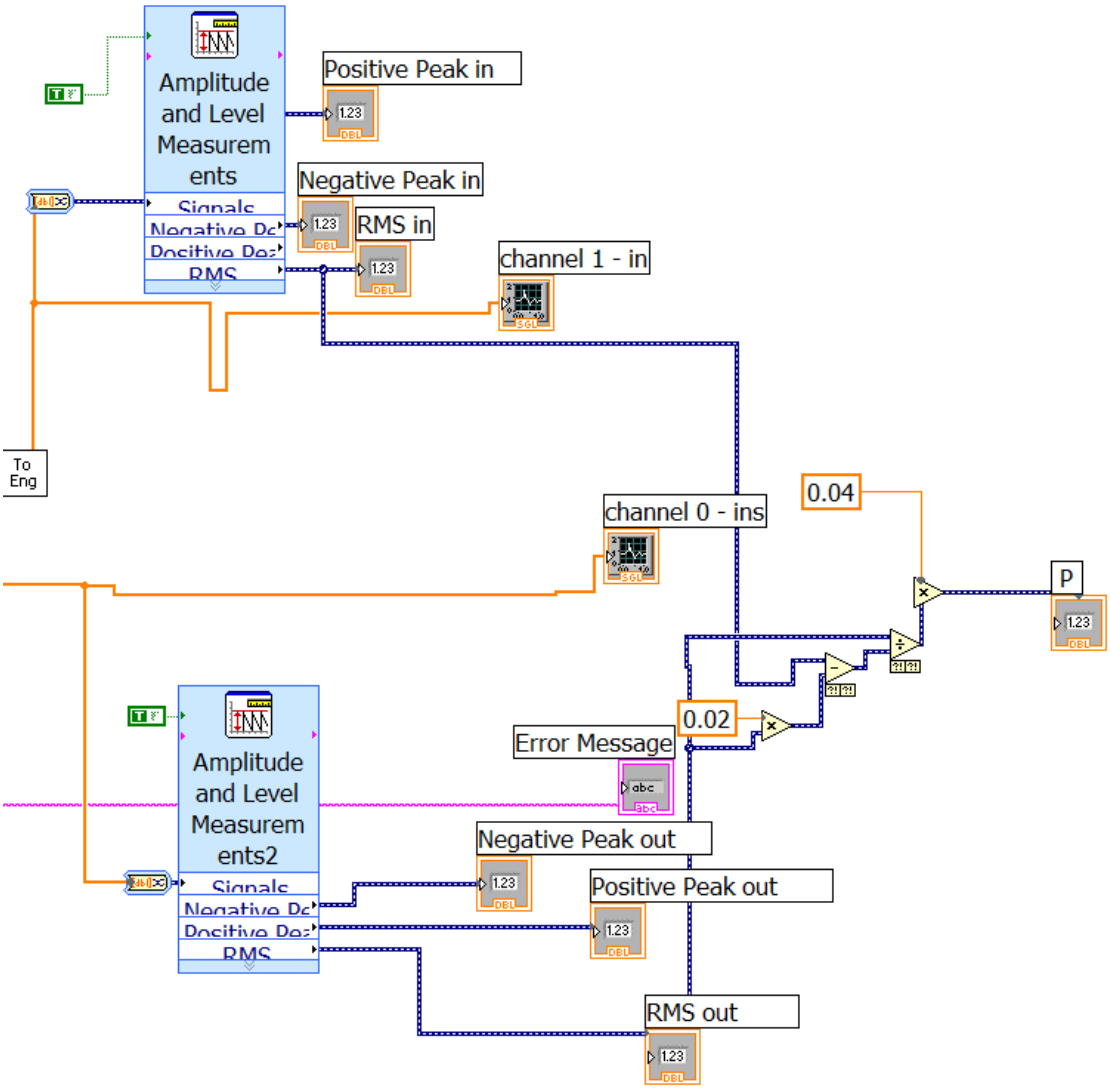

Figure 68. Block Diagram *P-Measurements* B